PAUL SCHERRER INSTITUT

**PSI**

Department Logistics
Division for Radiation Safety and Security

# International Intercomparison Exercise of Airborne Gammaspectrometric Systems of Germany, France and Switzerland in the Framework of the Swiss Exercise ARM07

Benno Bucher, Ludovic Guillot, Christopher Strobl, Gernot Butterweck, Sébastien Gutierrez, Michael Thomas, Christian Hohmann, Ingeborg Krol, Ladislaus Rybach and Georg Schwarz

Department Logistics
Division for Radiation Safety and Security

# International Intercomparison Exercise of Airborne Gammaspectrometric Systems of Germany, France and Switzerland in the Framework of the Swiss Exercise ARM07

**Benno Bucher[1], Ludovic Guillot[2], Christopher Strobl[3], Gernot Butterweck[4],
Sébastien Gutierrez[2], Michael Thomas[3], Christian Hohmann[3], Ingeborg Krol[3],
Ladislaus Rybach[5], Georg Schwarz[1]**

[1] Eidgenössisches Nuklearsicherheitsinspektorat, 5232 Villigen ENSI, Schweiz

[2] Laboratoire Mesures Sol et Aéroportées, Commissariat à l'énergie atomique,
   91680 Bruyères-le-Châtel, France

[3] Abteilung Überwachung der Radioaktivität in der Umwelt, Bundesamt für Strahlenschutz
   85764 Oberschleißheim, Deutschland

[4] Abteilung Strahlenschutz und Sicherheit, Paul Scherrer Institut, 5232 Villigen PSI, Schweiz

[5] Institut für Geophysik, ETH Zürich, 8092 Zürich, Schweiz

**Abstract**

The aeroradiometric exercise ARM07 was a joint project of the measurement teams of France, Germany and Switzerland. The measurement flights of the exercise ARM07 were performed between 27th and 31st of August 2007 under the direction of G. Scharding of the National Emergency Operations Centre (NAZ) and coordination by the Expert Group for Aeroradiometrics (FAR).

According to the alternating schedule of the annual ARM exercises, the environs of the nuclear power plants Mühleberg (KKM) and Gösgen (KKG) were surveyed. The measurements showed similar results to those obtained in former years. The results from the three teams agree well.

The region of Basel, where the borders of Germany, France and Switzerland meet, was chosen for a composite aeroradiometric mapping. It was shown that the data measured by each team in adjacent areas could be uniformly processed and integrated within hours into joint radiological maps of the complete region. The methods for data aquisition, data processing and integration are described.

**CONTENTS**

**TABLES**

**FIGURES**

## 1 INTRODUCTION

Adequate emergency response in the case of nuclear accidents, lost radioactive sources, radioactive satellite debris or intentional dispersion of radioactive materials requires appropriate information based on measurements in the environment. Airborne gamma-spectrometry is able to obtain fast radiological information over large areas, yielding a first impression of the radiological situation to decision makers. Basing on these measurements ground measuring teams can be deployed with significantly increased efficiency.

The affected area in a radiological emergency is dependent on the type of radio-nuclide release. Large scale contamination, as could be expected in the cases of severe nuclear accidents, obviously calls for international collaboration and data exchange. In the case of localized emergencies, as for example lost radioactive sources, national radiometric capabilities may be supplemented by international assistance from unaffected countries.

International collaboration in radiological emergencies requires preparation. Measurement techniques, measurements protocols and data formats have to be compatible to integrate measurements obtained by measuring teams of different countries to a unified estimate of the radiological situation.

International exercises are the best tool to provide and test this necessary compatibility.

Following a series of international comparison exercises of airborne gamma-spectrometric systems, teams of France and Germany joined the Swiss annual aero-radiometric exercise 2007. The region of Basel where the countries of France, Germany and Switzerland meet was chosen as location of the exercise.

## 2 INTEGRATION INTO NATIONAL EMERGENCY RESPONSE ORGANISATIONS

### 2.1 France

The Helinuc system is operated by the French Atomic Energy Commission (CEA). The system can be deployed by the French Ministry of Defense, the French Civil Defence and Protection Directorate (DDSC) and the nuclear industry. The measuring system is located at the Ile de France site of CEA. The CEA site is equipped with a helicopter landing pad. In an emergency case, the helicopter is provided and operated by the French Air Force. During working hours, the measuring system is operative in less than three hours. The deployment time increases to less than twelve hours over weekends and holidays.

### 2.2 Germany

The airborne gamma-spectrometry is designed, maintained and operated by the Federal Office for Radiation Protection (BfS) which is the central reponse organi-

sation for emergencies associated with radioactive materials. The helicopters are provided and operated by the German Federal Police.

The measuring systems are located at the sites of BfS in Berlin and Munich. The Federal Police operates helicopter bases in both cities, which enables a start of measuring operations in less than five hours throughout Germany.

## 2.3 Switzerland

Swiss aeroradiometric measurements started in 1986. Methodology and software for calibration, data aquisition and mapping were developed at the Institute of Geophysics of the Swiss Federal Institute of Technology Zurich (ETHZ). Between 1989 and 1993 the environs of Swiss nuclear installations were measured annually on behalf of the Swiss Federal Nuclear Safety Inspectorate (ENSI). This schedule was changed to bi-annual inspections in 1994, together with an organisatorical inclusion of the airborne gamma-spectrometric system into the Emergency Organisation Radioactivity (EOR) of the Federal Office for Civil Protection (FOCP). The deployment of the airborne gamma-spectrometric system is organized by the National Emergency Operations Centre (NEOC). Aerial operations are coordinated and performed by the Swiss Air Force. The gamma-spectrometric equipment is stationed at the military airfield of Dübendorf. The gamma-spectrometry system can be airborne within four hours.

Responsibility for scientific support, development and maintenance of the aeroradiometric measurement equipment passed from ETHZ to the Radiation Metrology Section of the Paul Scherrer Institut (PSI) in 2003 in cooperation with ENSI. General scientific coordination and planning of the annual measuring flights is provided by the Expert Group for Aeroradiometrics (FAR). FAR was a working group of the Swiss Federal Commission for NBC-protection (ComNBC) and consists of experts from all Swiss institutions concerned with aeroradiometry. FAR was re-organized as an expert group of the NEOC in 2008. Additional information can be found at http://www.far.ensi.ch/.

## 3 MEASURING SYSTEM

### 3.1 France

The survey of a site consists of a series of gamma measurements recorded along a predefined flight plan. Two types of detectors are used, a NaI crystals pack and two Ge detectors. Every 2 seconds, a NaI and/or a Ge spectrum is recorded together with the center position (X, Y, Z) of the helicopter during the measurement. The area to be surveyed is divided into a grid by equidistant flight lines (Fig. 1). The line spacing, the altitude and the speed of the helicopter are defined before the flight according to the required detection limit and the flight time available to cover the area. These parameters are monitored continuously by the operator and the helicopter pilot.
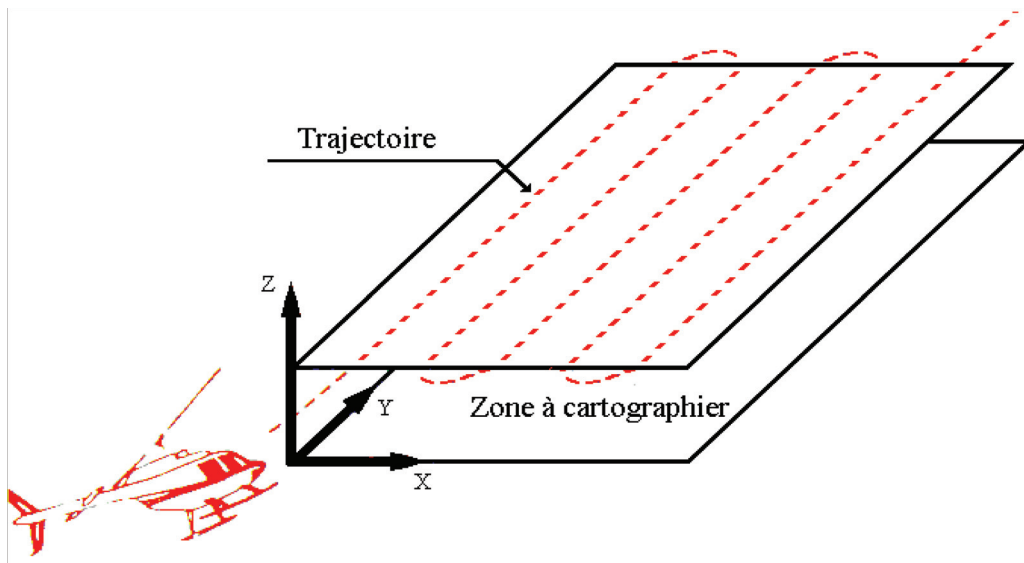
**Figure 1: Coverage of the area to be mapped.**

The main detector is a 16 litres sodium iodide crystals pack inside a dedicated container fitted under the helicopter. In such configuration, the gamma signal is unaffected by the floor of the aircraft. There is also a 70% Ge detector on both sides of the container. The system is described in Table 1 and presented in Figure 2. The NaI spectra are stored in 512 Channels between 40 keV and 2800 keV, whereas the Ge spectra are stored in 2048 channels between 40 keV and 2050 keV. The NaI Measurement is managed by an Exploranium GR-820 airborne spectrometer. The gain is set automatically by continuously monitoring the position of the photo-peak of a natural radionuclide, usually potassium or thorium. Two Ortec DSpec spectrometers process the Ge data. A real time gain monitoring is also performed to avoid energy drifts of the spectra. The position of the helicopter is given each second by a GPS, which can be used in real-time differential mode to obtain a sub-metric precision. The ground clearance is given by a radio-altimeter with a precision of 1 meter. The data processing is performed by a recording rack inside the cabin. An operator can control the acquisition process and the real-time data-processing. The system can be installed on-board of a helicopter within two hours.

**Table 1: System description**

| Detection system A | NaI pack of 16 litres |
|---|---|
| Sample time | 2 s |
| Spectrometer | Exploranium GR-820 |
| Energy range | 40 keV to 2800 keV |
| | |
| Detection system B | 2 Ge detectors of 70% |
| Sample time | 2 s |
| Spectrometer | 2 Ortec Dspec |
| Energy range | 40 keV to 2050 keV |
| | |
| Positioning system | GPS Trimble, type AG 132 |
| Altimetry system | Radio-altimeter Thomson ERT 011 |
| Hardened PC | Kontron FW 8500 |



**Pilot indicator**

**Recording rack**

**Measurement pod:**
· NaI of 16 litres
· 2 Ge detectors (option)
· 1 radioaltimeter

**Figure 2: The French Helinuc system installed on-board an AS355 helicopter.**

The acquisition process is controlled by the Gr-660 software, developed by the Exploranium company and modified by the CEA for Ge data recording. A preliminary processing of NaI data is done in real time. The results are displayed in different windows presented in Figure 3. The first window displays the charts of count rate or activity of specified nuclides, or dose rate. A "rainbow" graph, showing the last fifty spectra is also displayed. In case of alarm the spectrum can be displayed to identify the anomaly. A navigation display is in front of the pilot. Planned and actual flightlines are displayed together with the flight parameters (speed, line spacing and ground clearance). At the end of the flight, the data are transferred on a PCMCIA memory card for post-processing.



Chart of activities of 4 radionuclides       "Rainbow" graph

Pilot indicator       GPS plot
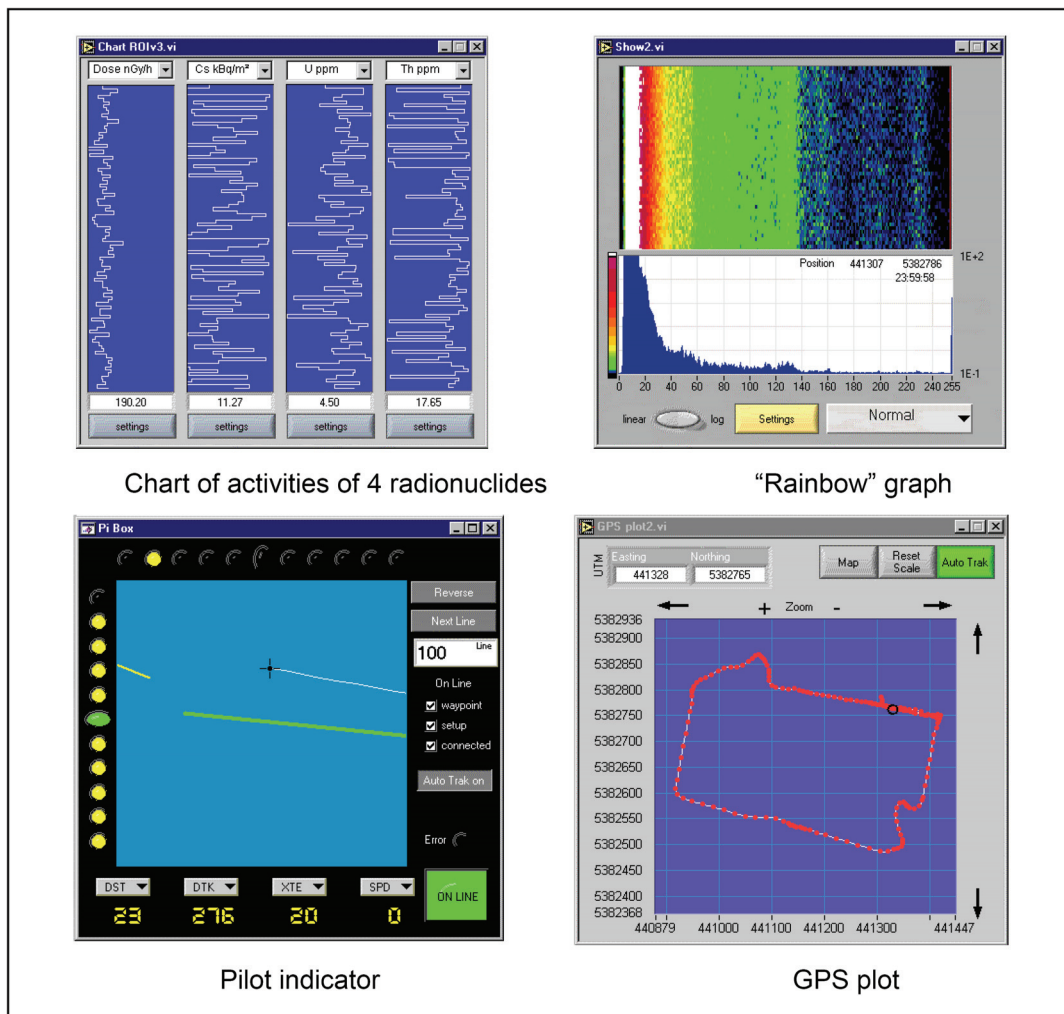
**Figure 3: Information displayed by the acquisition software.**

The Helinuc system is usually installed on a Eurocopter helicopter AS 355 or AS 555. With such a light helicopter, it is possible to fly at a ground clearance of 50 m without too much disturbance to people or animals at ground level. The use of Hélinuc with an AS 355 or AS 555 is agreed by French aeronautic authorities. The system has also been mounted on Eurocopter Allouette III, Bell UH-1H, Bell 205

and Kamov 26 (Fig. 4). For each type of helicopter, a specific flight box was designed in accordance with the anchor points of the helicopter.



**Figure 4: Helinuc system mounted on several types of helicopter.**

The field data processing system is operated on a laptop PC. In an emergency situation, the data processing can be done in the field in two hours. This can be done everywhere in autonomy in the processing van presented in Figure 5. This van contains two processing units, with PC, printer and scanner.



**Figure 5: Processing van.**

## 3.2 Germany

The measuring system of the German team consists of four NaI(Tl)-detectors with a volume of four liters each located at the walls of the helicopter cargo bay. An additional HPGe-detector is located in the rear of the helicopter (Fig. 6). The mounting platforms are adapted to the Eurocopter EC135 helicopter of the German Federal Police (Fig. 2). All relevant data are displayed on the operator screen giving a direct picture of the radiological situation in the measurement area (Fig. 8).



**Figure 6: The German measuring system installed in the cargo bay of an Eurocopter EC135 helicopter. Right and left side: NaI(Tl)-Detectors. Center: Data processing unit.**



**Figure 7: EC135 helicopter of the German Federal Police during a measuring flight.**

8
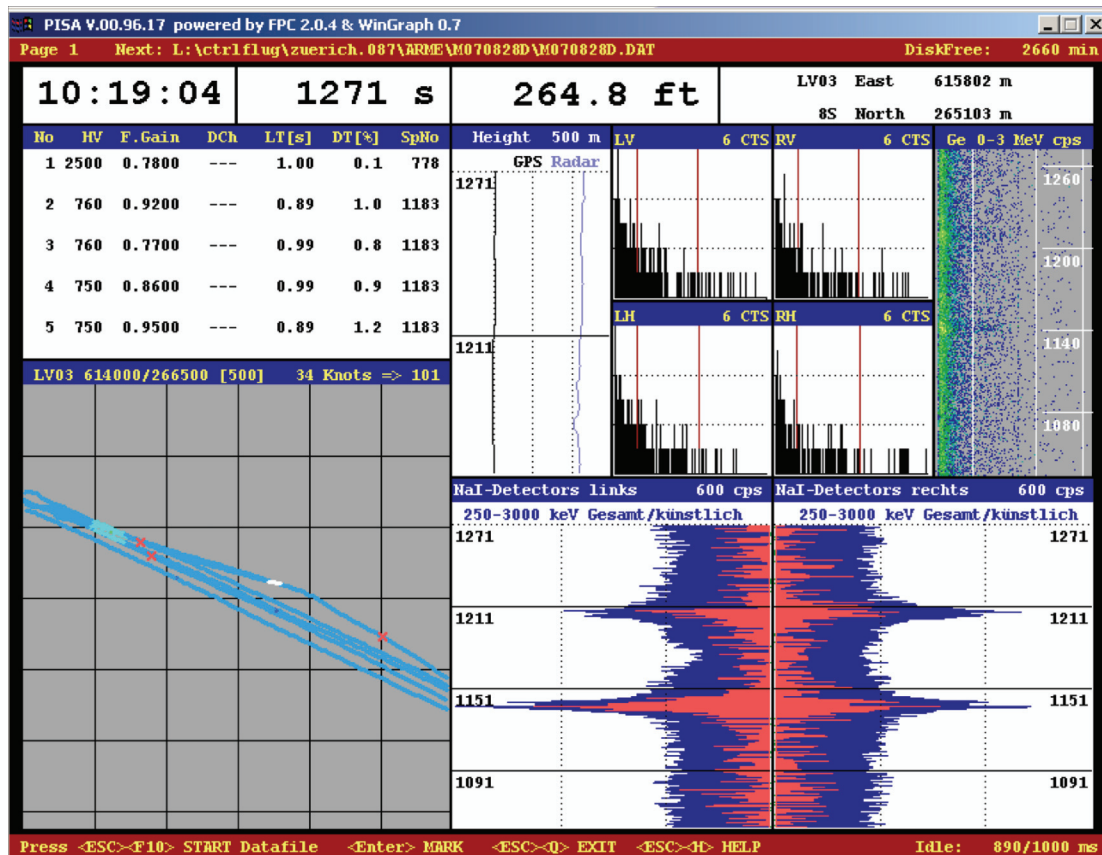


**Figure 8: Screen shot of the data aquisition and evaluation software.**

## 3.3 Switzerland

The measuring system consists of four NaI-detectors with a total volume of 16.8 l. The spectrometer includes for each detector a 256-channel analyser with automatic gain control. The measurement control, data acquisition and storage are performed with an industrial grade personal computer. A second, identically configured PC is present in the electronics rack (Fig. 9) as redundance. Under normal operation conditions, this PC is used for real-time evaluation and mapping of the data.
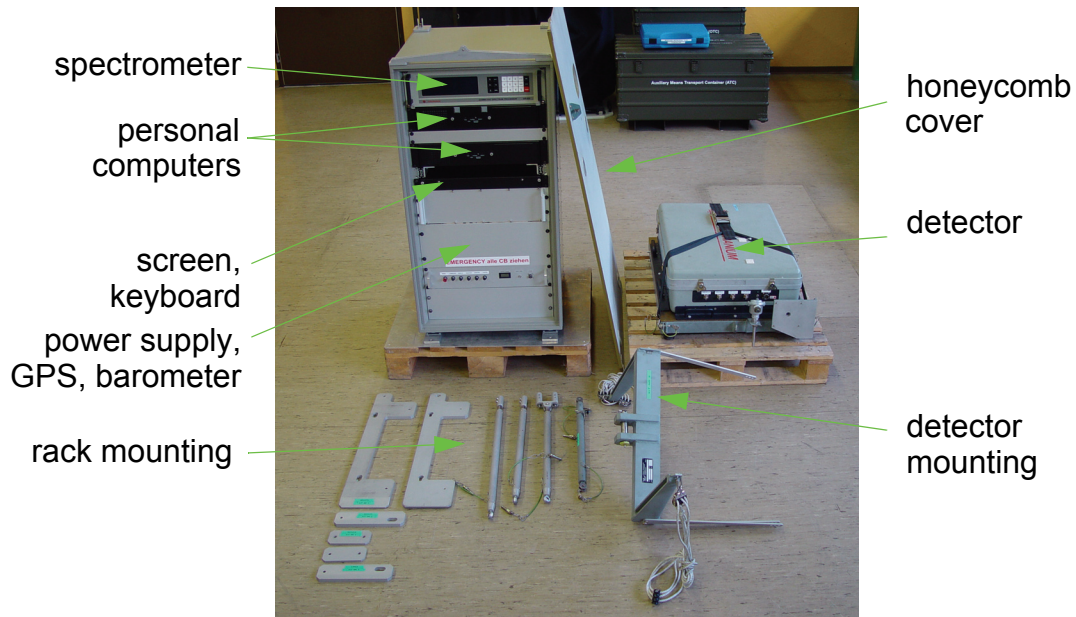
**Figure 9: Measurement system of the Swiss team.**

The positioning uses GPS (Global Posistioning System) in the improved EGNOS (European Geostationary Navigation Overlay Service ) mode. Together with spectrum and position, air pressure, air temperature and radar altitude are registered.

The measuring system is mounted in an Aérospatiale AS 332 Super Puma helicopter of the Swiss Air Force (Fig. 10). This helicopter has excellent navigation properties and allows emergency operation during bad weather conditions and nighttime. The detector is mounted in the cargo bay below the center of the helicopter. The cargo bay is covered with a lightweight honeycomb plate to minimise photon absorption losses.



**Figure 10: Super Puma helicopter of the Swiss airforce.**

## 4 DATA EVALUATION

The advantage of aeroradiometric measurements lies in the high velocity of measurements in a large aera, even over rough terrain.

Uniform radiological information of an area is obtained from a regular grid of measuring points. This grid is composed from parallel flightlines which are 100 m to 500 m apart, dependent on the scope of the measurement (Fig. 11). The flight altitude above ground is kept constant during the measuring flight. Typical values lie between 50 m and 100 m above ground. The spectra are recorded in regular time intervals of typical one or two seconds, yielding an integration over 28 meters to 56 meters of the flight line at a velocity of 100 km/h.
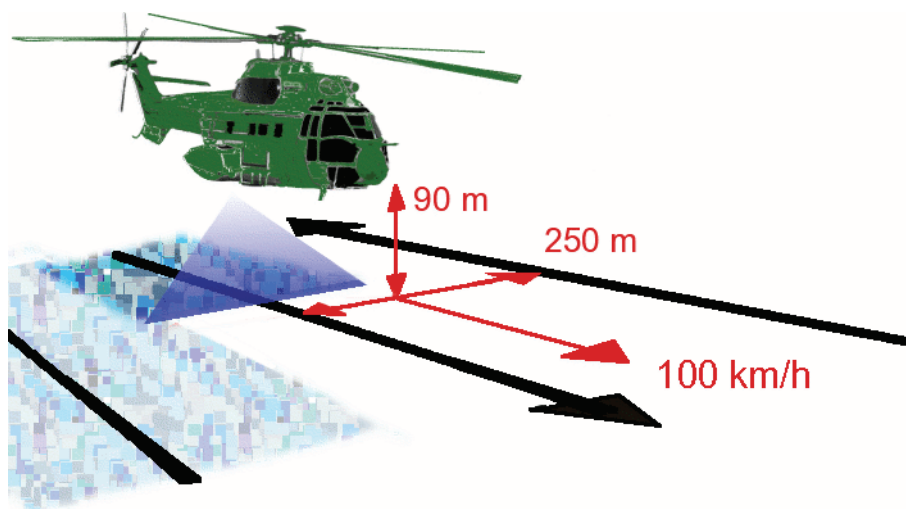


**Figure 11: Schematic diagram of a measuring flight.**

## 4.1 France

The measuring flights are typically performed with a speed of 70 km/h at a flight altitude of 40 m. Line spacing varies between 50 m and 500 m according to the measurement task.

The GPS provides geographical coordinates (WGS 84) which are converted for mapping purposes either into the UTM system (cylindrical projection) or the Lambert system (conic projection), which is generally used in France. Previously-scanned geographical maps appear as transparent overlays on each map. Two bars in the bottom left-hand corner indicate the map scale in X and Y direction.

The objective of the data analysis is to find all radionuclides which produce gamma emission on the area and if possible to calculate the activity of each one everywhere. To achieve these tasks, several data analysis algorithms are used. Some of them have been developed at CEA. Generally the mapping of raw measurements starts the data processing in order to evaluate the main changes in gamma signal. Secondly the mapping of natural radionuclides is performed. It's very helpful

to know activities and spatial distribution of natural radionuclides to detect low amount of man-made radionuclides. Then man-made contributions are isolated with several analysis methods, depending on the energy range of the gamma emission.

### 4.1.1 Raw Measurements

The mapping of total count rate between 40 keV and 2800 keV is always the first step of data processing. It provides a first view of spatial distribution of the gamma emission. A radioactive orphan source can be located very quickly by this method. Maps showing the count rate in different energy windows, known as 'interest windows', centred on the major absorption peaks of the radionuclides can also be produced. If the background in the energy window is low compared to the net count rate, these maps show very quickly spatial distribution of the radionuclide. The results are expressed in normalized counts per second at a standard ground clearance, while the ratios between windows are expressed as relative values. The maps generated from raw measurements must be interpreted with caution. In particular, large changes in the background (Compton effect) generated by radionuclides with higher energy lines can significantly affect the count rates in a specific window. When an anomaly is observed, it is necessary to check that it is not caused by a sudden change in the activity of another radionuclide.

### 4.1.2 Spectral Analysis of NaI data

The windows method is recommended by IAEA (IAEA, 1991) and Eccomags project (Sanderson et al., 2003) to process AGRS data. Gross count rates for potassium, uranium and thorium are calculated. A background count rate for each window (determined from flight above the water) is then subtracted. After the stripping procedure, an altitude correction to estimate count rate at ground level is applied. The altitude correction and calibration coefficients are determined for each nuclide from hovering manoeuvres over the calibration sites. This method provides good performances if all the radionuclides are known before the processing and if the number of radionuclides is not to high. For example the mapping of very low levels of caesium in France is usually performed with this method (sometimes less than 1 kBq/m²).

An absorption peak isolation algorithm adapted to characteristics of poor statistic NaI spectra has been developed to extract these peaks from the raw spectrum (Guillot, 1996). The performances obtained are comparable with that of the windows method, conventionally used for measuring natural radionuclides. The feature of this new processing method is that, in contrast to existing methods, it does not require any assumptions about the number or nature of the radionuclides. Radionuclides with emission lines over the entire measurement energy range (40 to 2800 keV) can now be detected but the performances are optimal at energies higher than 400 keV.

Both previous methods are not very efficient at low energy (40 keV to 400 keV) because the intensity of the background is higher in this energy range. A third method has been developed to estimate the low energy background with a better

accuracy. A stripping coefficient between the low energy window and a reference window at higher energy is calculated considering the complete data set. This coefficient is then used to calculate the low energy contribution generated by all radionuclides which have gamma lines in the high energy window. After stripping, the signal from low energy emitters is remaining.

The ground level dose rate is estimated by the spectral dose index method (Sanderson et al., 2003). A calibration factor is determined from a hovering manoeuvre above the calibration sites.

4.1.3 Spectral Analysis of Ge data

The Ge data are used to detect the radionuclides by adding together the spectra recorded in the same area. Ge data are also used to estimate radionuclide specific activities if the net count rates calculated are significant. Depending on the activity and the detection limit of a nuclide, a data set re-gridding is performed to increase statistics. Regridding consists in summing the Germanium measurements relative to the same "elementary measurement mesh" that represents the ground emission surface area of the detected signal. It is assumed that the activity in the area during measurement is uniform. As the detector is not collimated, the solid detection angle is about $2\pi$. Under standard conditions (altitude of 40 m and speed of 20 m/s), 90% of the signal comes from an area which radius is between 150 and 200 meters. To avoid spatial dilution of the gamma-ray information, regridding is limited to the closest neighbours, by summing the data whose centres are included in the mesh of the central point. Regridding must be the result of a compromise between gain in terms of detection limits and spatial smoothing. A peak isolation method (Gutierrez, 2002) developed at CEA is then used. This method includes standard algorithms of peak search, optimised for low statistics. Height correction and efficiency coefficients determined for each nuclide from hovering manoeuvres data are then applied.

4.1.4 Altitude correction

During each survey, hovering manoeuvres are performed to adjust the attenuation parameter and the efficiency for each radionuclide. After processing each data set by the windows method and the peak isolation method, the attenuation parameter is fitted using the following expression to normalize the count rate at ground level (Grasty, 1975).

$$C_{groundlevel} = \frac{C_h}{e^{-\mu h} - \mu h E_1(\mu h)}$$

with  $C_h$:             count rate at ground clearance h
      $C_{groundlevel}$ :   count rate at ground level
      $E_1$:             exponential function of first order.

4.1.5 Calibration

An experimental device simulating the hovering conditions of a superficial activity was developed in the laboratory in order to study the changes in spectral profiles with detection altitude. A grid of point sources is used, and the atmosphere around the detector in flight is reproduced by wood particle board screens. The effect of the vertical distribution of the activity in the ground is then determined numerically using the Monte-Carlo method. This original calibration method enables all the data required for qualitative and quantitative analysis of the measurements to be obtained in the laboratory. The instrument background noise and the cosmic background radiation are determined by flights over the sea. These calibration techniques have been validated in flight over the last few years, and in particular during international exercises comparing airborne spectrometry means in August 1995 (Bourgeois et al., 1996) and in May 2002 (Sanderson et al., 2003).

$^{40}$K and the $^{238}$U and $^{232}$Th families at secular equilibrium are in the ground in various proportions. When assessing their activity, it is assumed that their vertical distribution in the first 50 centimetres from the surface is uniform. It is also assumed that the activity in the emission area during a measurement is uniform. As the detector is not collimated, the solid angle of detection is close to $2\pi$. However, it is possible to estimate the ground area from which a defined proportion of the signal is emitted. For the three major peaks of $^{40}$K, $^{214}$Bi and $^{208}$Tl, 90% of the signal comes from a disc with a radius of between 160 and 200 metres (Fig. 12). During a 2-second acquisition, the helicopter travels approximately 40 metres.

The photon detection area is in fact an ellipse, whose major axis is approximately 40 metres longer than its minor axis.

When interpreting the maps, it is important to consider this notion of area of emission, which represents the calibration unit cell of the map. The activity expressed at any place on the map corresponds to the activity from a uniform active area whose surface area is at least equal to the unit cell. As the natural activity is assumed to be uniform in the ground, it is expressed in becquerels per kilogram of soil. For calibration, the photon transport properties of the soil are represented by those of a standard soil defined by Beck et al. (1972).

Anthropic radionuclides are usually located in the upper few centimetres of the ground, with variations in vertical distribution according to the sites. The measured activities are expressed per unit area (Bq/m²) with an assumption on the depth distribution. In the same way as for the natural radionuclides, the activity in the area hovered during a measurement is assumed to be uniform. For $^{137}$Cs at 662 keV, 90% of the signal comes from an ellipse with a minor axis of approximately 120 metres (Fig. 12).
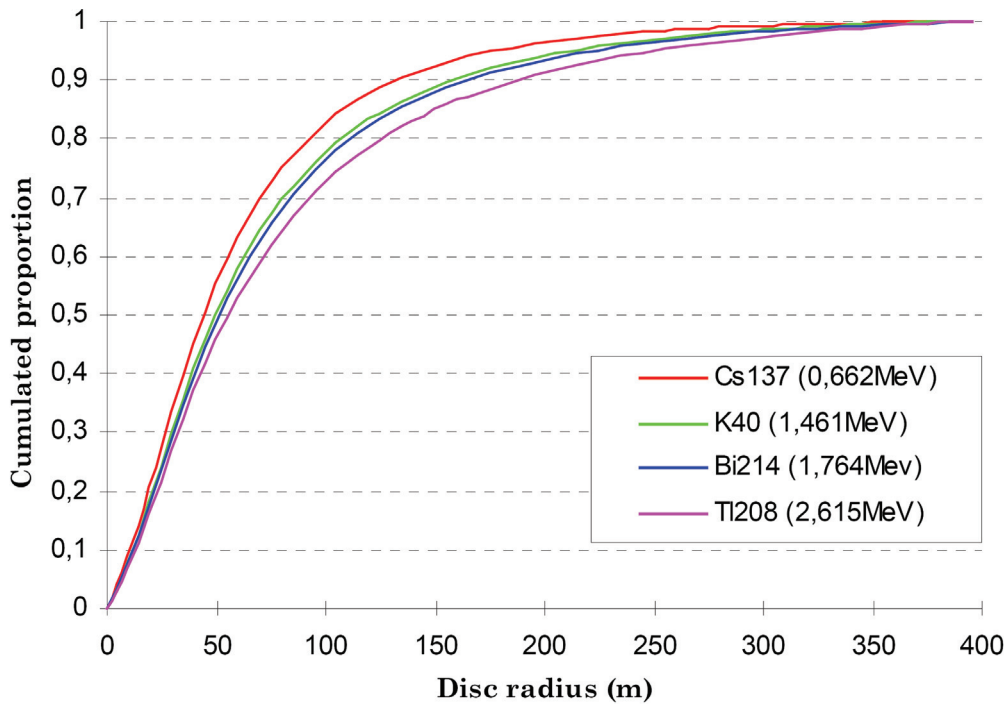
**Figure 12: Proportion of gamma signal emitted by a circular active area at a ground clearance of 40 metres, normalised with respect to an infinite area.**

4.1.6 Quality check

A detailed calibration of a detector is done before the first use. All along it's life, checks of the efficiency are then performed before and after each survey. Figure 13 shows the monitoring of a 16 litres crystals pack. The aim of these tests is to detect any change in the detector response. A measurement is performed in the same experimental conditions and the efficiency calculated must stay between two reference values.

Spectral analysis methods considering counts in specific energy windows of NaI spectra require very precise energy stabilization of the spectrometer throughout the flight. The summation of Ge spectra to increase statistic requires also a very accurate energy stability. The energy stabilization is checked all along each flight in order to detect abnormal variations which would disturb spectral analysis. The peak isolation algorithm is used to detect and calculate the central channel of the absorption peaks for each spectrum. Figures 14 and 15 show the changes in the position of the main absorption peaks of caesium, potassium, uranium and thorium during a flight, for NaI and Ge detectors respectively. In this example, no significant drift in the automatic energy stabilization is observed. The central energy of the peak is determined with a standard deviation between 8 keV and 32 keV for NaI data, depending of the counting statistic. For Ge spectra, the standard deviation is less than 2 keV, in agreement with the better resolution of the detector.
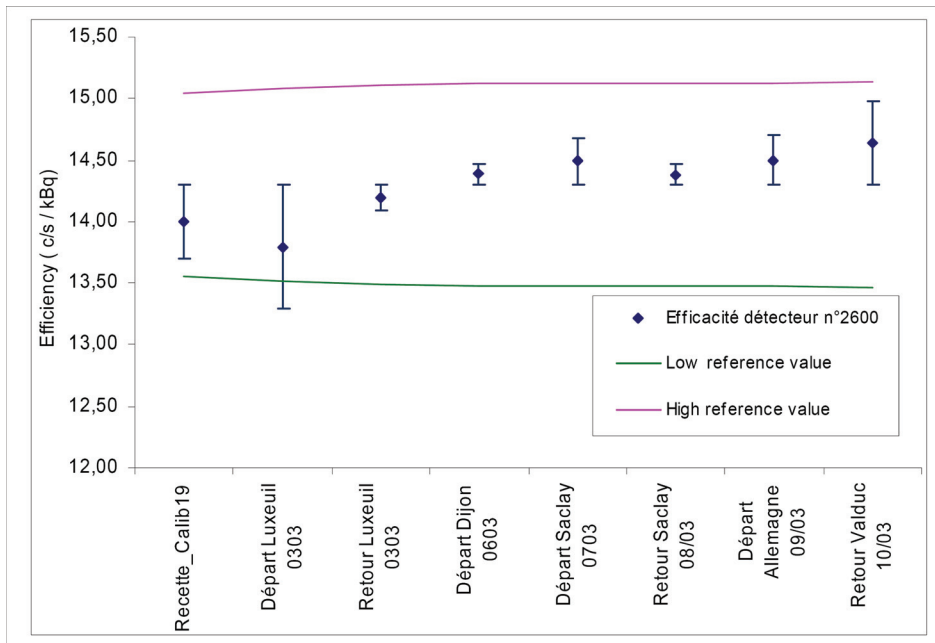
**Figure 13: Efficiency controls of a NaI crystals pack. This chart shows the response to a $^{137}$Cs point source in the standard configuration.**
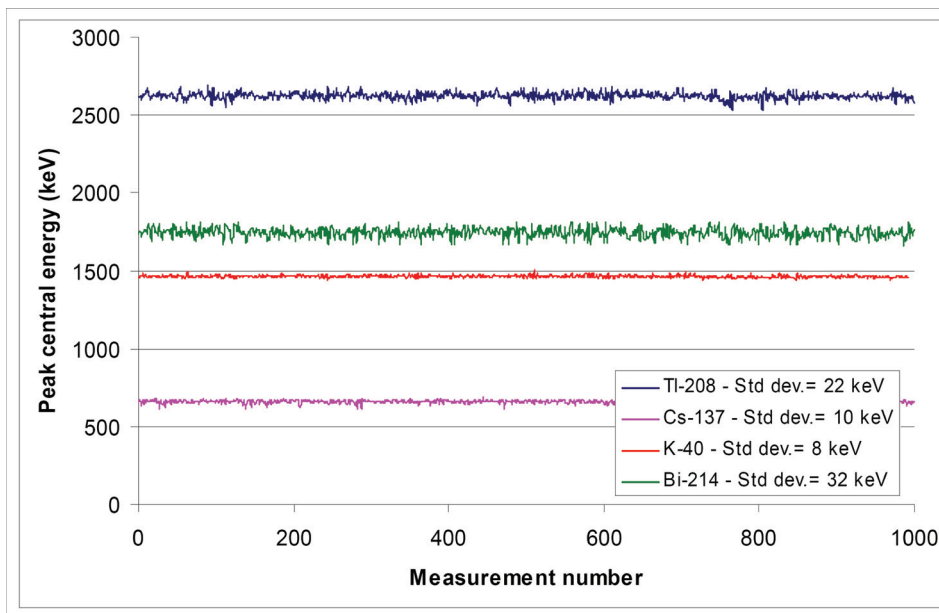


**Figure 14: Changes in the central channel of the main absorption peaks isolated from NaI spectra. The sample time is 2 seconds.**
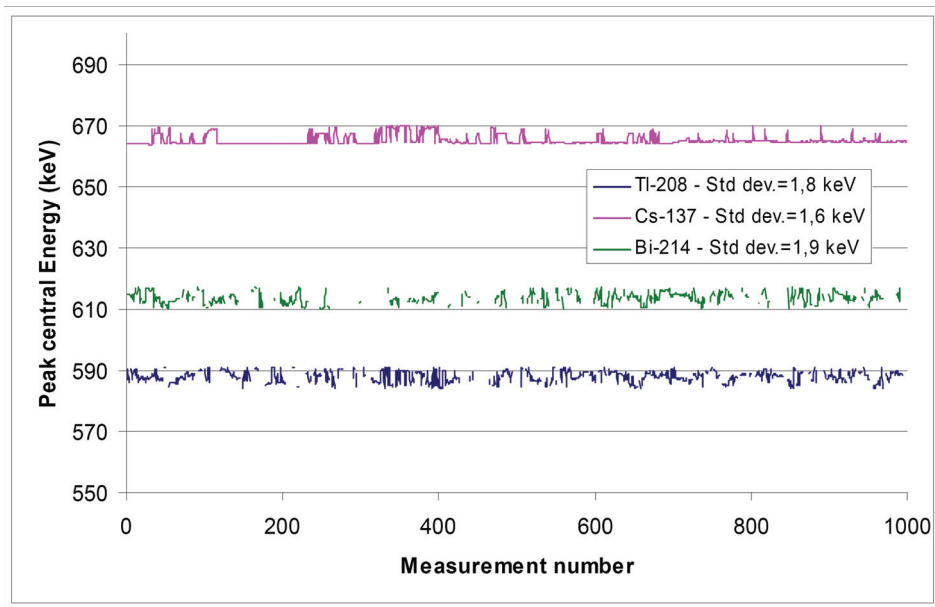
**Figure 15: Changes in the central channel of the main absorption peaks isolated from Ge spectra. The sample time is 60 seconds.**

The amplification gains of each input channel of the spectrometer are monitored individually throughout the flight in order to detect any spectral changes. Faulty stabilization of one of the crystals would generate a distortion of the spectral profile, which would result in a widening of the full width at half-maximum of the peaks. Figure 16 illustrates the stability of NaI detectors. The full width at half maximum of the absorption peaks at 662 keV ($^{137}$Cs) and 2615 keV ($^{208}$Tl) are presented. The main changes in resolution are mainly generated by the statistical fluctuations of the spectral shape. There are also weak oscillations in the mean resolution. These oscillations, with a period of about 500 measurements (1000 seconds), are generated by variation in amplification gains around the mean value. However these variations are weaker than statistical ones.

Figure 17 illustrates the stability of Ge detectors. FWHM of caesium peak is between 3 and 4 keV most of the time, but it can sometimes increase up to 7 keV. This comes from the summation of Ge spectra which can be recorded with some minutes or hours of time difference. The central channel of the peaks can be slightly different for one spectra to an other and generate this widening when peaks are added. In this example, the widening of caesium spectra is significant and should be taken into account for data processing. These data quality checking of raw data is of major importance to guarantee the performance of data processing methods.
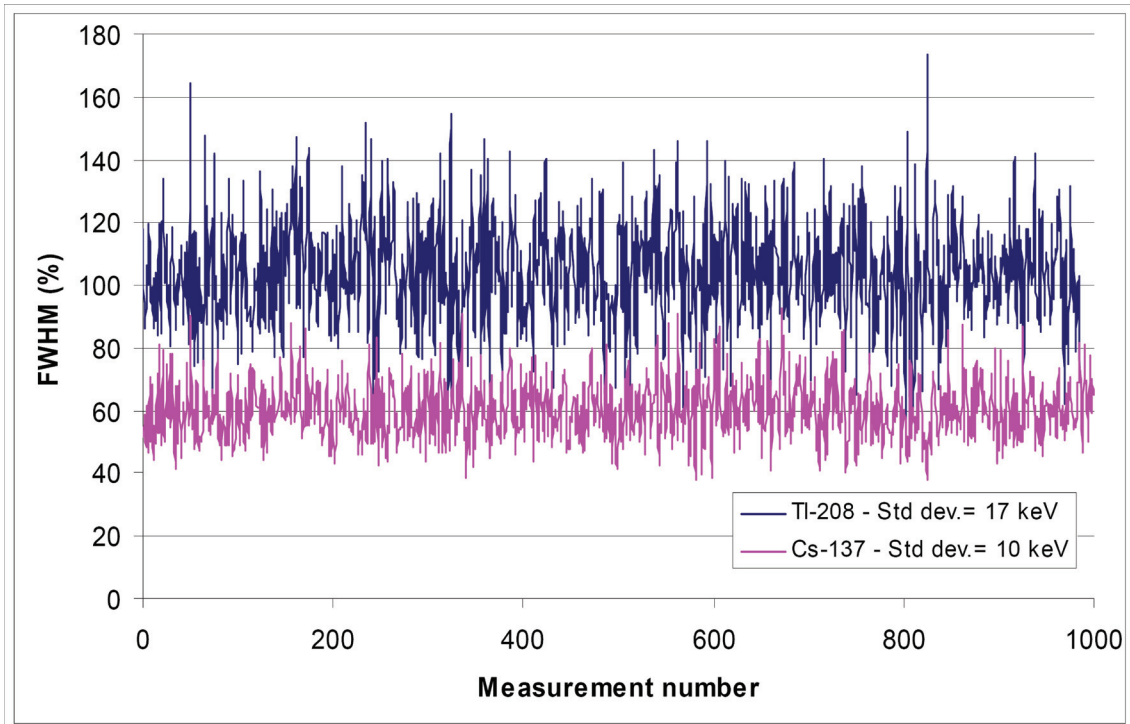
**Figure 16: Variation in full width at half maximum of the $^{137}$Cs peak (662 keV) and $^{208}$Tl peak (2615 keV) of NaI spectra.**
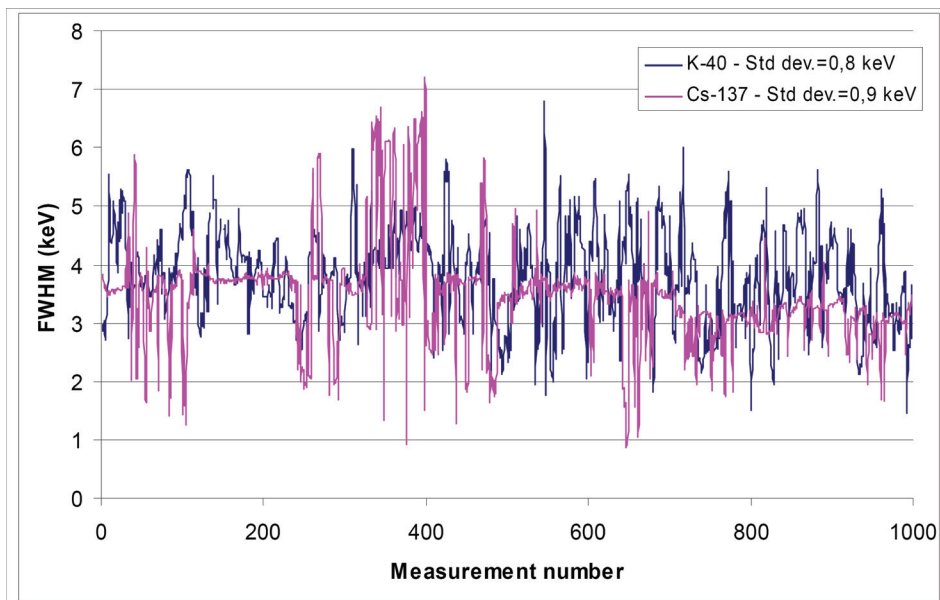


**Figure 17: Variation in full width at half maximum of the $^{137}$Cs peak (662 keV) and $^{40}$K peak (1460 keV) of HPGe spectra.**

## 4.1.7 Nuclide identification

The examination of the average spectrum over the area surveyed can provide a preliminary identification of the radionuclides. An example of average airborne gamma ray spectrometry (AGRS) spectra is presented in Figure 18. Only the main radionuclides can be identified from NaI detector because of its low resolution. The Ge provides a precise identification of radionuclides with a contribution in a significant proportion of the spectra. Traces of radionuclides distributed over the area can easily be detected. The Ge spectral shape averaged over several thousands of spectra demonstrates the good energy stability of the system.
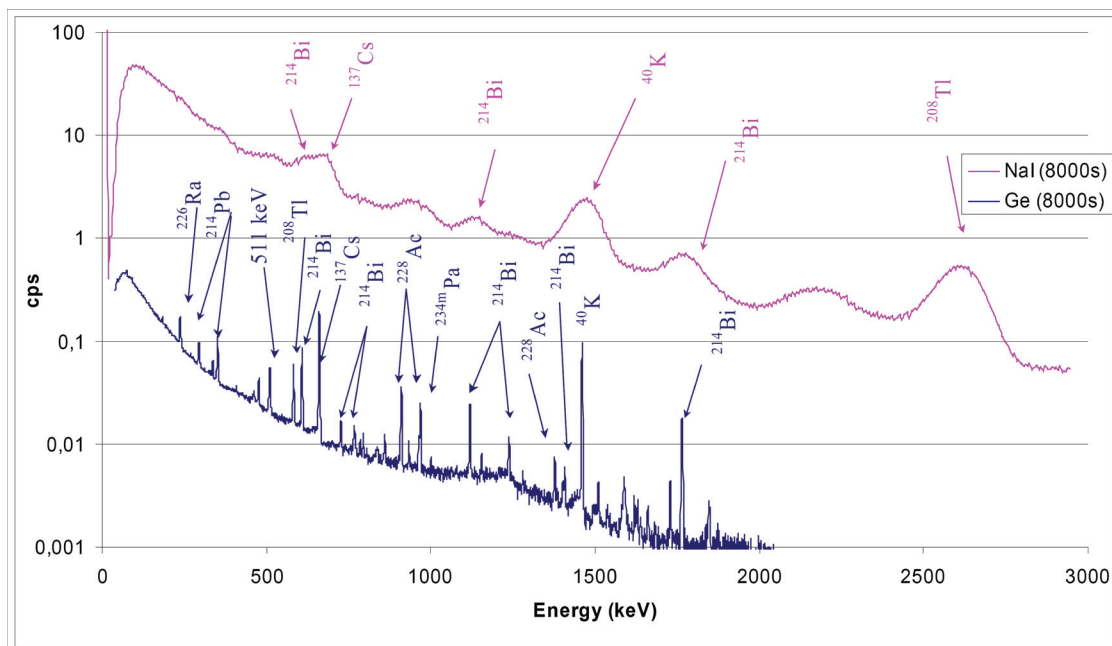


**Figure 18: AGRS spectra recorded with a 16 litres NaI detector and two 70% Ge detectors. 4000 gamma spectra of 2 seconds are considered in these average spectra.**

## 4.1.8 Detection limits

The detection limit associated with any radiation measuring instrument is an essential parameter, since it is used to select the appropriate measurement means for the activities to be measured. Other criteria, such as the area covered per hour or measurement costs, then influence the choice. Knowledge of the detection limits in airborne gamma spectrometry is particularly important because many parameters are involved in their calculation: energy, sample time, ground clearance, line spacing, radiological background of the site, etc. A detection limit is associated with a set of experimental parameters. The knowledge of the influence of each parameter enables the appropriate flight conditions to be defined to obtain the desired detection limits.

Calculation of the activity corresponding to the minimum detectable count rate requires an assumption about the distribution of the radionuclides in the ground.

The activity detected over the elementary emission area is considered as being locally uniform with respect to area or to volume in the ground.

Table 2 presents the typical detection limits for radionuclides of major interest in AGRS. These results are obtained with a sample time of 2 s. A range of activities is given for each radionuclide because the detection limit is strongly depending of activities of other radionuclides. Activity levels of $^{40}$K, $^{238}$U, $^{232}$Th and $^{137}$Cs in France are also mentioned to compare to the detection limits. Most of detection limits obtained with a sample time for 2 s are lower than current activities, but data can be added one to each other to reduce the detection limit if needed. The detection of trace amounts of radioactivity requires accurate knowledge of the detection limits. Consequently, these limits must be calculated for each area surveyed. Depending on the radiological background of the site, the choice of flight parameters (ground clearance and sample time) is determined by the detection limit that must be obtained.

**Table 2: Detection limits with a 16 litres NaI detector (detection probability at 1$\sigma$; acquisition time = 2 s; altitude = 40 m)**

| Radionuclide | Unit | Typical activities in France | Detection limit |
|---|---|---|---|
| $^{241}$Am | kBq / m$^2$ | - | 15 - 40 |
| $^{131}$I | kBq / m$^2$ | - | 2 - 5 |
| $^{137}$Cs | kBq / m$^2$ | 1 - 20 | 1 - 4 |
| $^{60}$Co | kBq / m$^2$ | - | 0.5 - 3 |
| $^{40}$K | Bq / kg | 100 - 700 | 30 - 80 |
| $^{238}$U | Bq / kg | 10 - 50 | 15 - 40 |
| $^{232}$Th | Bq / kg | 5 - 50 | 2 - 10 |

The ground clearance and the energy of gamma photons are the main parameters which influence the detection limit. Figure 19 points out the importance of ground clearance in the detection limit, particularly for low-energy radionuclides. The mapping of activities close to the detection limit requires high precision in the ground clearance monitoring in order to have constant performances over the study zone. The amplitude of the radiological background and the flight altitude are the two major parameters affecting the detection limit, but the acquisition time and the desired confidence level must also be taken into account.
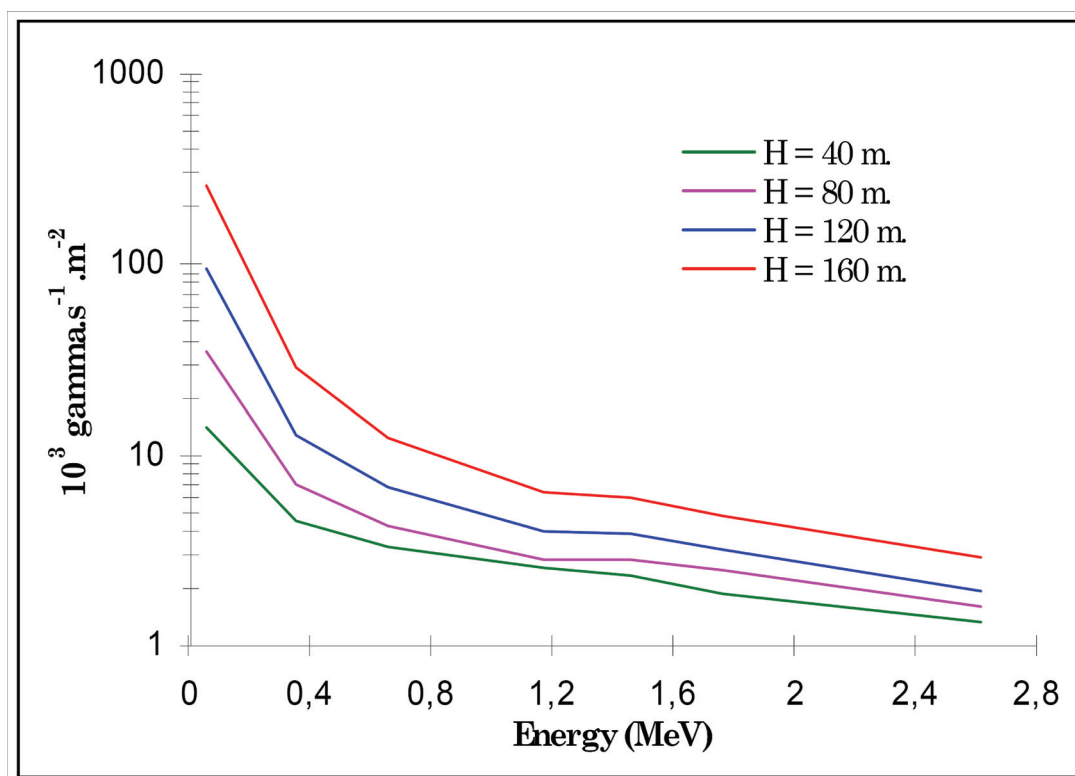
**Figure 19: Effect of ground clearance on detection limit of a 16 litres Nal detector. The depth distribution of activity is assumed superficial. The detection limit is expressed in photons emitted per second per squaremeter.**

The study of the detector response to a point source has enabled calibration of a model for the variation in the count rate as a function of the various parameters that govern changes in the counts, in particular the position of the helicopter with respect to the source during the measurement. The detection limit of a gamma source depends on the following parameters:
- energy of the emission lines of the source,
- intensity of the local radiological background,
- ground clearance,
- flight speed,
- sample time,
- line spacing,
- centring of the acquisition on the source,
- required confidence level.

The influence of each parameter on the detection limit has been studied (Figs. 20 - 23). Study of the various parameters enables the influence of each factor to be compared. The detection altitude and the energy of the emitted radiation (Fig. 20) are the parameters that generate the largest variations. To an even greater extent than for measurement of activities per unit area or per unit volume, the detection of point sources requires the lowest possible flight altitude, between 30 and 50 metres if possible. At these altitudes, the offset of the source from the flight line generates considerable variation (Fig. 21), whereas the speed of the helicopter is not a critical factor (Fig. 22). The results confirm

that, for source detection in a given time, it is preferable to reduce line spacing and to increase the speed in order to increase the probabilities of hovering and detecting the source. At ground clearances between 30 and 50 metres, the detection limits obtained with acquisition times from 2 to 5 seconds are very similar (Fig. 23). However, these results must be analysed with caution, as the different parameters studied are not independent. In particular, all the parameters that determine the position of the helicopter are strongly correlated. The flight parameters are therefore adapted to the required detection limit with the following order of decreasing influence: altitude, line spacing, speed, acquisition time. The position of the helicopter in comparison with the point source is never known precisely. Consequently the estimated activity is always expressed in the form of a range of activities.
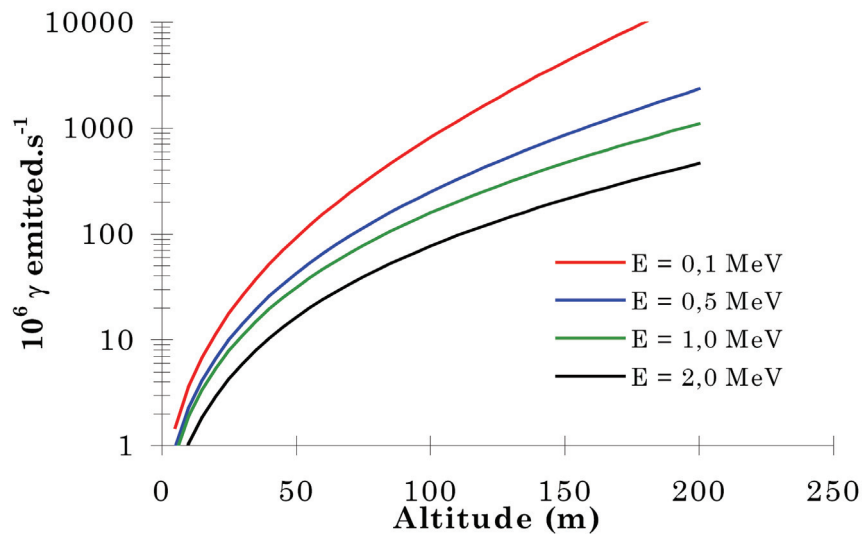


**Figure 20: Influence of emission line energy; Detection probability = 90 %; Source offset = 0 m; Speed = 20 m/s; Acquisition time = 2 s.**
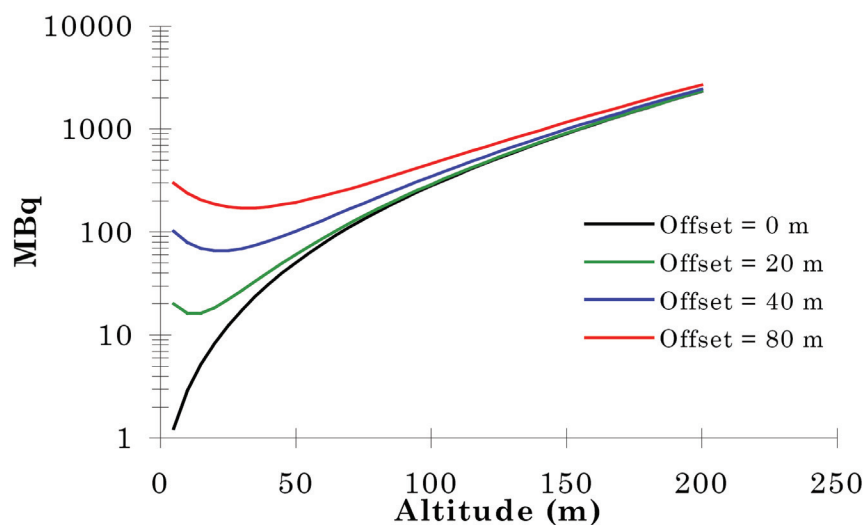


**Figure 21: Influence of source offset; $^{137}$Cs source; Detection probability = 90 %; Acquisition time = 2 s; Speed = 20 m/s.**
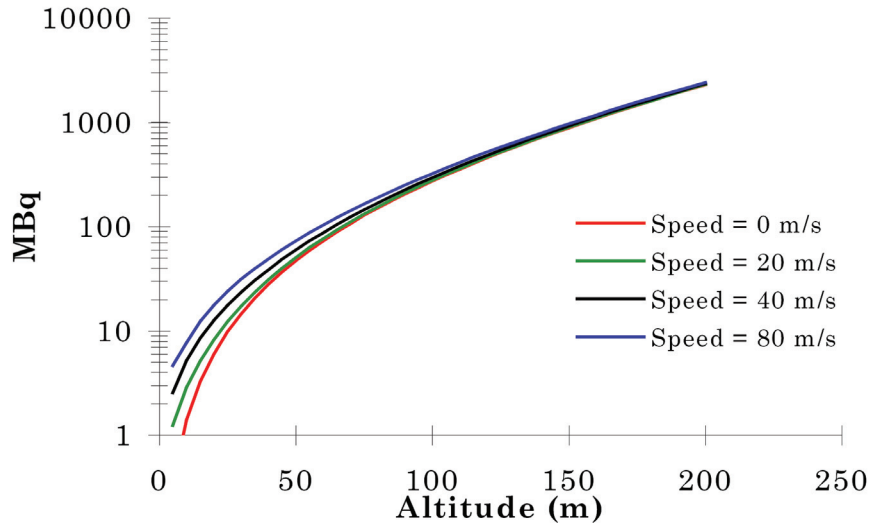
**Figure 22: Influence of flight speed; <sup>137</sup>Cs source; Detection probability = 90 %; Source offset = 0 m; Acquisition time = 2 s.**
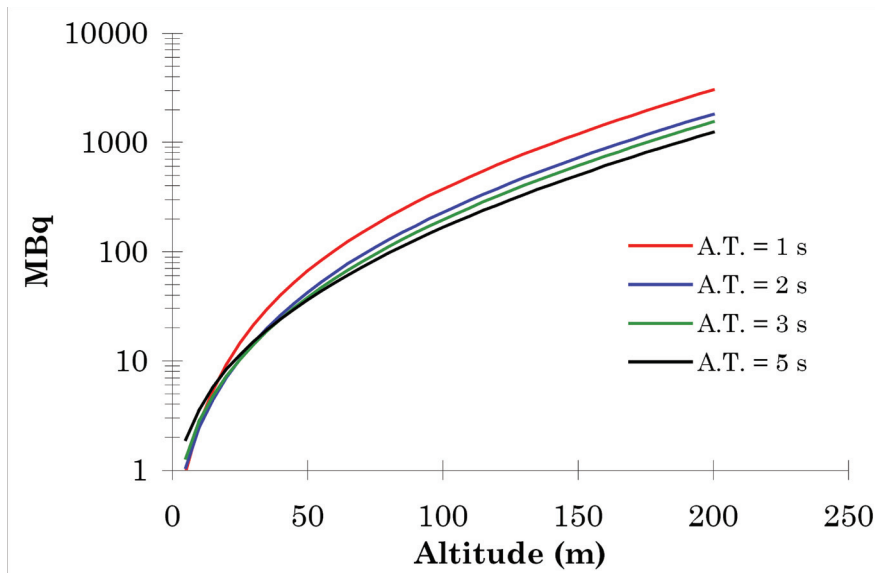


**Figure 23: Influence of acquisition time; <sup>137</sup>Cs source; Detection probability = 90%; Source offset = 0 m; Speed = 20 m/s; Acquisition centred.**

### 4.2 Germany

The airborne spectrometers are calibrated similarly to the procedure used for the calibration of in situ-gamma-spectrometers which is described in more detail in Beck et al. 1972, DIN 25462 and IAEA report 323. The detector response and the angular dependency as a function of energy are determined with the help of point sources. The attenuation of the gamma-rays due to the helicopter components is taken into account. The unscattered flux of photons depending on the distribution of radionuclides in the soil at the position of the detector for the given altitude is calculated. The calibration is additionally checked by measurements over areas with a known content of natural and

artificial radionuclides.

To calculate the specific activities of $^{137}$Cs, $^{40}$K, $^{238}$U ($^{214}$Bi) and $^{232}$Th ($^{208}$Tl) the following equation is used:

$$A = \frac{N_f}{P_\gamma} \cdot c_f; \qquad c_f = \left(\frac{1}{R_0}\right)\left(\frac{1}{R_G}\right)\left(\frac{1}{F_G}\right)$$

with: A:    Specific activity [Bq/kg] or [Bq/m$^2$]
   N$_f$:    Full-energy peak count rate
   P$_\gamma$:    Intensity of the gamma line of interest
   c$_f$:    Calibration factor [kBq s/kg] or [Bq s/cm$^2$]
   R$_0$:    Detector response [m$^2$/(kBq s)]
   R$_G$:    Angular correction factor
   F$_G$:    Geometrical factor [kg/m$^2$]

After landing, a software written by the Federal Office for Radiation Protection calculates the ambient dose rate, the specific activities of the natural radionuclides ($^{40}$K, $^{214}$Bi, $^{232}$Th) and the contamination due to artificial radionuclides (e.g. $^{137}$Cs) which are determined from the NaI(Tl) and HPGe spectra at each point of the flight path. Within a time period of 10 minutes the radiological situation along the trajectory is presented on the screen. Additional information, for example the method of data evaluation (stripping, altitude correction, statistical values) are given and provide an overview of the range of the count rates or specific activities from the considered radionuclide. The data are further integrated onto digital maps, which are available at different scales. Thus regions of low or elevated natural and artificial radionuclides can easily be located.

4.2.1 Evaluation of the NaI(Tl)- spectra

For the evaluation of the specific activities of $^{137}$Cs, $^{40}$K, $^{238}$U and $^{232}$Th we used the so-called "windows method". Here the total count rates within the selected energy windows (Table 3) were determined. For the background correction separate flights over lakes in high altitudes were performed to calculate the contributions due to the activity of the system itself, the helicopter components, the crew, and the cosmic radiation to each energy window. The factors for the background correction of each radionuclide are listed in Table 3.

Because of scattering processes in the air, in the ground and in the detector itself the contribution of scattered photons originating from radionuclides with higher energies are also measured in lower energy windows. To obtain the net count rate of each energy window the amount of the scattered photons has to be removed by stripping all the NaI(Tl)-spectra. The stripping coefficient matrix was determined by measurements on a set of calibration pads with a diameter of 70 cm doped with potassium, uranium and thorium nuclides and is documented in Table 4.

**Table 3: Parameters for the evaluation of the NaI(Tl)-spectra**

| Nuclide | Energy window [keV] | | P$\gamma$ | Background [cps] | Calibration factor ($c_f$) | $c_f$ Unit |
|---|---|---|---|---|---|---|
| $^{232}$Th ($^{208}$Tl) | 2415 | 2815 | 0.359 (0.991) | 1.6 | 2.86 | Bq kg$^{-1}$ IPS$^{-1}$ |
| $^{214}$Bi | 1655 | 1885 | 0.230 | 3.1 | 3.86 | Bq kg$^{-1}$ IPS$^{-1}$ |
| $^{40}$K | 1360 | 1560 | 0.107 | 4.3 | 3.63 | Bq kg$^{-1}$ IPS$^{-1}$ |
| $^{137}$Cs | 600 | 720 | 0.860 | 8.8 | 500 | Bq m$^{-2}$ IPS$^{-1}$ |

$^{137}$Cs: Surface; $c_f$ at 300 ft

**Table 4: Stripping coefficient matrix**

| Source / Destination | $^{137}$Cs | $^{40}$K | $^{214}$Bi | $^{208}$Tl |
|---|---|---|---|---|
| $^{137}$Cs | x | 0.57 | 2.65 | 1.68 |
| $^{40}$K | 0 | x | 0.99 | 0.57 |
| $^{214}$Bi | 0 | 0 | x | 0.33 |
| $^{208}$Tl | 0 | 0 | 0.09 | x |

4.2.2 Evaluation of the HPGe-spectra

The gamma lines from the high-purity germanium (HPGe)-spectra used for the calculation of the specific activities of $^{238}$U, $^{208}$Tl, $^{40}$K and $^{137}$Cs are listed in Table 5 together with factors employed in the calculation. A typical spectrum is plotted in Figure 24. For the evaluation of the HPGe-spectra a program is used, which is especially adapted to low counting statistics. It identifies the total absorption peaks of the individual radionuclides and calculates their net count rate. In Table 5 the energies and the calibration factors for the radionuclides are listed for one of the HPGe-detectors used by the German team.
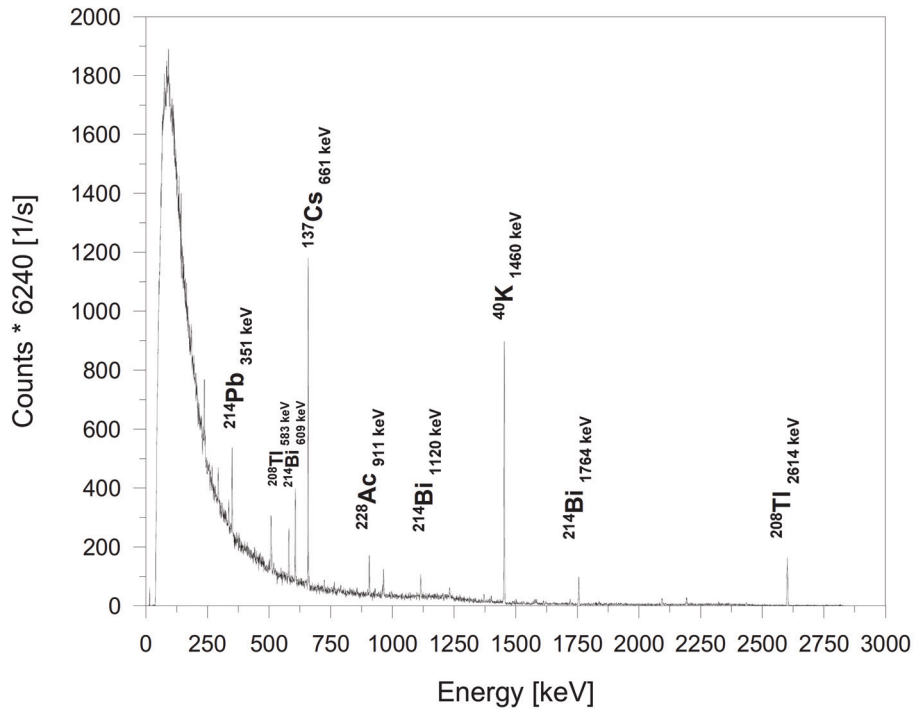
**Figure 24: Typical HPGe-sum-spectrum of a flight path.**

**Table 5: Parameters for the evaluation of the HPGe-spectra**

| Nuclide | Energy [keV] | $P_\gamma$ | Calibration factor $c_f$ | $c_f$ Unit |
|---------|--------------|------------|--------------------------|------------|
| $^{232}$Th ($^{208}$Tl) | 2615 | 0.359 (0.991) | 53.4 | Bq kg$^{-1}$ IPS$^{-1}$ |
| $^{214}$Bi | 1764 | 0.230 | 54.9 | Bq kg$^{-1}$ IPS$^{-1}$ |
| $^{40}$K | 1461 | 0.107 | 53.9 | Bq kg$^{-1}$ IPS$^{-1}$ |
| $^{137}$Cs | 662 | 0.860 | 660 | Bq m$^{-2}$ IPS$^{-1}$ |

$^{137}$Cs: Surface; $c_f$ at 300 ft

## 4.3 Switzerland

The impulses in eight photon energy windows of each spectrum are summed for further evaluation (Table 6). The right hand column of Table 6 notes the energy of the relevant photon emission. The „total"-energy window sums counts for photon energies between 400 keV and 3000 keV.

Three energy windows are associated with natural radionuclides. The „potassium" window measures photon emissions of $^{40}$K at 1461 keV. The determination of the activities of uranium and thorium utilises high energy emissions of the decay products $^{214}$Bi and $^{208}$TI to minimize absorption losses in the air between ground and detector.

Four energy windows are employed for a determination of artificial radioactivity. Those at 662 keV and 1250 keV measure the emissions of $^{137}$Cs and $^{60}$Co, respectively. The remaining two MMGC (Man Made Gross Count) energy windows measure in the photon energy interval 400 keV to 1400 keV (MMGC1) radiation from artificial and natural radionuclides and in the photon energy interval 1400 keV to 3000 keV (MMGC2) mainly natural radionuclides. The ratio of the count rates in these energy windows can be used for the search of radioactive sources.

Additional to the acquired spectra, a special channel is dedicated for the measurement of photon energies between 3000 keV and 6000 keV. This channel is used to determine the fraction of the mesured counts in the spectra, which are correlated to cosmic radiation. Simplifying, this channel (measured separately from the spectrum) is called cosmic window.

**Table 6: Energy windows for data evaluation**

| Window | Lower energy limit [keV] | Upper energy limit [keV] | Peak energy [keV] |
|---|---|---|---|
| Total | 400 | 3000 | - |
| Potassium ($^{40}$K) | 1369 | 1558 | 1461 |
| Uranium ($^{214}$Bi) | 1664 | 1853 | 1765 |
| Thorium ($^{208}$TI) | 2407 | 2797 | 2615 |
| Caesium ($^{137}$Cs) | 600 | 720 | 662 |
| Cobalt ($^{60}$Co) | 1100 | 1400 | 1173, 1332 |
| MMGC1 | 400 | 1400 | - |
| MMGC2 | 1400 | 3000 | - |

The photons registered in the detector origin from several different sources. Goal of the measurement is the determination of the part of the signal, which is correlated to radionuclides in the soil. The signal has to be reduced in respect to other sources of photon radiation, which therefore have to be identified and quantified.

Additionally, the measuring signal is dependent on several influencing parameters, which may vary during a measuring flight. For optimum quality of the derived results, the influence of these parameters has to be corrected. The steps for data processing are described in the following sections in detail.

Corrections are applied either in the energy windows described above or for each channel of the spectrum separately.

### 4.3.1 Dead time Correction

During the processing of an impulse, the detector and spectrometer are blocked from registering further impulses. This effect reduces the number of counted impulses at high count rates. The dead time of the spectrometer is measured directly and can be utilised for the according correction.

$$CR_{corr, t} = CR_{raw} \frac{t_{meas}}{t_{meas} - t_{dead}}$$

with:

$CR_{corr,t}$:   Deadtime corrected count rate [IPS]
$CR_{raw}$:   Measured count rate [IPS]
$t_{meas}$:   Measuring time of the spectrometer (constant 990 ms) [s]
$t_{dead}$:   Time during which the spectrometer was blocked [s]

Typical values for $t_{dead}$ are between 40 ms (central Switzerland) and 200 ms (Swiss nuclear power plant Leibstadt) in 990 ms measuring time, yielding an associated correction factor between 1.04 and 1.25.

### 4.3.2 Detector Background and cosmic radiation

The detector measures photons which originate from the detector itself and the surrounding helicopter. Both components are assumed constant for an individual detector and helicopter. To this background is added a second component generated by cosmic radiation. The primary cosmic radiation consists of 87% protons, of 12% alpha particles and of 1% heavy nuclei. Photons are generated during interaction of the primary cosmic radiation with the atmosphere. The effect of these photons on the measuring signal is dependent on elevation, air pressure and latitude. A linear relationship between the count rate produced by cosmic radiation in any channel of the spectrum and the count rate in the cosmic window was found experimentally. Thus, the count rate in the cosmic window can be used for the direct correction in other energy windows. The correction for background and cosmic radiation can be formulated as

$$CR_{corr, B} = CR_{corr, t} - (CR_B + S_c CR_c)$$

with:

$CR_{corr,B}$:  Background corrected count rate [IPS]

$CR_B$:  Background count rate of detector and helicopter [IPS]

$CR_c$:  Count rate in cosmic window [IPS]

$S_c$:  Cosmic correction factor [ ]

The two constants $CR_B$ and $S_c$ are determined with an ascent over large water bodies. Due to the absorption in water the terrestric radiation is mainly shielded yielding a direct measurement of the term $CR_B + S_c CR_c$ for each energy window. The background is independent of the flight altitude, whereas the effect of cosmic radiation increases with altitude. Thus, both effects can be separated with a linear regression of the measured count rates.

The measured count rates during an ascent over the British Channel in the year 2002 are summed in Table 7. Figure 25 shows exemplarily the measured count rates and the respective linear regression for the caesium energy window. The constants $CR_B$ and $S_c$ are listed together with their uncertainties according to the Guide to the Expression of Uncertainty in Measurement (GUM, extension factor k=1) for all energy windows in Table 8.

**Table 7: Measured count rates in three different altitudes**

| Altitude [m] | 1888 | 2864 | 3750 |
|---|---|---|---|
| Energy window | Count rate [IPS] | | |
| Cosmic | 105.0 | 162.4 | 252.0 |
| Total | 283.9 | 359.2 | 506.9 |
| Potassium | 22.9 | 27.6 | 35.8 |
| Uranium | 9.9 | 13.3 | 19.3 |
| Thorium | 9.6 | 12.2 | 19.5 |
| Caesium | 42.2 | 50.5 | 65.4 |
| Cobalt | 28.4 | 36.7 | 50.6 |
| MMGC1 | 217.0 | 274.6 | 383.6 |
| MMGC2 | 67.7 | 85.8 | 125.0 |

y = 0.159x + 25.2
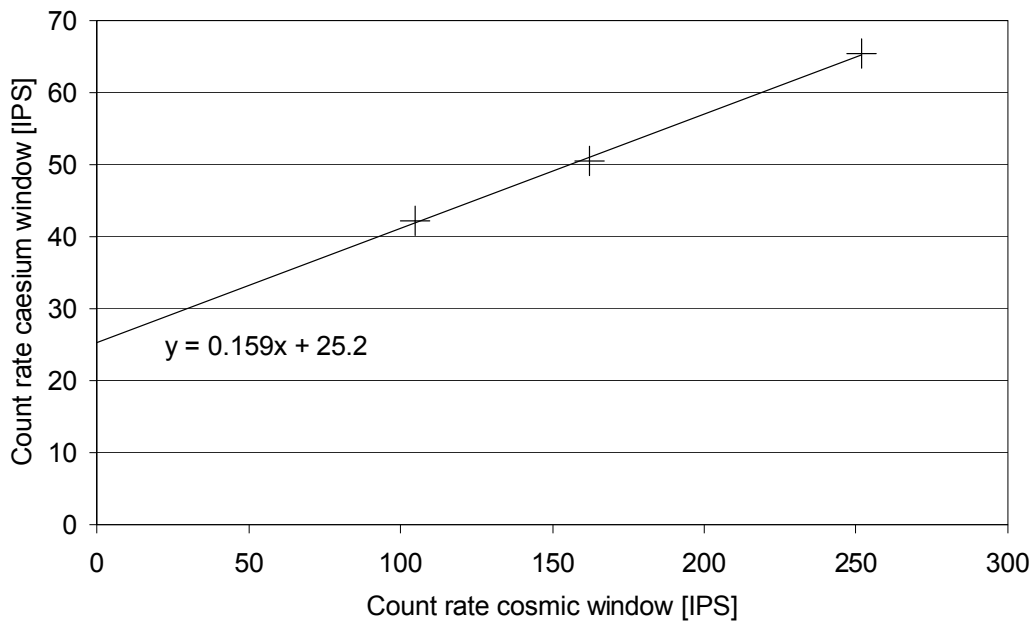
**Figure 25: Count rate in the caesium energy window for three different altitudes and according linear regression.**

**Table 8: Correction factor $S_c$ and background count rate $CR_B$ determined by linear regression together with their uncertainties**

| Energy window | $S_c$ | $U(S_c)$ | $CR_B$ [IPS] | $U(CR_B)$ [IPS] |
|---|---|---|---|---|
| Total | 1.528 | 0.090 | 118.7 | 16.6 |
| Potassium | 0.088 | 0.002 | 13.5 | 0.4 |
| Uranium | 0.064 | 0.002 | 3.1 | 0.3 |
| Thorium | 0.068 | 0.010 | 2.0 | 1.8 |
| Caesium | 0.159 | 0.005 | 25.2 | 1.0 |
| Cobalt | 0.151 | 0.003 | 12.4 | 0.5 |
| MMGC1 | 1.141 | 0.058 | 94.3 | 10.5 |
| MMGC2 | 0.394 | 0.034 | 24.6 | 6.2 |

4.3.3 Energy resolution and Compton scattering

Photons emitted from the soil are scattered due to the Compton effect in the soil, in buildings, in vegetation, in the air between surface and helicopter and in the detector. The associated energy loss may lead to a registration of the photon in a lower photon energy window.

The poor energy resolution of a NaI-detector compared to modern solid-state de-

tectors causes the possibility that photons with energies near the energy limits of a photon energy window are registered in the adjacent energy window.

The influence of both effects on the signal is determined experimentally. The count rate $CR_{korr,B}(i)$ in the energy window i is composed from contributions of all photon sources j, weighted with a stripping coefficient $f_{i,j}$.

$$CR_{corr,B}(i) = \sum_{j=1}^{8} f_{i,j} CR_{corr,S}(j)$$

with:

$f_{i,j}$:  Stripping coefficient of component j into energy window i [ ]

For the derivation of the contributions of the different photon sources $CR_{corr,S}(j)$ from measured count rates $CR_{corr,B}(i)$, the system of linear equations has to be solved. The equation above can be formulated as

$$\overline{CR}_{corr,B} = \overline{\overline{f}}\, \overline{CR}_{corr,S}$$

with:

$\overline{\overline{f}}$:  Matrix of stripping coefficients [ ]

$\overline{CR}_{corr,B}$:  Vector of count rates in the eight energy windows [IPS]

$\overline{CR}_{corr,S}$:  Vector of contributions of eight photon sources [IPS]

Matrix f is then inverted with the help of the LU-algorithm (reduction to two triangular matrices, L(ower) and U(pper), which yields

$$\overline{CR}_{corr,S} = \overline{\overline{f}}^{-1} \overline{CR}_{corr,B}$$

with:

$\overline{\overline{f}}^{-1}$:  Inverse Matrix of stripping coefficients [ ]

The stripping coefficients $f_{i,j}$ can be determined with measurements of radioactive point sources near to the detector, which are then corrected for altitude and scattering in soil for the natural radionuclides.

$$f_{i,j} = g_{i,j} + f_{i,j,point}$$

with:

$g_{i,j}$:  Correction for altitude and scattering in soil  [ ]
$f_{i,j,point}$:  Stripping coefficients derived from measurements with point sources [ ]

These steps are demonstrated with a numerical example in the following paragraphs. Formally, the stripping factors are calculated for all energy windows and all radiation sources. The stripping correction is obsolete for the group energy windows Total, MMGC1 and MMGC2. Measurements showed that $^{137}$Cs does not render counts in energy windows with higher photon energies. With these restrictions, the determination of stripping coefficients is reduced to the radioactive sources $^{60}$Co, $^{40}$K, uranium and thorium, the latter two in natural isotope composition.Table 9 summarises exemplarily results of measurements of these four radioactive sources together with a background measurement performed in the year 2000. After substracting the background count rates, the net count rate is normalized to the component energy window (Table 10). The matrix is completed with the given values in the group windows (Table 11). After applying the corrections for altitude and soil scattering $g_{i,j}$, the system of equations can be solved by formation of the inverse matrix.

**Table 9: Measured count rates with four different point sources in 1 m distance to the detector**

| Energy window | Component count rate [IPS] | | | | |
|---|---|---|---|---|---|
| | Background | $^{40}$K | Uranium | Thorium | $^{60}$Co |
| Potassium | 160.2 | 210.6 | 255.7 | 233.3 | 210.4 |
| Uranium | 40.4 | 39.4 | 173.1 | 83.0 | 42.6 |
| Thorium | 39.6 | 40.0 | 47.1 | 247.7 | 42.8 |
| Caesium | 200.3 | 210.9 | 720.2 | 577.5 | 255.7 |
| Cobalt | 155.7 | 173.9 | 428.9 | 263.8 | 378.0 |

**Table 10: Relative fraction of count rates in the respective energy window**

| Energy window | Relative fraction of component | | | |
|---|---|---|---|---|
| | $^{40}$K | Uranium | Thorium | $^{60}$Co |
| Potassium | 1.00 | 0.72 | 0.35 | 0.23 |
| Uranium | -0.02 | 1.00 | 0.20 | 0.01 |
| Thorium | 0.01 | 0.06 | 1.00 | 0.01 |
| Caesium | 0.21 | 3.92 | 1.81 | 0.25 |
| Cobalt | 0.36 | 2.06 | 0.52 | 1.00 |

**Table 11: Extended matrix of relative count rate fractions in the respective energy window**

| Energy window | Relative fraction of component | | | | | | | |
|---|---|---|---|---|---|---|---|---|
| | Total | $^{40}$K | U | Th | $^{137}$Cs | $^{60}$Co | MMGC1 | MMGC2 |
| Total | 1.00 | 0.00 | 0.00 | 0.00 | 0.00 | 0.00 | 0.00 | 0.00 |
| Potassium | 0.00 | 1.00 | 0.72 | 0.35 | 0.00 | 0.23 | 0.00 | 0.00 |
| Uranium | 0.00 | -0.02 | 1.00 | 0.20 | 0.00 | 0.01 | 0.00 | 0.00 |
| Thorium | 0.00 | 0.01 | 0.06 | 1.00 | 0.00 | 0.01 | 0.00 | 0.00 |
| Caesium | 0.00 | 0.21 | 3.92 | 1.81 | 1.00 | 0.25 | 0.00 | 0.00 |
| Cobalt | 0.00 | 0.36 | 2.06 | 0.52 | 0.00 | 1.00 | 0.00 | 0.00 |
| MMGC1 | 0.00 | 0.00 | 0.00 | 0.00 | 0.00 | 0.00 | 1.00 | 0.00 |
| MMGC2 | 0.00 | 0.00 | 0.00 | 0.00 | 0.00 | 0.00 | 0.00 | 1.00 |

4.3.4 Altitude, air pressure, air temperature and atmospheric radioactivity
Normalisation of the measured data to a fixed altitude of 100 m above ground improves the comparability of the multitude of point measurements along the flight lines. An exponential dependence between photon attenuation and altitude is assumed.

$$CR_{corr,\,h} = CR_{corr,\,S}\,\frac{e^{-\mu_{ref}h_{ref}}}{e^{-\mu h}}; \quad \mu = \mu_{ref}\,\frac{T_{ref}}{T}\,\frac{P}{P_{ref}}$$

with:
$CR_{corr,h}$: Count rate corrected to reference altitude $h_{ref}$ [IPS]
$\mu_{ref}$: Attenuation coefficient at reference conditions [m$^{-1}$]
$\mu$: Attenuation coefficient at measurement conditions [m$^{-1}$]
$h_{ref}$: Reference altitude $h_{ref}$ = 100 m
h: Altitude above ground [m]
$T_{ref}$: Reference temperature $T_{ref}$ = 273.15 K
T: Air temperature [K]
$P_{ref}$: Reference pressure $P_{ref}$ = 101325 Pa
P: Air pressure [Pa]

A more complex method, which takes into account topographic effects with the help of the Swiss digital terrain model is used only in special cases.
The attenuation coefficients for the respective radiation components are determi-

ned with ascents over flat terrain. The measured net counts for different altitudes are fitted to an exponential curve using the least squares method. The so determined attenuation coefficient is extrapolated with the measured values of air temperature and air pressure to the reference conditions.

The detector registers photon emissions from radionuclides contained in the atmosphere, mainly radon decay products attached to aerosol particles. The influence of these radionuclides can be observed during the determination of the attenuation coefficient of the uranium component. The measurement of this component including the expected temporal variation during a measuring flight with additional instrumentation is neither performed nor planned for the near future.

Ascents for the determination of the attenuation coefficients are performed during the annual aeroradiometric exercises. The attenuation coefficients for the artificial radionuclides $^{137}$Cs and $^{60}$Co are revised only in the case that the peaks are clearly identifyable in the photon spectrum. Table 12 sums the results of an ascent over the airfield of the Swiss town Locarno measured during the exercise ARM05. Figure 26 shows the decrease of the $^{137}$Cs count rate together with a approximated exponential interpretation of the measurement results. The attenuation coefficients determined from this flight and normalised to reference conditions are listed in Table 13 together with the uncertainties according to GUM (extension factor k=1).

**Table 12: Results of the ascent over the airfield of Locarno, 2005**

| Altitude [m] | Count rate of component $CR_{corr,S}$ [IPS] | | | | | | |
|---|---|---|---|---|---|---|---|
| | Total | $^{40}$K | Uranium | Thorium | $^{137}$Cs | MMGC1 | MMGC2 |
| 27.4 | 2436 | 162 | 38 | 55 | 184 | 2044 | 401 |
| 59.3 | 1952 | 122 | 30 | 44 | 118 | 1646 | 313 |
| 93.7 | 1571 | 96 | 26 | 34 | 75 | 1323 | 254 |
| 118.4 | 1358 | 79 | 25 | 30 | 45 | 1143 | 221 |
| 162.4 | 1064 | 59 | 22 | 22 | 22 | 894 | 175 |
| 247.4 | 726 | 33 | 16 | 14 | 8 | 613 | 116 |
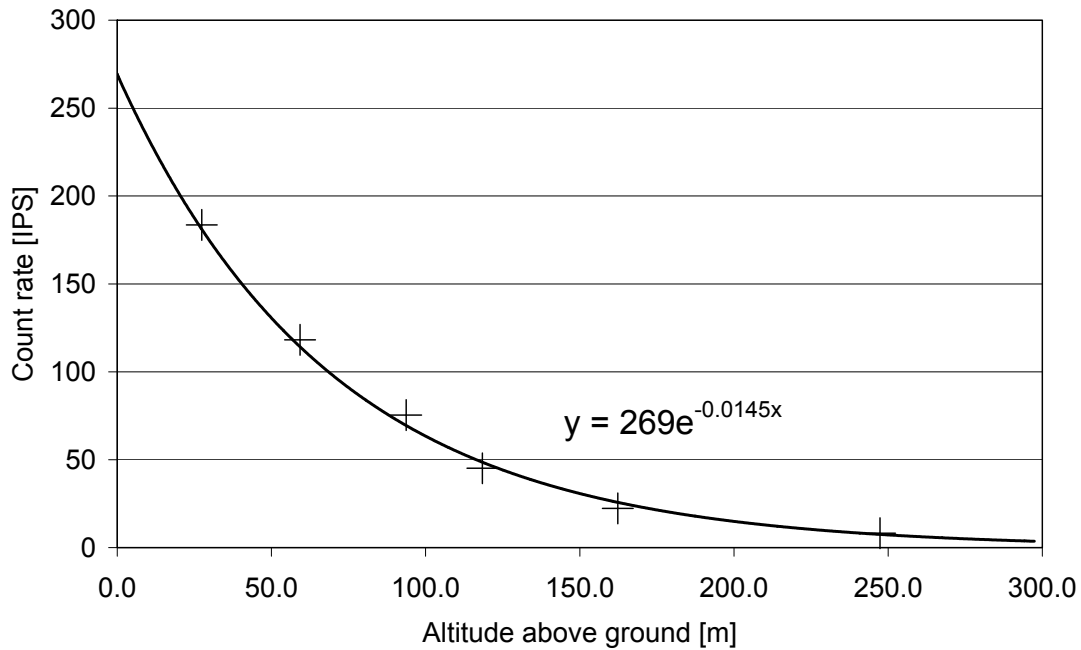
**Figure 26: Decrease of $^{137}$Cs count rate in dependence on flight altitude.**

**Table 13: Experimentally determined attenuation coefficients**

| Component | $\mu_{ref}$ [m$^{-1}$] | $U(\mu_{ref})$ [m$^{-1}$] |
|---|---|---|
| Total | 5.48E-03 | 2.53E-04 |
| $^{40}$K | 7.19E-03 | 1.66E-04 |
| Uranium | 3.53E-03 | 2.99E-04 |
| Thorium | 6.18E-03 | 2.99E-04 |
| $^{137}$Cs | 1.45E-02 | 5.83E-04 |
| $^{60}$Co | not detectable ||
| MMGC1 | 5.46E-03 | 2.55E-04 |
| MMGC2 | 5.54E-03 | 2.47E-04 |

4.3.5 Specific activity calibration

Activity concentrations of radionuclides in soil can be estimated from the norma-lised measured count rates $CR_{corr,h}$. In the case of natural radionuclides, a homo-geneous distribution in soil is assumed, whereas for artificial radionuclides the activity is assumed to be located in a thin layer of topsoil. The calibration factors (Table 14) are determined by comparing the measured count rates with results from radioanalytical measurement of soil samples and in-situ gamma-spectrome-

tric measurements.

**Table 14: Calibration factor for calculating specific activity from net count rate**

| Component | Nuclide | Calibration factor [Bq kg$^{-1}$ IPS$^{-1}$] |
|---|---|---|
| Potassium | $^{40}$K | 8.3 |
| Uranium | $^{214}$Bi | 4.0 |
| Thorium | $^{208}$Tl | 1.7 |
| Caesium | $^{137}$Cs | 2.0 |

4.3.6 Dose rate calibration

The specific activities determined in the prior paragraph can be used for a determination of terrestric dose rate H*(10) one meter above ground. As used for measurements with in-situ gammaspectrometry, the air kerma is estimated using conversion factors listed in ICRU report 53. Further multiplication with factors 1.1 Sv/Gy (uranium- and thorium-decay series) or 1.2 Sv/Gy (Caesium) renders terrestric dose rate H*(10), assuming radioactive equilibrium in the decay series (Table 15).

**Table 15: Dose rate conversion factors**

| Nuclide | Conversion factor [nSv h$^{-1}$ Bq$^{-1}$ kg] |
|---|---|
| $^{40}$K | 0.044 |
| $^{214}$Bi | 0.55 |
| $^{208}$Tl | 0.77 |
| $^{137}$Cs | 0.20 |

A second approach consist of a direct calculation of the terrestric dose rate with the spectrum dose index (SDI) method. This method utilises the energy deposition in the detector as a direct measure of dose rate H*(10). Due to the automatic gain stabilisation of the measuring system with the help of the $^{40}$K photon emission, the assignment of channel to energy interval can be considered constant. The SDI is then calculated as sum of the products of channel number and net count rate.

$$SDI = \sum_{k=0}^{255} k \, CR_{raw}(k)$$

with:

CR$_{raw}$(k):  Raw count rate in channel k [IPS]
SDI:           Spectrum dose index [IPS]

In a next step the SDI is corrected for background and cosmic radiation.

$$SDI_{Corr} = SDI - SDI_{Back} - SDI_{Cosmic}$$

The contribution of the background is calculated using a background spectrum of the aircraft and the equipment. The value used currently for SDI$_{Back}$ is 12640 IPS.

$$SDI_{Back} = \sum_{k=0}^{255} k \, CR_{Back}(k)$$

with:

CR$_{Back}$(k): Raw count rate of the background spectrum in channel k [IPS]
SDI$_{Back}$:    SDI of the background spectrum [IPS]

The contribution of the cosmic radiation is calculated using the count rate of the cosmic window and the cosmic stripping coefficients of each channel. The value of f$_{cosmic}$ currently used is 95.5.

$$SDI_{Cosmic} = CR_{Cosmic} f_{Cosmic} = CR_{Cosmic} \sum_{k=0}^{255} k \, S(k)$$

with:

CR$_{Cosmic}$:  Raw count rate in the cosmic window [IPS]
f$_{Cosmic}$:    Bulk stripping factor for the influence of cosmic radiation [ ]
S(k):          Cosmic stripping coefficient for channel k [ ]
SDI$_{Cosmic}$: SDI derived from counts in the cosmic window [IPS]

The SDI reduced for backround and cosmic radiation is corrected to reference altitude h$_{ref}$ = 100 m.

$$SDI_{Alt} = SDI_{Corr} \, e^{\mu_{air}(h - h_{ref})}$$

with:

$\mu_{air}$:    Attenuation coefficient in air [m$^{-1}$]
h:             Flight altitude [m]
h$_{ref}$:      Reference altitude [m]
SDI$_{Alt}$:    SDI at reference altitude [IPS]

A comparison to dose rate measurements at ground level yields directly the calibration factor to the dose rate H*(10).

$$DR_{Terr} = \alpha \, SDI$$

with:

$DR_{Terr}$: Terrestrial dose rate H*(10) 1 m above ground [nSv h$^{-1}$]

$\alpha$: Calibration factor $\alpha$ = 0.00096 [nSv h$^{-1}$ IPS$^{-1}$]

The total dose rate consists of two components, terrestric and cosmic dose rate. The cosmic dose rate in dependence of height above sea level can be approximated with an exponential function. The total dose rate is then obtained by adding the cosmic dose rate to the terrestric dose rate estimated with the SDI-method.

$$DR_{Cosmic} = 37 \, e^{0.38z}$$

with:

$DR_{Cosmic}$: Cosmic dose rate H*(10) at height z above sea level [nSv h$^{-1}$]

z: Height above sea level [km]

Table 16 shows a comparison of dose rates in 1 m above ground estimated with both methods in the year 2006. The slight decrease of the dose rate estimated from specific activities can be assigned to the influence of airborne radon decay products, which led to an overcompensation of Compton scattering. Nevertheless, both methods agree well inside the uncertainties according GUM (extension factor k=1).

**Table 16: Dose rate H*(10) in 1 m above ground**

| Altitude [m] | Dose rate [nSv h$^{-1}$] | |
|---|---|---|
| | Activities | SDI |
| 45 | 130 ± 6 | 120 ± 6 |
| 60 | 126 ± 6 | 120 ± 6 |
| 89 | 125 ± 7 | 118 ± 6 |
| 120 | 120 ± 8 | 116 ± 8 |
| 149 | 119 ± 9 | 118 ± 10 |
| 175 | 119 ± 10 | 117 ± 10 |
| 209 | 118 ± 11 | 121 ± 10 |

## 5 APPLICATION OF THE ERS FORMAT

The European Radiometric and Spectrometry (ERS) format described in the appendix was used during the tri-national exercise ARM07. One task of the ARM07 exercise was the composite mapping of the area around the city Basel. Therefore the participating teams agreed in quantities and units which should be delivered during the exercise (see Table 17). It was also agreed that the dose rate should be reported as ambient dose rate equivalent dH*(10)/dt in nSv/h in 1 m above ground. The dose rate should be reported with and without cosmic contribution. Each quantity should be reported together with its corresponding uncertainty.
The coordinates should be reported in the World Geodetic System WGS84 reference system or in the Swiss National Grid reference system. Raw and processed data should be delivered in separate files.

**Table 17: Quantities and units defined for the Exercise**

| Nuclide | Distribution | Relaxation mass depth [g cm$^{-2}$] | Unit |
|---|---|---|---|
| $^{40}K$ | Uniform | - | Bq kg$^{-1}$ |
| $^{238}U$ | Uniform | - | Bq kg$^{-1}$ |
| $^{232}Th$ | Uniform | - | Bq kg$^{-1}$ |
| $^{137}Cs$ | Surface | 0 | Bq m$^{-2}$ |

The algorithm for the composite mapping was integrated in the existing data processing and mapping software of the Swiss team. The identifiers of the ERS format are now also used within the software for configuration purposes. To map data from different origins it has to be brought to the same format and structure.
In the software a survey is created, which acts as a container for the data files. The data files can be either raw data files of the Swiss team or ERS data files of any team. Depending on the data format the data file is processed or parsed, the coordinates transformed to the defined projection and the data filled into a buffer file. From this buffer file the gridding routine is reading the data and creates specified data grids using the method described in Schwarz et al. (1992). Finally, the grids are displayed together with map information (Fig. 27).  The grids can be exported in ASCII format for use with third party geographic information software (GIS).
The modification of the software was tested with ERS data files which were supplied by the French team. On request of the French team, the coordinates systems employed for the exercise were extended with the Universal Transverse Mercator (UTM) projection of WGS84 coordinates.

During the exercise a few minor problems in the data format were detected when the teams delivered their data:
- different data delimiters were used;
- "<" was used as symbol for values below detection limit;
- no date and time was delivered.

In the reported quantities also a few deviations were registered:
- Activity per dry weight or activity per wet weight was reported;
- Dose rate to air (DAR identifier in ERS format) instead of ambient dose equivalent rate (dH*(10)/dt, DHSR identifier) was reported;
- No uncertainties corresponding to the values were delivered.

These problems could be solved during the exercise. The values which contained the "<" symbol were set to "no value". The values given in activity per wet weight were recalculated to activity per dry weight using a factor of 1.25. The delivered dose rate to air was converted to ambient dose rate equivalent using a factor 1.2.

```
┌──────────────┐        ┌──────────────┐
│  Raw data    │        │  ERS data    │
│  file CH     │        │  file        │
└──────────────┘        └──────────────┘
   Data processing         Data parsing, transformation of
                           coordinate system
            ┌──────────────┐
            │  Buffer file │
            └──────────────┘
                   │
            ┌──────────────┐
            │  Gridding    │
            └──────────────┘
                   │
            ┌──────────────┐
            │  Mapping     │
            └──────────────┘
```
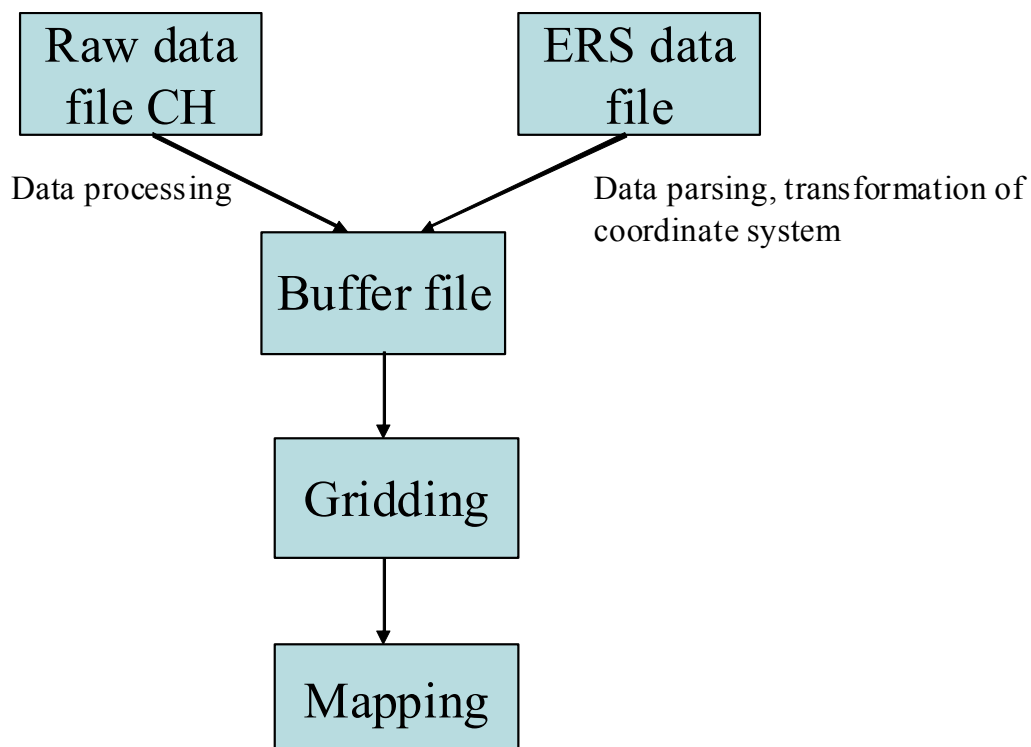
**Figure 27: Data flow within the software used for composite mapping.**

# 6 RESULTS

The exercise ARM 2007 consisted of measurements over the Swiss nuclear power plants Mühleberg (KKM) and Gösgen (KKG), composite mapping in the region of Basel and a search for radioactive sources at the freight depot in Muttenz. Due to inclement weather, some flights had to be cancelled and some data are not available for all three teams. A summary of all results is listed in Table 18, the detailed analysis can be found in chapters 6.1 to 6.6.

**Table 18: Average measured values for different areas**

| | | Measurement Team | | |
|---|---|---|---|---|
| **Quantity** | **Aera** | **F** | **D** | **CH** |
| Flight Altitude [m] | KKM | - | 97 ± 22 | 107 ± 16 |
| | KKG | 60 ± 20 | 98 ± 21 | 109 ± 13 |
| | Basel | 47 ± 11 | 94 ± 17 | 107 ± 17 |
| Total Dose Rate H*(10) [nSv/h] in 1 m above ground | KKM | - | 110 ± 19 | 117 ± 19 |
| | KKG | 93 ± 10 | 107 ± 15 | 100 ± 10 |
| | Basel | 92 ± 14 | 94 ± 17 | 95 ± 14 |
| Terrestric Dose Rate H*(10) [nSv/h] in 1 m above ground | KKM | - | - | 71 ± 20 |
| | KKG | 53 ± 10 | - | 57 ± 10 |
| | Basel | 52 ± 14 | 57 ± 16 | 53 ± 13 |
| $^{40}$K Activity concentration [Bq/kg] | KKM | - | 363 ± 121 | 491 ± 139 |
| | KKG | 381 ± 122 | 251 ± 77 | 328 ± 107 |
| | Basel | 403 ± 119 | 397 ± 150 | 336 ± 110 |
| $^{238}$U Activity concentration [Bq/kg] | KKM | - | 51 ± 20 | 72 ± 24 |
| | KKG | 57 ± 15 | 69 ± 26 | 58 ± 21 |
| | Basel | 49 ± 16 | 55 ± 28 | 47 ± 20 |
| $^{232}$Th Activity concentration [Bq/kg] | KKM | - | 26 ± 12 | 22 ± 9 |
| | KKG | 21 ± 6 | 27 ± 12 | 21 ± 9 |
| | Basel | 23 ± 8 | 37 ± 15 | 23 ± 11 |

## 6.1 Flight data

The flightlines of the German and the Swiss team in the environs of the KKM nuclear power plant are shown in Figures 55 and 56, respectively. The frequency distribution of the flight altitude above ground for the KKM area shows that the distributions of altitudes around the target altitude of 100 m are similar for the Swiss (CH) and German (D) team (Fig. 28) with a higher average flight altitude of the Swiss team (Table 18). The slightly narrower distribution for the Swiss team may be explained with the larger flight altitude, the terrain being more familiar to the Swiss pilots and the better rate of climb (8.2 m/s) of the Super-Puma helicopter compared to the EC 135 helicopter (7.6 m/s).

The environs of the Swiss nuclear power plant Gösgen (KKG) were inspected by all teams. The flightlines are mapped in Figures 67, 68 and 69. The frequency distribution of flight altitude (Fig. 29) shows distributions of the teams from Germany and Switzerland which are similar to the distributions obtained in the environs of KKM. The altitude distribution of the French team shows a significantly lower flight altitude. The frequency distribution is also less symmetric compared to the distributions of both other teams. Due to the lower average flight altitude, a larger amount of necessary height corrections to avoid obstacles has to be expected, leading to the positive slant of the distribution.

The environs of the city of Basel were apportioned between the three teams for the compilation of a composite gamma-spectrometric map. The flightlines for all three teams are mapped in Figure 88. The interpretation of the frequency distributions in Figure 30 has thus the restriction that the altitude samples are derived from different areas. The terrain of the French area of the measuring aera was flat compared to the German and Swiss areas, resulting in a less pronounced positive slant of the altitude frequency distribution of the French data compared to the environs of KKG (Fig. 29). The frequency distribution of the french altitude data seems narrower due to the lower average of altitudes. This effect can be eliminated by plotting the relative frequency distribution (Fig. 31), which shows that the relative variation of flight altitudes of all three teams is similar for the environs of Basel.
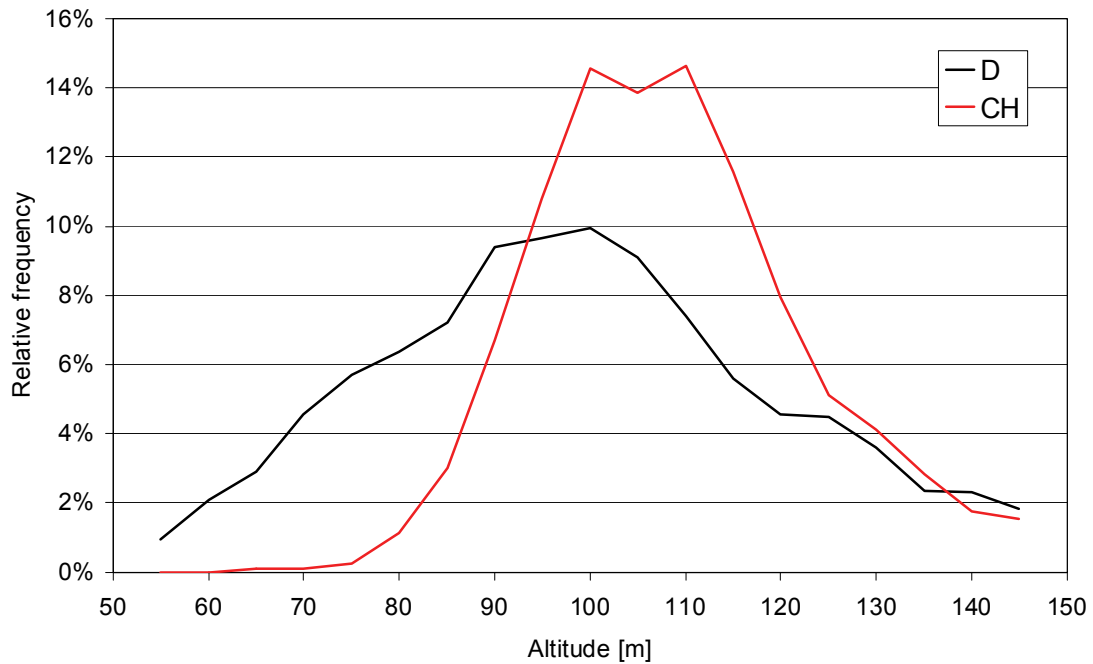
**Figure 28: Frequency distribution of flight altitudes in the environs of the Swiss nuclear power plant Mühleberg (KKM).  D: German team; CH: Swiss team.**
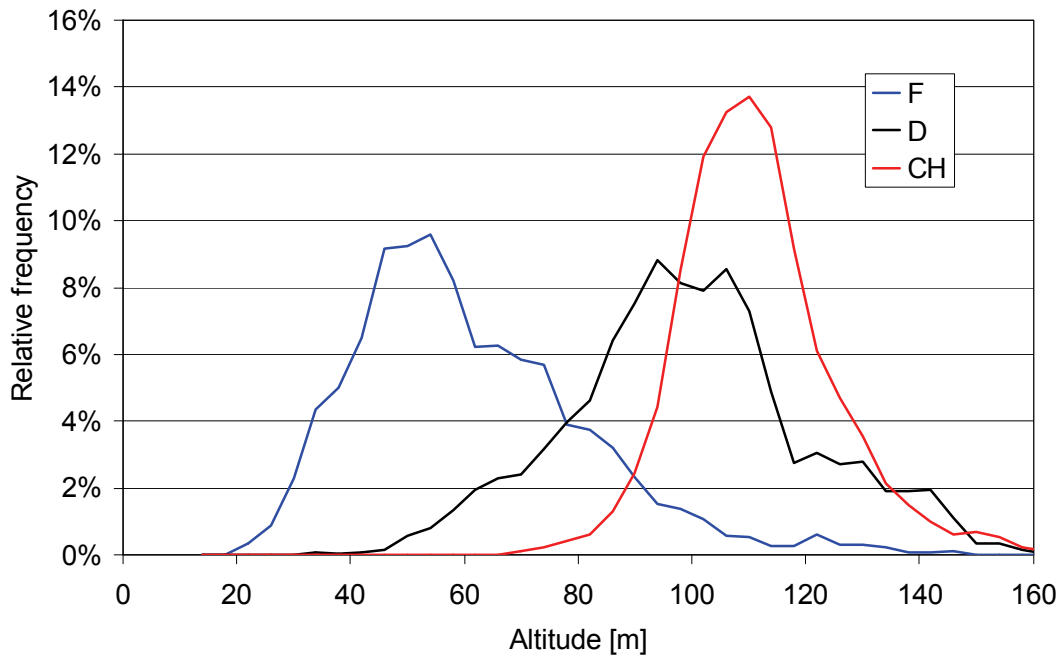


**Figure 29: Frequency distribution of flight altitudes in the environs of the Swiss nuclear power plant Gösgen (KKG).  F: French team; D: German team; CH: Swiss team.**

**Figure 30: Frequency distribution of flight altitudes in the environs of Basel. F: French team; D: German team; CH: Swiss team.**



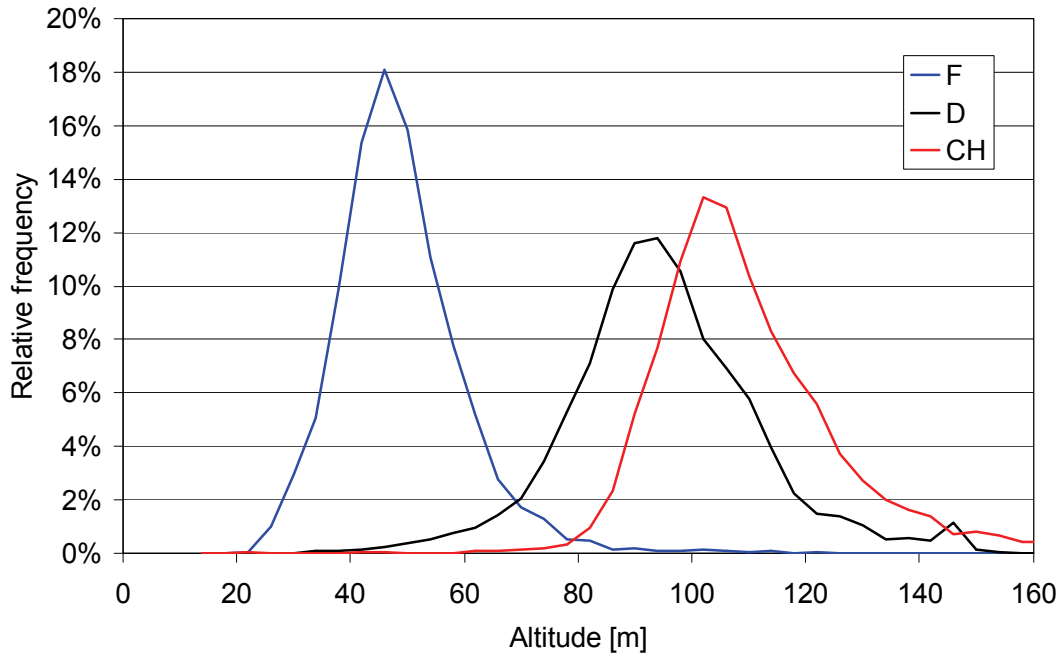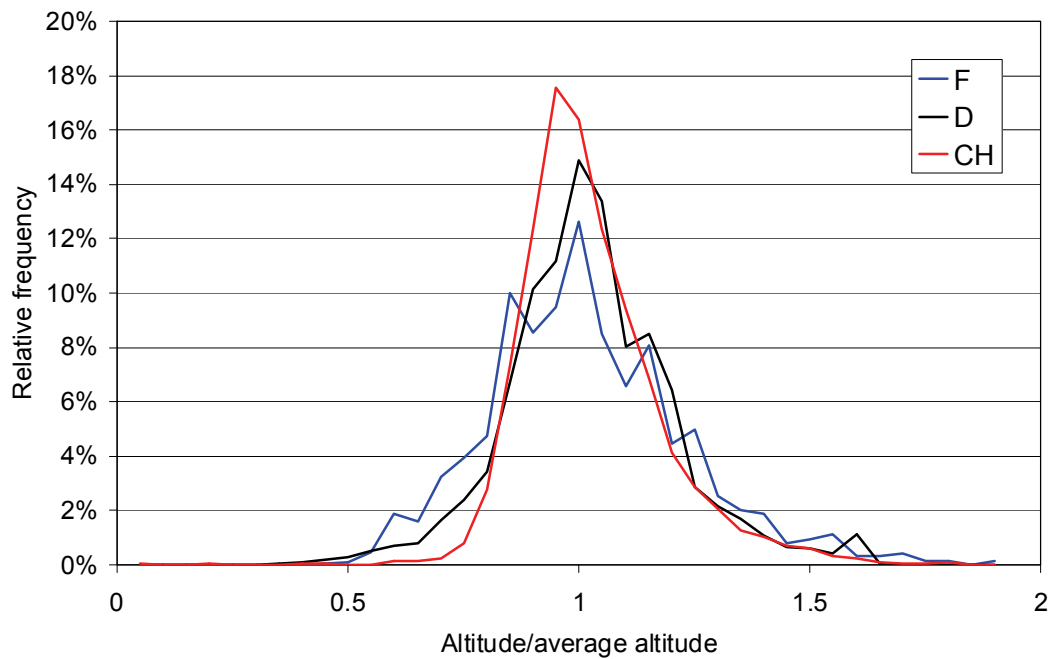**Figure 31: Relative frequency distribution of flight altitudes in the environs of Basel. F: French team; D: German team; CH: Swiss team.**

## 6.2 Dose Rate

Photons produced from cosmic rays in the atmosphere, emissions from radionuclides located in soil and rock and emissions from airborne radionuclides contribute to the total dose rate. The dose rate measured at flight altitude is extrapolated to a standard height of 1 m above ground. The dose rate is expressed in dose quantity H*(10) per unit time.

Figures 57 and 58 show maps of the total dose rate in the environs of the KKM nuclear power plant. The reactor of KKM was switched off for the annual revision between August 5$^{th}$ and September 2$^{nd}$. Some components containing $^{60}$Co were stored outside of the reactor containment for maintenance in the time of the measuring flights.

The dose rate clearly depicts the topography of the area, especially low values over water bodies, where the photon emissions of natural radionuclides are attenuated during the passage through the water layer. The KKM power plant generates a distinct peak in the dose rate maps. A comparison of photon spectra (Fig. 32) inside and outside of KKM premises identifies the radionuclide $^{60}$Co as source for the elevated dose rate of 800 nSv/h extrapolated to a heigt of 1 m above ground. The dose rate peak at KKM is less pronounced in the map derived from the measurements of the German team. This difference can be attributed to the different distances of the flightlines from the source of KKM photon emissions (Figs. 55 and 56), as the frequency distributions of the dose rate over the complete measurement area are very similar for both teams (Fig. 33).

The area which is influenced by the photon emissions of the KKM nuclear power plant is small compared to the complete measurement area. Therefore, the influence of KKM on the frequencey distribution can be neglected and Figure 33 can be considered to represent the background readings of the total dose rate.

In contrast to the boiling water reactor KKM, where during operation steam containing $^{16}$N is piped to the generator building, the pressurized reactor of KKG keeps radioactivity inside the well shielded reactor building. Thus, the dose rate maps (Figs. 70, 71 and 72) of the KKG environs show topographic effects, but a dose rate peak for KKG is not detected.

The frequency distributions of the total dose rates in the environs of KKG nuclear power plant are plotted in Figure 34. The distributions of the Swiss and French team display a similar shape with a not significant difference between the mean values of 5 nSv/h. The dose rate distribution measured by the German team is slightly broader with higher mean value (see also Table 18).

The standard deviation for each cell (cell size 125 m x 125 m) with terrestric dose rate measurements from all three teams relative to the cell average is mapped for the KKG measurement area in Figure 85. The map shows a pattern according to the underlaying topography, indicating an uncompletely corrected influence of topography and flight parameters on the calculated dose rates of the three teams.

Figure 89 shows the composite map of terrestric dose rate in the environs of Basel, which represents the total dose rate minus the dose rate of about 40 nSv/h caused by cosmic rays. The most distinct feature in this map is the Rhine river due to the attenuation of photons passing the water layer. A slight elevation of terrestric dose rate can be observed in the north-eastern part of the measurement area, which was measured by the German team. Accordingly, the total dose rate frequency distribution of the German team has a higher average value compared to the nearly identical frequency distributions of the total dose rates measured by the French and Swiss teams in the western and southern part of the Basel measurement area (Fig. 35).
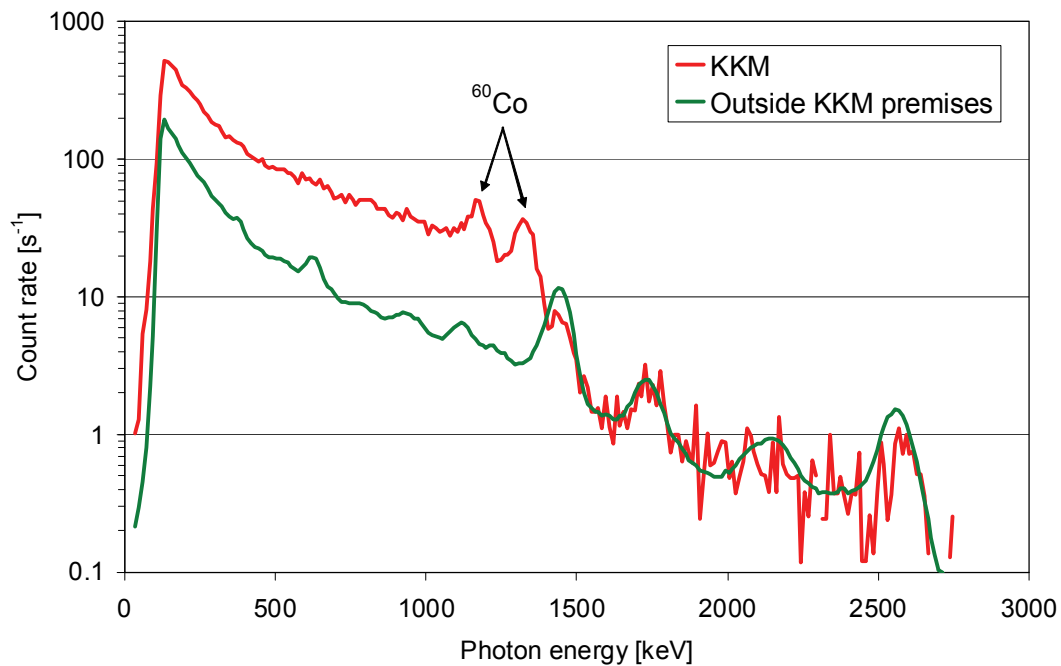


**Figure 32: Photon spectra inside and outside of KKM premises.**
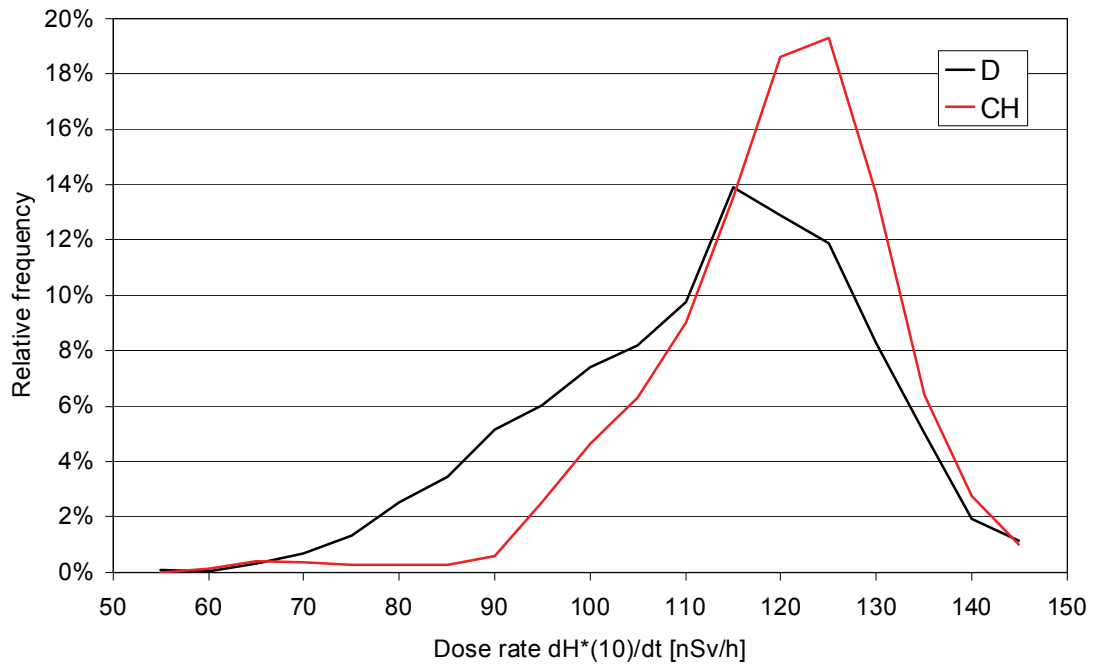
**Figure 33: Frequency distribution of dose rates in the environs of the Swiss nuclear power plant Mühleberg (KKM).
D: German team; CH: Swiss team.**
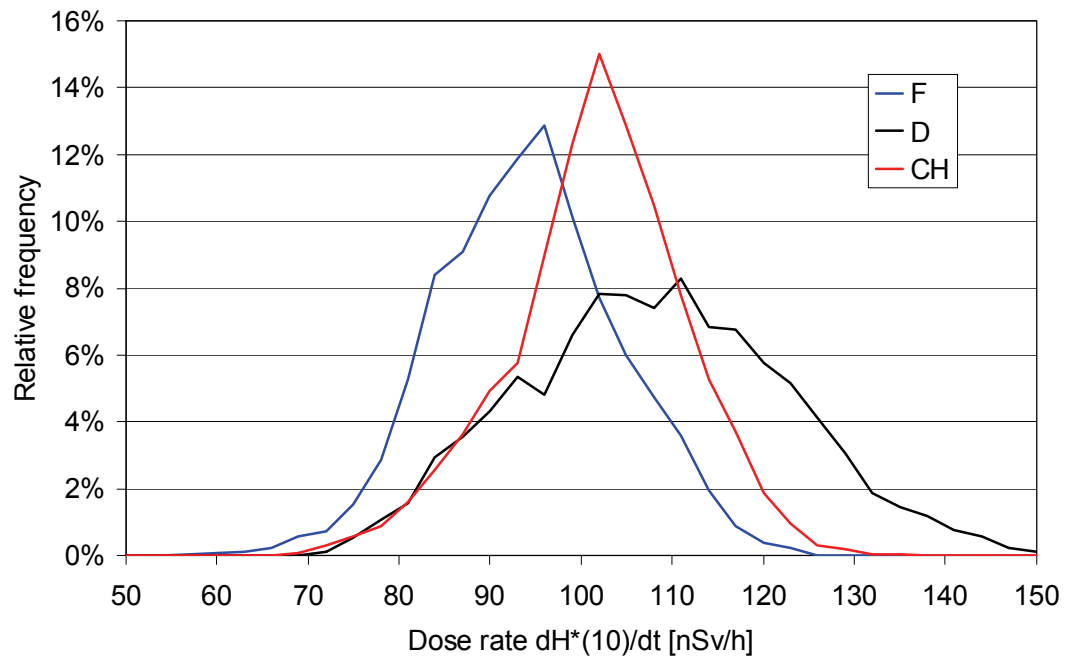


**Figure 34: Frequency distribution of dose rates in the environs of the Swiss nuclear power plant Gösgen (KKG).
F: French team; D: German team; CH: Swiss team.**
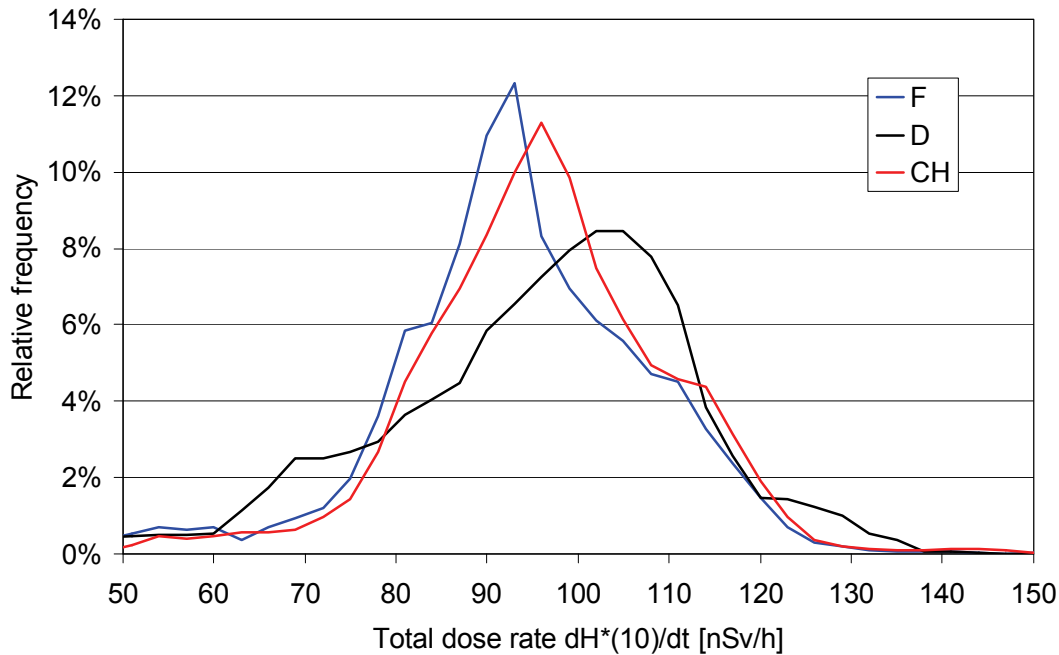
**Figure 35: Frequency distribution of dose rates in the environs of Basel.
F: French team; D: German team; CH: Swiss team.**

## 6.3 Radiocaesium

The major source of $^{137}$Cs contamination in western Europe was the accident at Chernobyl power plant in 1986. As Switzerland was mainly affected in the southern and eastern region, the inspected areas of the intercomparison exercise are expected to show low $^{137}$Cs contamination values.

The $^{137}$Cs acitivity concentration measured by the German and Swiss teams in the environs of KKM nuclear power plant are mapped in Figures 59 and 60. Both maps show a $^{137}$Cs peak at the location of KKM power plant. The photon spectrum obtained over the KKM premises (Fig. 32) shows clearly photon peaks at 1173 keV and 1332 keV associated with $^{60}$Co, but no indication of the 662 keV photon emission of $^{137}$Cs.
Therefore, the elevated $^{137}$Cs concentrations at KKM depicted in both maps have to be attributed to an undercorrection of the influence of the scattered photons emitted by $^{60}$Co on the energy window used to derive the $^{137}$Cs activity concentration.
The majority of measurement points outside the KKM premises yields $^{137}$Cs concentration values well below the detection limit of both measurement systems. For example, the average value of the Swiss team over the complete measurement area can be calculated to -70 Bq m$^{-2}$ with a standard deviation of 1100 Bq m$^{-2}$.

The large uncertainties of the measured $^{137}$Cs activity concentrations render the interpretation of results meaningless and thus the $^{137}$Cs values were neither included in the result table (Table 18) nor analysed with the help of frequency distributions. Rarely, single data points with elevated activity concentrations can be observed due to the large uncertainties of both signal and correction factors (Fig. 73). These data points require further examination to assure their origin from a numeric artefact.

These considerations are also valid for the measuring areas KKG and Basel. The according measurement results are mapped for all teams in Figures 73, 74, 75 and 90 as a matter of completeness.

## 6.4 Potassium

Like the map of total dose rate (Figures 57 and 58), the activity concentrations of the long-lived natural radioactive isotope of potassium, $^{40}$K, reflects clearly the topography of the measurement area around the KKM nuclear power plant (Figures 61 and 62).
The frequency distributions of $^{40}$K activity concentrations (Fig. 36) measured by the German and Swiss teams have practically identical shapes. The deviation of the average values (Table 18) between the data of both teams results in an offset between the distributions.

The activity concentrations of $^{40}$K in the environs of KKG nuclear power plant measured by the three teams are mapped in Figures 76, 77 and 78. The according frequency distributions (Fig. 37) show a similar offset between the measurement results of the German and Swiss team as was observed at the KKM site, although with both distributions shifted to a lower average. The frequency distribution measured by the French team shows the same pattern displaced to higher activity concentrations.
The sharp decline of the frequency distribution of the German data toward low activity concentrations is caused by a different data reporting strategy compared to the two other teams. Activity concentrations below the detection limit measured by the German team are replaced with an indicator that the result was below the detection limit. These data points were removed from the frequency distribution, thus reducing the frequency in the classes below the detection limit.
In contrast to the variation of the terrestric dose rate (Fig. 85), the map of the standard deviation of the $^{40}$K measurements (Fig. 86) shows no pattern reflecting the terrain. This indicates that the differences between the results of the different teams are mainly determined by stochastic effects.

The composite map of the $^{40}$K activity concentration in the environs of Basel (Fig. 91) shows clearly the Rhine river similar to the composite map of the terrestric

dose rate (Fig. 89). Elevated $^{40}$K activity concentrations are registered north-east of the Rhine river in the foothills of the Black Forest. This region was measured by the German team. Coincidentially, the elevated potassium concentration in the area measured by the German team compensates the offset between the averages of $^{40}$K activities measured by the German and Swiss teams observed for the KKM and KKG areas (Table 18), yielding nearly identical frequency distributions (Fig. 38). Measurements of soil samples performed by the State Laboratory of Canton Basel Town confirmed the elevated potassium contents measured by the Swiss team. The highest $^{40}$K-concentrations (1200 Bq/kg) were measured in samples of granitic gravel located at a decommissioned railway yard.

A sharp decline of the frequency distribution towards low activity concentration values as oberved for the German data in the KKG area can also be detected for $^{40}$K activity concentrations of the Basel region. The raw data of the measurements from the German team in the Basel region were completely re-evaluated after the exercise. All composite maps are based on the revised data. The German colleagues used this opportunity to comply to the request for reporting also values below the detection limit, rendering Figure 39 as a revision of Figure 38. Besides a shift of the mean value of the revised frequency distribution from 354 Bq/kg (Table 18) to 397 Bq/kg, the decline on the left hand of the curve is less steep and similar to the shape of the distributions measured by the French and Swiss teams.
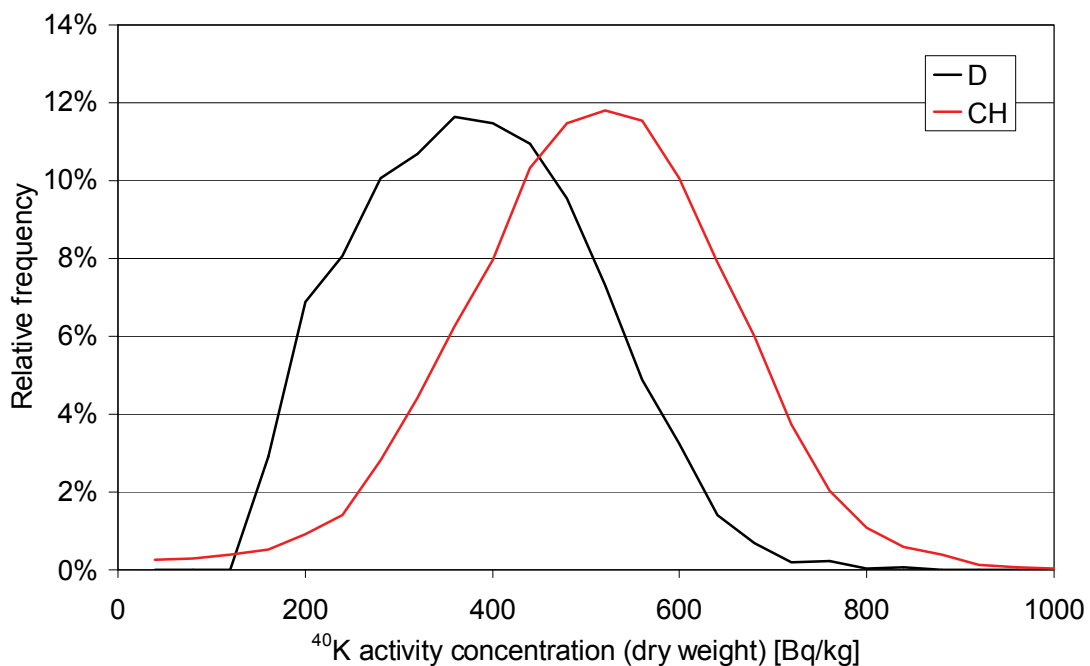


**Figure 36: Frequency distribution of $^{40}$K activity concentrations in the environs of the Swiss nuclear power plant Mühleberg (KKM). D: German team; CH: Swiss team.**
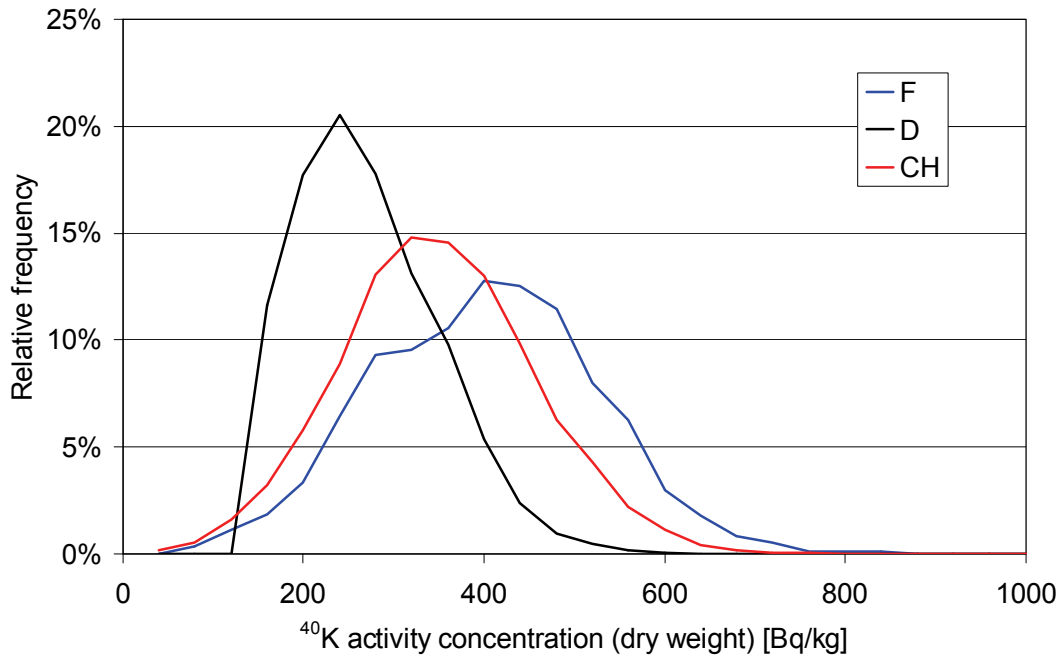
**Figure 37: Frequency distribution of $^{40}$K activity concentrations in the environs of the Swiss nuclear power plant Gösgen (KKG).
F: French team; D: German team; CH: Swiss team.**
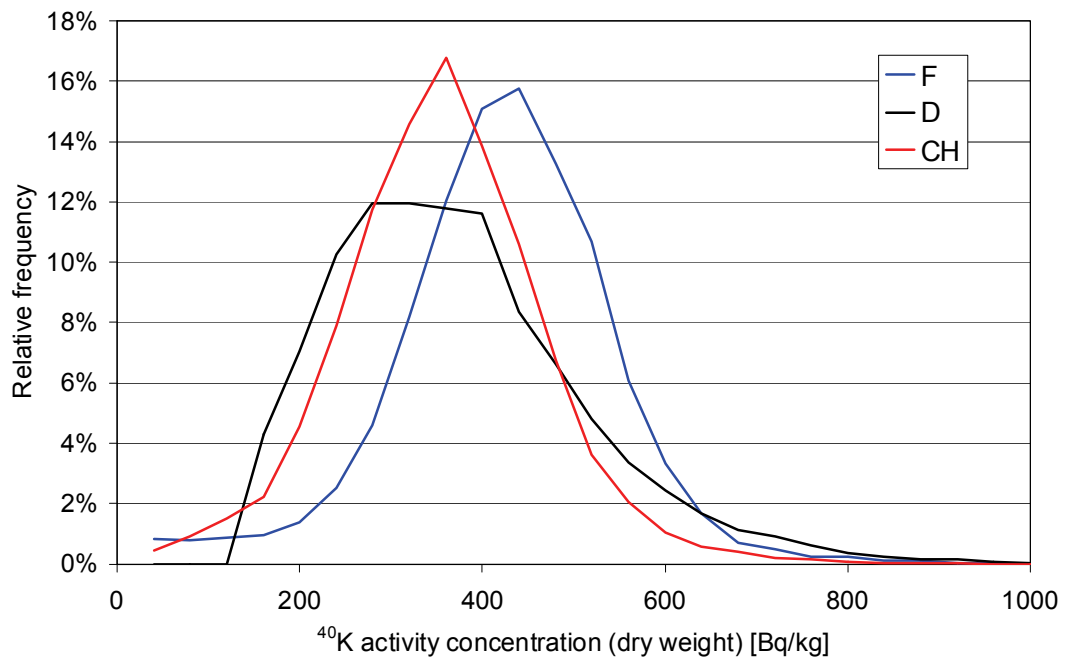


**Figure 38: Frequency distribution of $^{40}$K activity concentrations in the environs of Basel.
F: French team; D: German team; CH: Swiss team.**
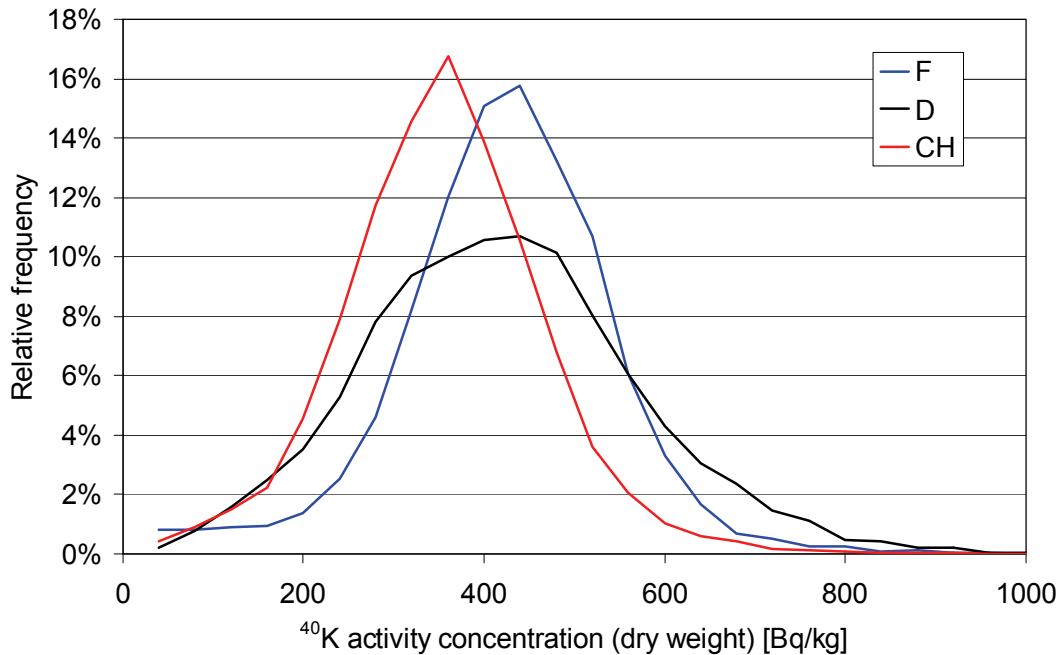
**Figure 39: Revised frequency distribution of $^{40}$K activity concentrations in the environs of Basel.**
**F: French team; D: German team; CH: Swiss team.**

## 6.5 Uranium

The uranium content of soil is determined from the measurement of the 1765 keV photon emission of the radionuclide $^{214}$Bi, which is produced in the uranium-radium decay chain. One of the predecessors of $^{214}$Bi in the decay chain is the noble gas radon ($^{222}$Rn). Due to its gaseous nature, radon is able to migrate from soil to air, yielding an airborne component of radionuclides of the uranium-radium decay chain including $^{214}$Bi. The advantage of utilising the high energy photon emission of $^{214}$Bi is thus partly compensated by the necessity to correct the measured signal for the influence of $^{214}$Bi in the air surrounding the aircraft.
The reported $^{238}$U concentrations between 45 Bq/kg and 69 Bq/kg are approximately twice the values reported for $^{232}$Th between 20 Bq/kg and 30 Bq/kg (Table 18). Typical uranium and thorium concentrations in soil are 3.0 ppm and 10.5 ppm, respectively (Ivanovich and Harmon, 1992), which results in expected activity concentrations of 37 Bq/kg for $^{238}$U and 43 Bq/kg for $^{232}$Th. Thus, the ratio of uranium and thorium activity concentration would be expected to be around unity or slightly below. The measured ratio of two may be an indication, that the signal attributed to airborne $^{214}$Bi is underestimated by all three teams.

The $^{238}$U concentrations measured in the environs of KKM nuclear power plant

are mapped in Figures 63 and 64 for the German and Swiss team. The measured values over KKM do not differ significantly from the values measured outside of the premises of KKM.

The frequency distributions of the $^{238}$U activity concentrations measured by the German and Swiss team are pictured in Figure 40. Whereas the frequency distribution of the $^{238}$U activity concentrations measured by the Swiss team is roughly symmetrical, the frequency distribution of the German data shows again a pronounced decline for lower activity concentrations due to the different reporting strategies . The distribution of $^{238}$U activity concentrations measured by the Swiss team is shifted to slightly larger values, resulting in a higher average over the measurement area (Table 18).

The environs of the KKG nuclear power plant show no unexpected variation of the $^{238}$U activity concentration in the according maps measured by the three teams (Figures 79, 80 and 81). The frequency distributions measured by the three teams are similar with  slight offsets between the distributions  (Fig. 41, Table 18). As the mean value over the measurement area KKG of the data measured by the German team is higher than observed for the environs of KKM (Fig. 40), the influence of discounted values below the detection limit on the frequency distribution is less pronounced.

The Rhine river is the most distinct feature apparent in the composite map of $^{238}$U concentrations in the Basel region (Fig. 92). A small region with slightly elevated $^{238}$U concentrations can be observed in the northern part of the measurement area. The frequency distributions (Fig. 42) of all three teams are nearly identical, even though the data were obtained over different regions of the measurement area. The revised frequency distribution for the re-evaluated data of the German team (Fig. 43) shows a narrower distribution with a more symmetrical shape, while the average activity concentration of both distributions remains equal.

**Figure 40: Frequency distribution of $^{238}$U activity concentrations in the environs of the Swiss nuclear power plant Mühleberg (KKM). D: German team; CH: Swiss team.**



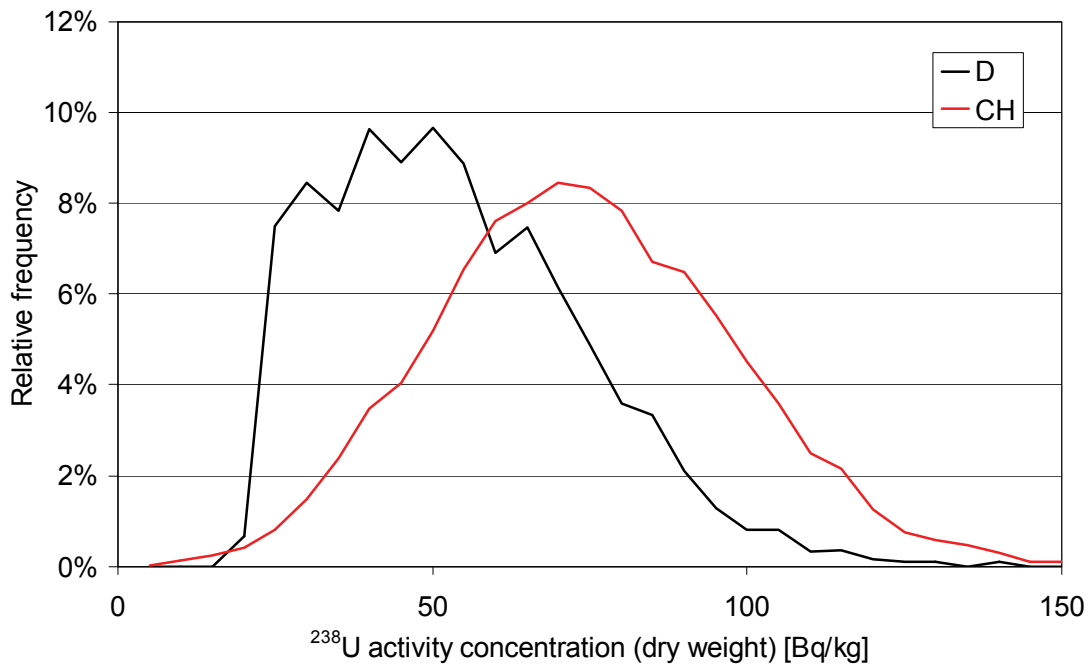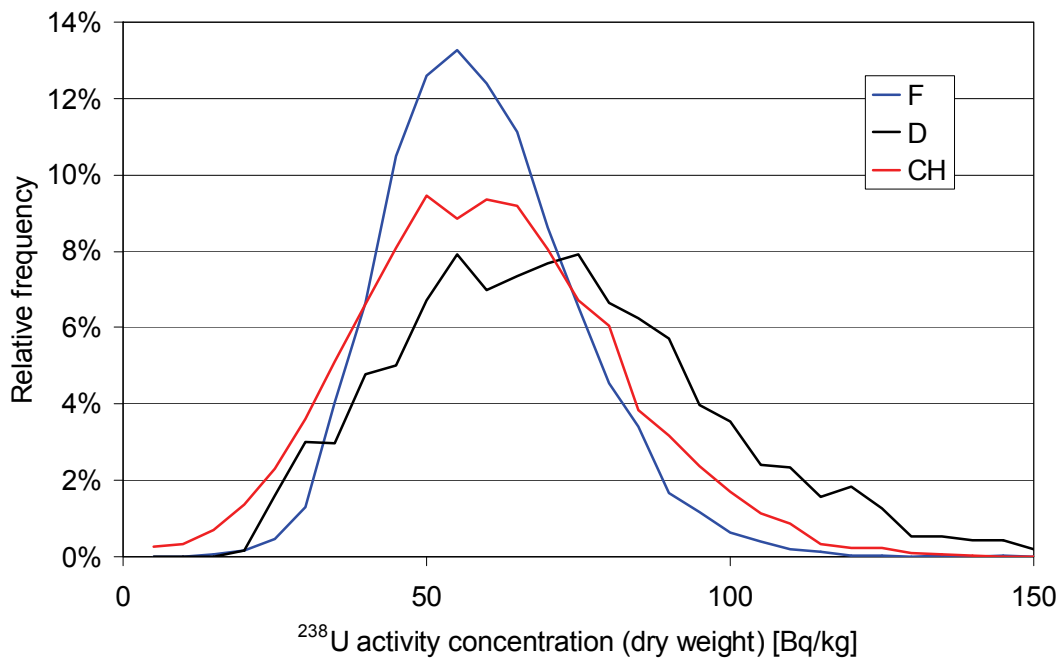**Figure 41: Frequency distribution of $^{238}$U activity concentrations in the environs of the Swiss nuclear power plant Gösgen (KKG). F: French team; D: German team; CH: Swiss team.**

**Figure 42: Frequency distribution of $^{238}$U activity concentrations in the environs of Basel.
F: French team; D: German team; CH: Swiss team.**



**Figure 43: Revised frequency distribution of $^{238}$U activity concentrations in the environs of Basel.
F: French team; D: German team; CH: Swiss team.**

## 6.6 Thorium

The thorium content of soil is determined by evaluating the 2615 keV photon emission of $^{208}$Tl, which is produced in the thorium decay chain.

The maps of $^{232}$Th activity concentrations measured by the German and Swiss teams (Figs. 65 and 66) over the environs of KKM nuclear power plant are showing a weak effect of topography. The values measured over the premises of KKM do not differ significantly from the values obtained over the rest of the measurement area. The frequency distributions (Fig. 44) of the $^{232}$Th activity concentrations measured by the German and Swiss teams are of similar shape with a slight offset between the average activity concentrations.

The according maps for the environs of KKG nuclear power plant (Figs. 82, 83 and 84) and the frequency distributions of the data measured by all three teams (Fig. 45) agree with the observations found in the environs of KKM. The map of the relative standard deviation of the $^{232}$Th concentration (Fig. 87) shows no pattern according to the topography of the measurement area, which is an indication that the variation between the measurement results of the three teams can be attributed to statistical uncertainties.

In the composite map of the $^{232}$Th activity concentration in the environs of Basel (Fig. 93), slightly elevated values are observed in the north-eastern part of the measurement area. The frequency distribution of the $^{232}$Th activity concentrations measured by the German team is significantly narrower for the re-evaluated data (Figs. 46 and 47). The relation between the revised frequency distributions replicates the pattern already observed for the environs of KKG nuclear power plant (Fig. 45).

**Figure 44: Frequency distribution of $^{232}$Th activity concentrations in the environs of the Swiss nuclear power plant Mühleberg (KKM).
D: German team; CH: Swiss team.**
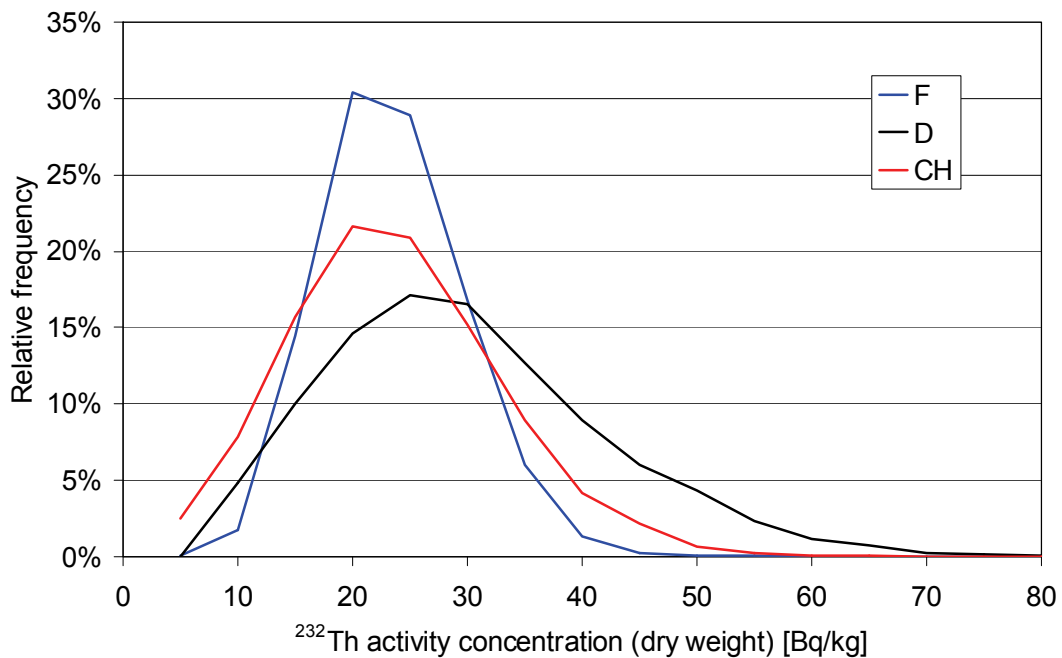


**Figure 45: Frequency distribution of $^{232}$Th activity concentrations in the environs of the Swiss nuclear power plant Gösgen (KKG).
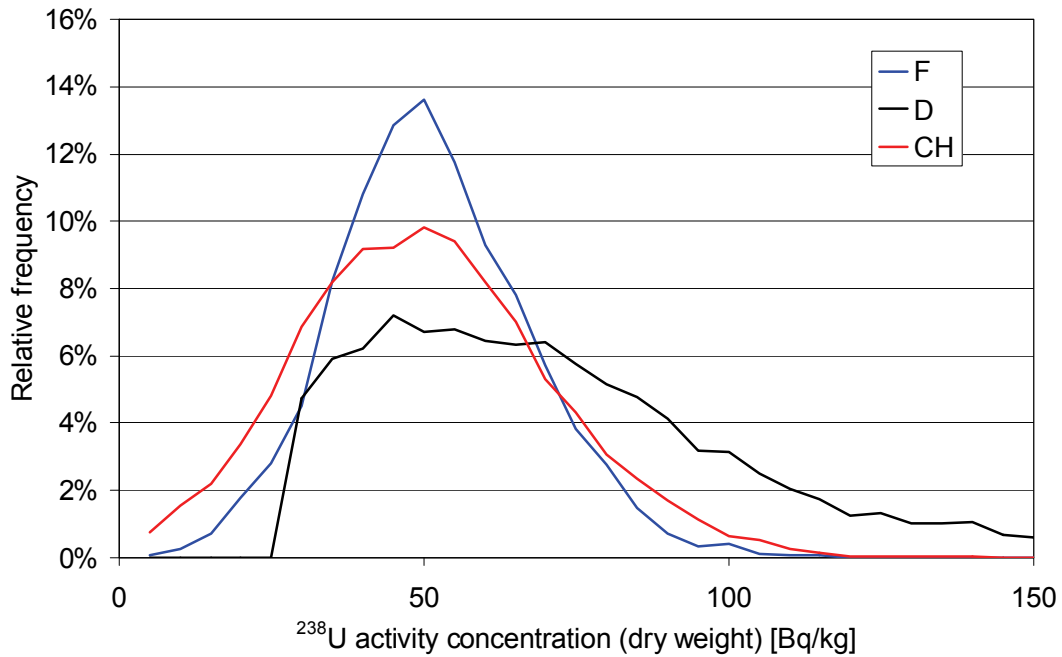F: French team; D: German team; CH: Swiss team.**

**Figure 46: Frequency distribution of $^{232}$Th activity concentrations in the environs of Basel.**
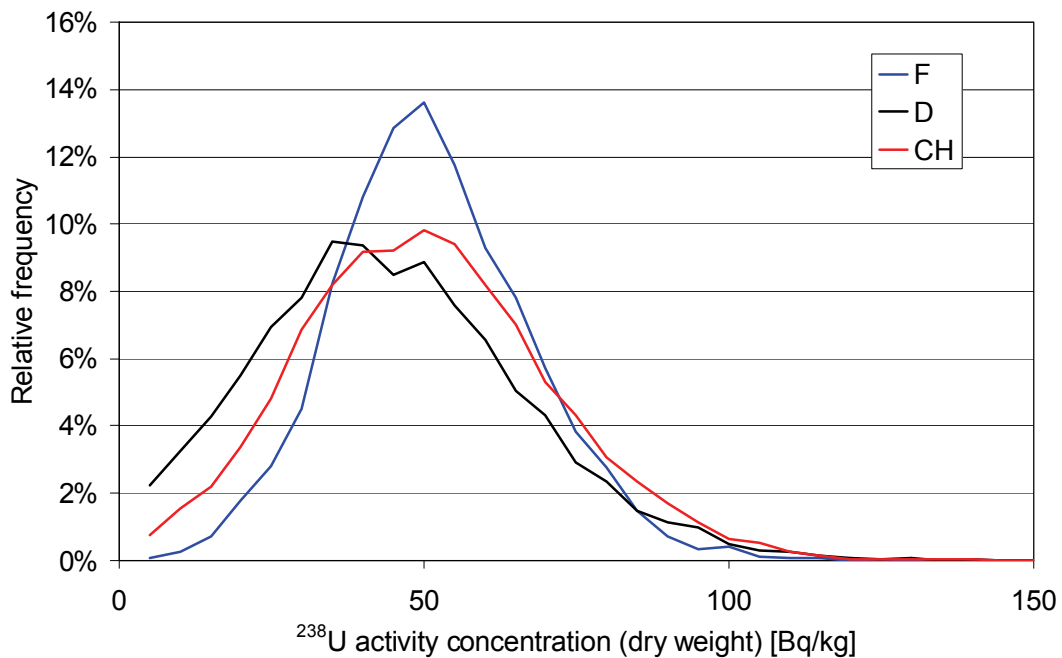**F: French team; D: German team; CH: Swiss team.**



**Figure 47: Revised frequency distribution of $^{232}$Th activity concentrations in the environs of Basel.**
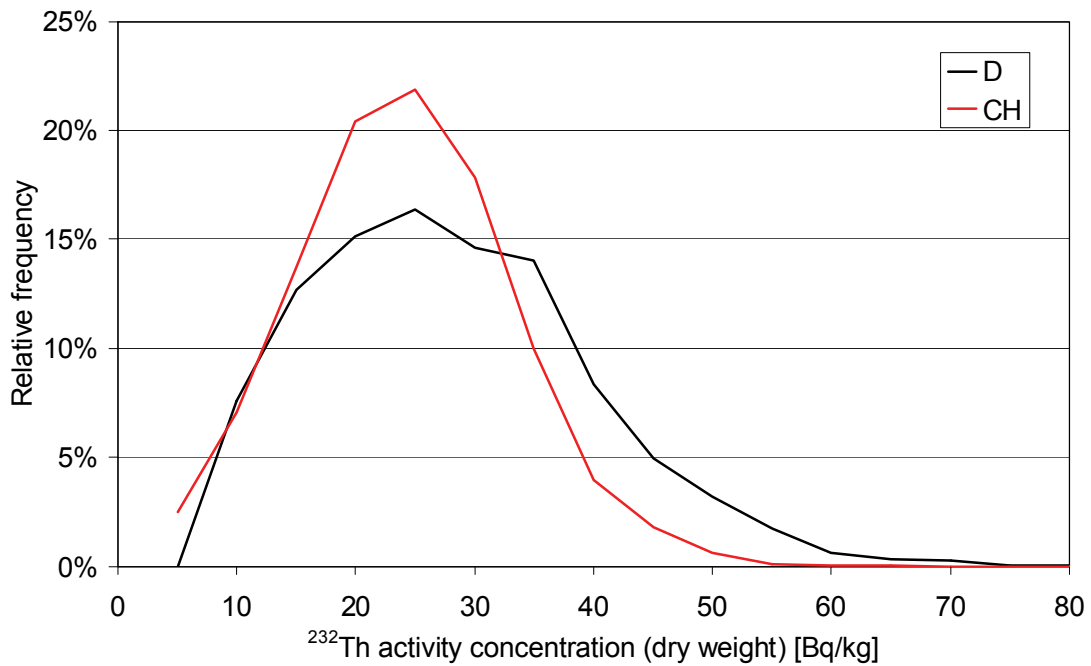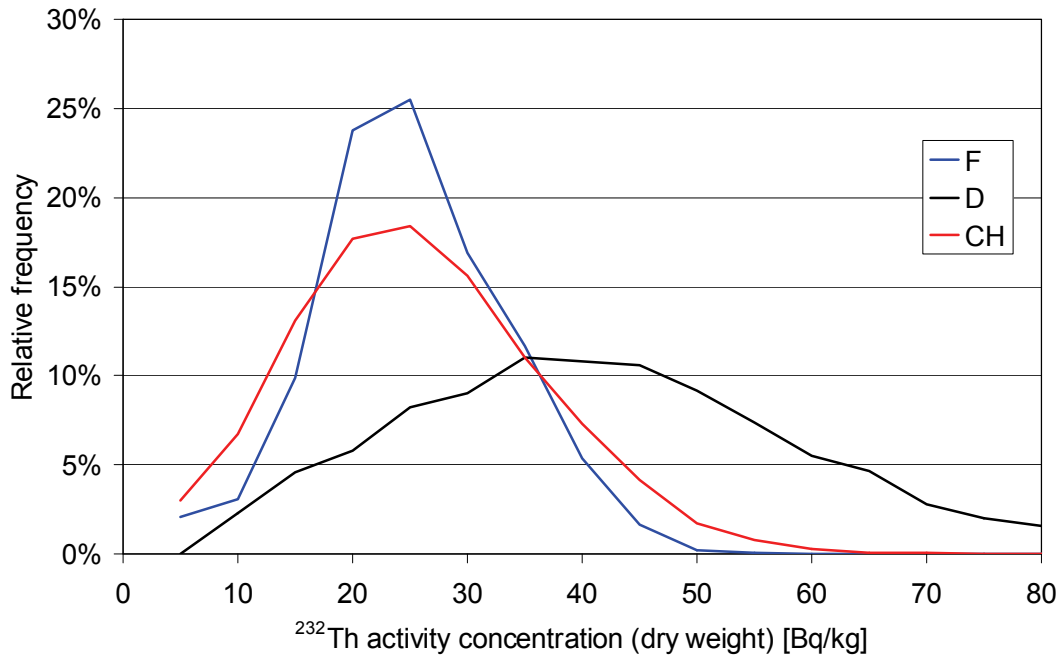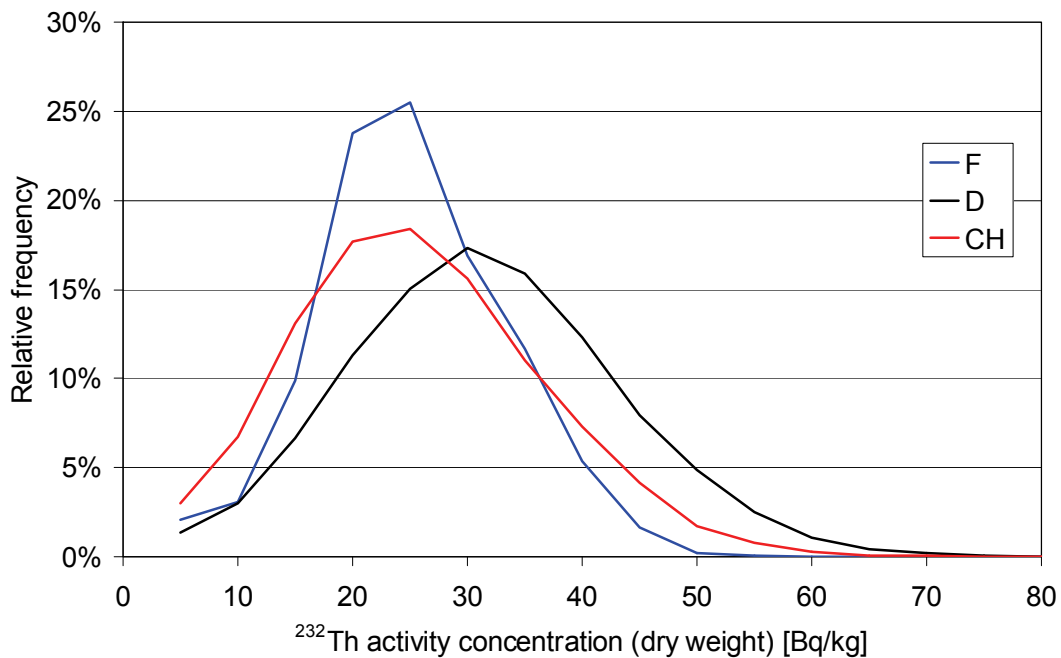**F: French team; D: German team; CH: Swiss team.**

## 7 SEARCH EXERCISE FOR RADIOACTIVE SOURCES

The Swiss National Railway (SBB) permitted the use of their freight depot located at Muttenz as location of the search exercise for orphaned radioactive sources. The exercise was organized in close collaboration with SBB and local emergency response forces. The railway yard was operative during the exercise. The radioactive sources were placed in the exercise area by radiation protection specialists of the Paul Scherrer Institute and guarded during the exercise by personnel of the Swiss Army.

Of the five radioactive sources concealed in the exercise area, three contained the radionuclide $^{60}$Co with activities of 660 MBq, 73 MBq and 7.3 MBq and two the radionuclide $^{137}$Cs with activities of 280 MBq and 234 MBq (Fig. 48).

For each team, a time slot of one hour was allocated. The flight pattern and flight parameters were at the discretion of the individual team. The flighlines are plotted for the three teams in Figures 49, 50 and 51. The French team used the lowest average flight altitude of 60 m, whereas the respective values for the German and Swiss teams were 88 m and 109 m.

The measurement teams had to report their findings promptly after the measuring flight for a realistic simulation of a search for orphaned radioactive sources. The French team reported the locations and activity estimates of one $^{60}$Co source with 700 MBq activity and two $^{137}$Cs sources with 120 MBq activity each (Fig. 52). The German team reported the locations of one $^{60}$Co and one $^{137}$Cs source without specifying estimated source activity (Fig. 53). Immediately after the flight, the Swiss team reported the location of one $^{60}$Co source without an estimate of source activity. In a later stage a small signal could be seen at the location of the 280 MBq $^{137}$Cs source (Fig. 54). Nevertheless, the signal at this point was very weak and was barely distinguishable from a statistical effect.

The different success rates of the teams for the location of radioactive sources demonstrate impressively the importance of flight altitude and density of flight pattern applied in the search strategy. A small helicopter, capable to obtain lower flight altitudes without damage to ground structures, has a definite advantage in limited search areas.

**Figure 48: Placement of the radioactive sources in the exercise area.**
**PK50©2008 swisstopo.**
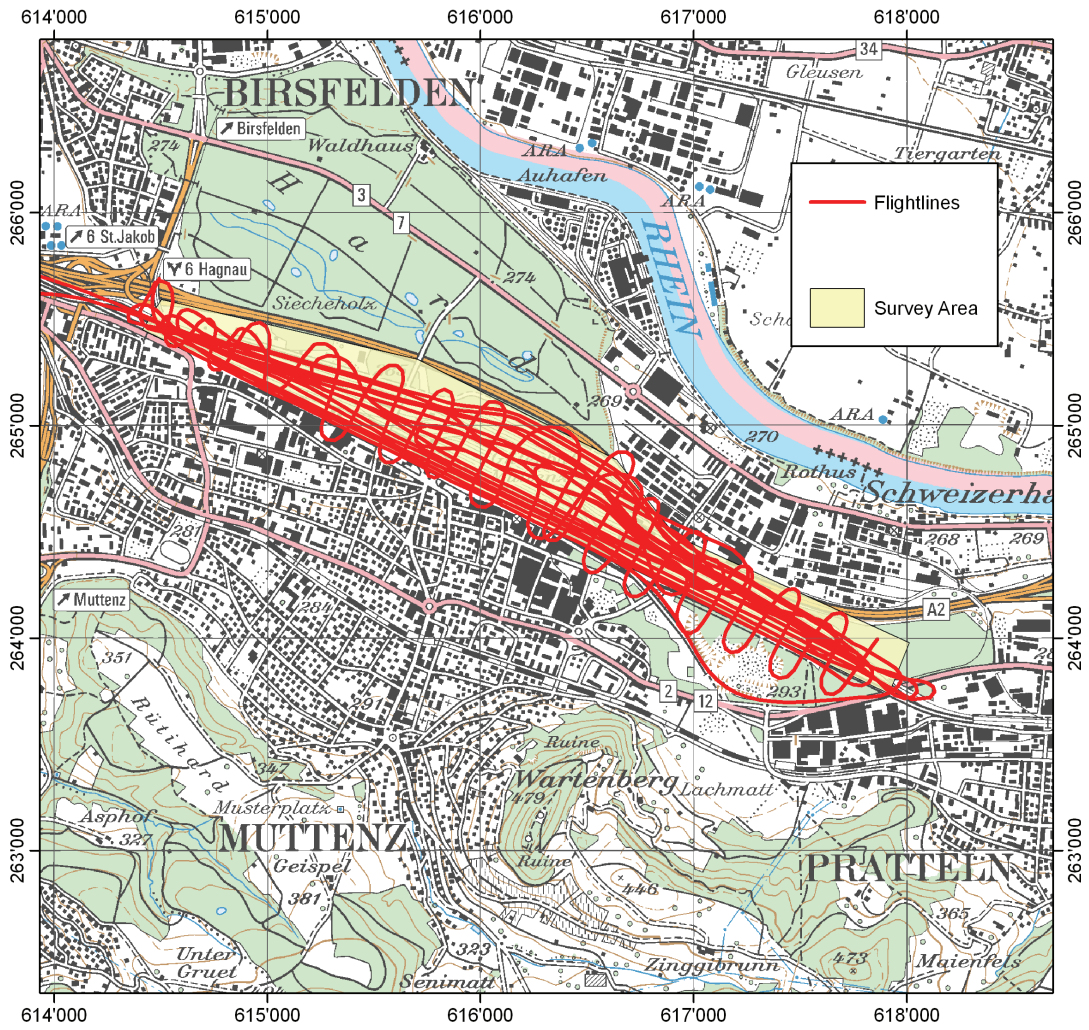
**Figure 49: Flightlines of the French team in the exercise area.
PK50©2008 swisstopo.**
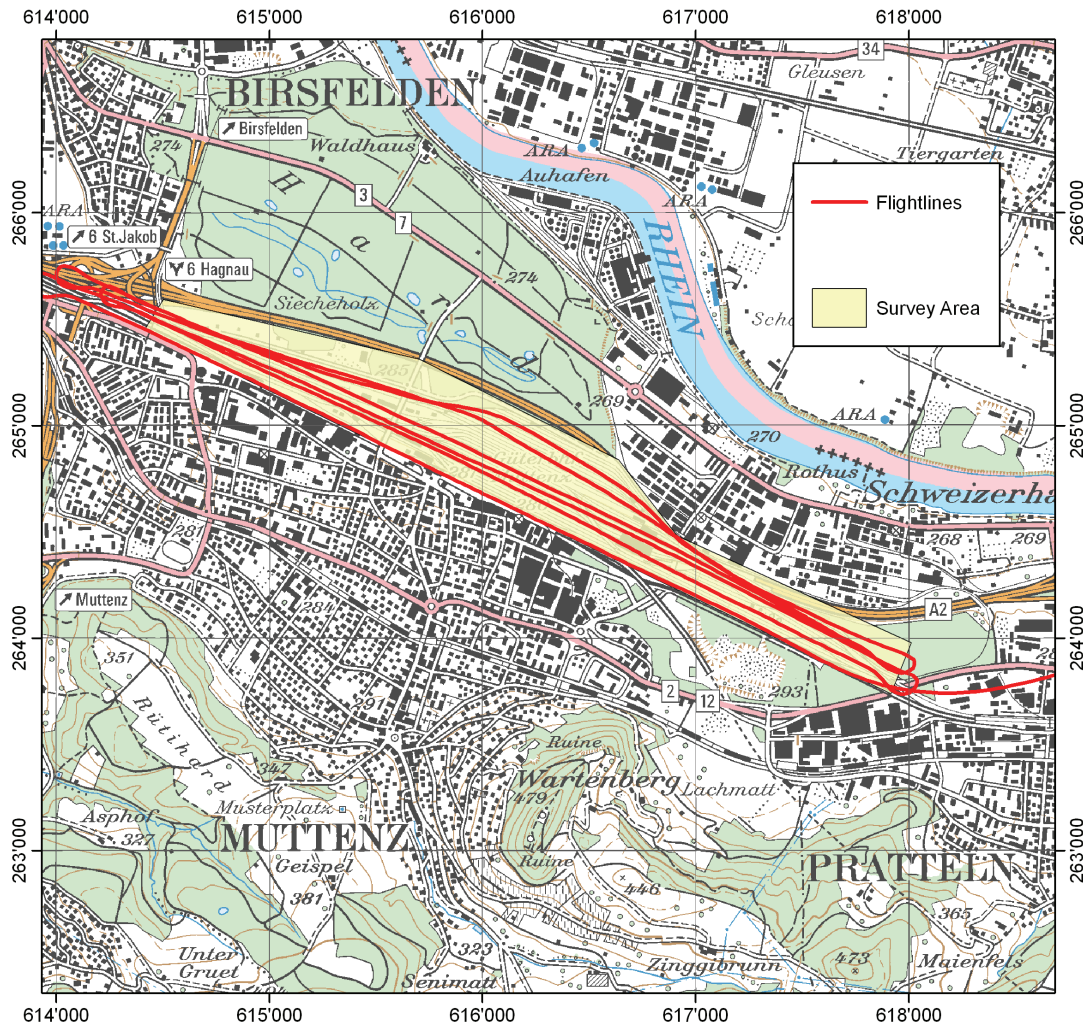
**Figure 50: Flightlines of the German team in the exercise area.
PK50©2008 swisstopo.**
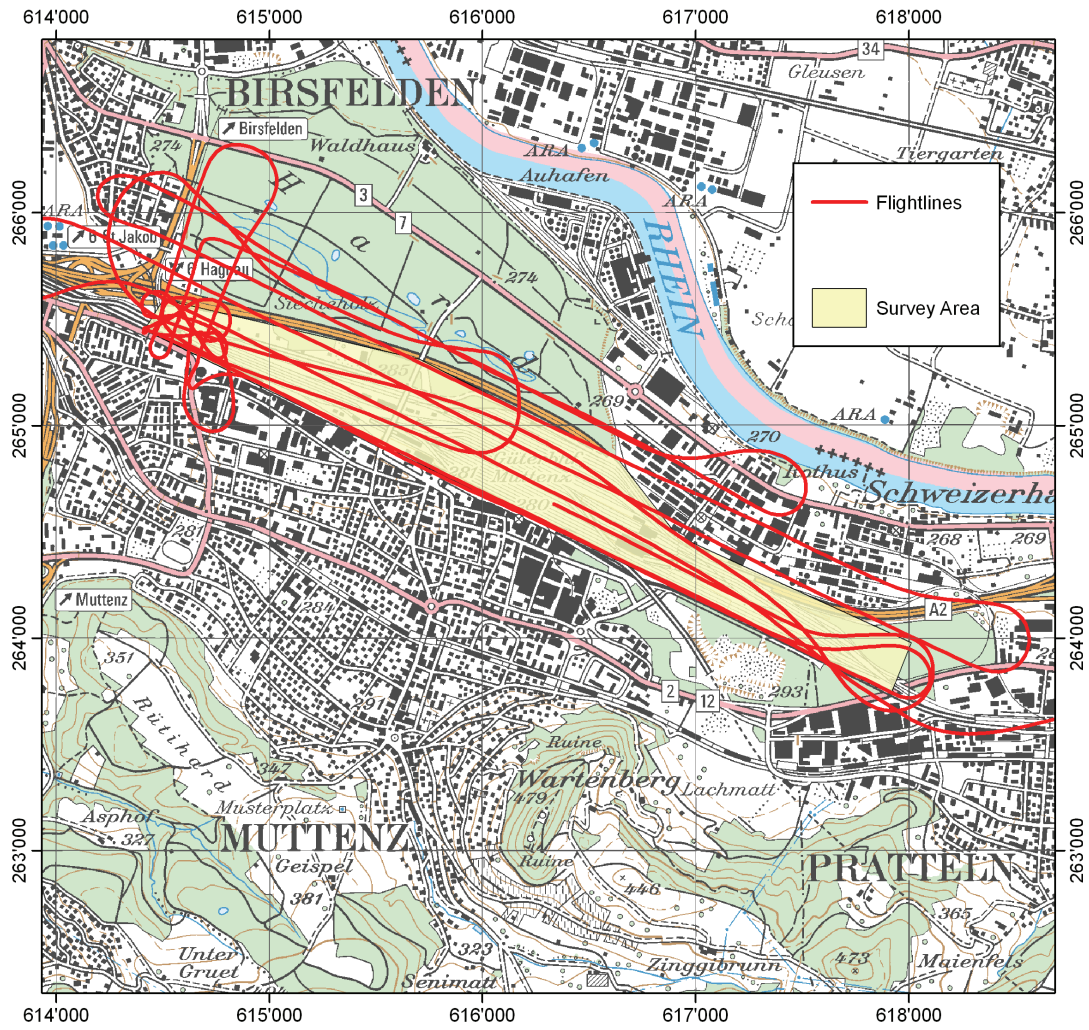
**Figure 51: Flightlines of the Swiss team in the exercise area.
PK50©2008 swisstopo.**
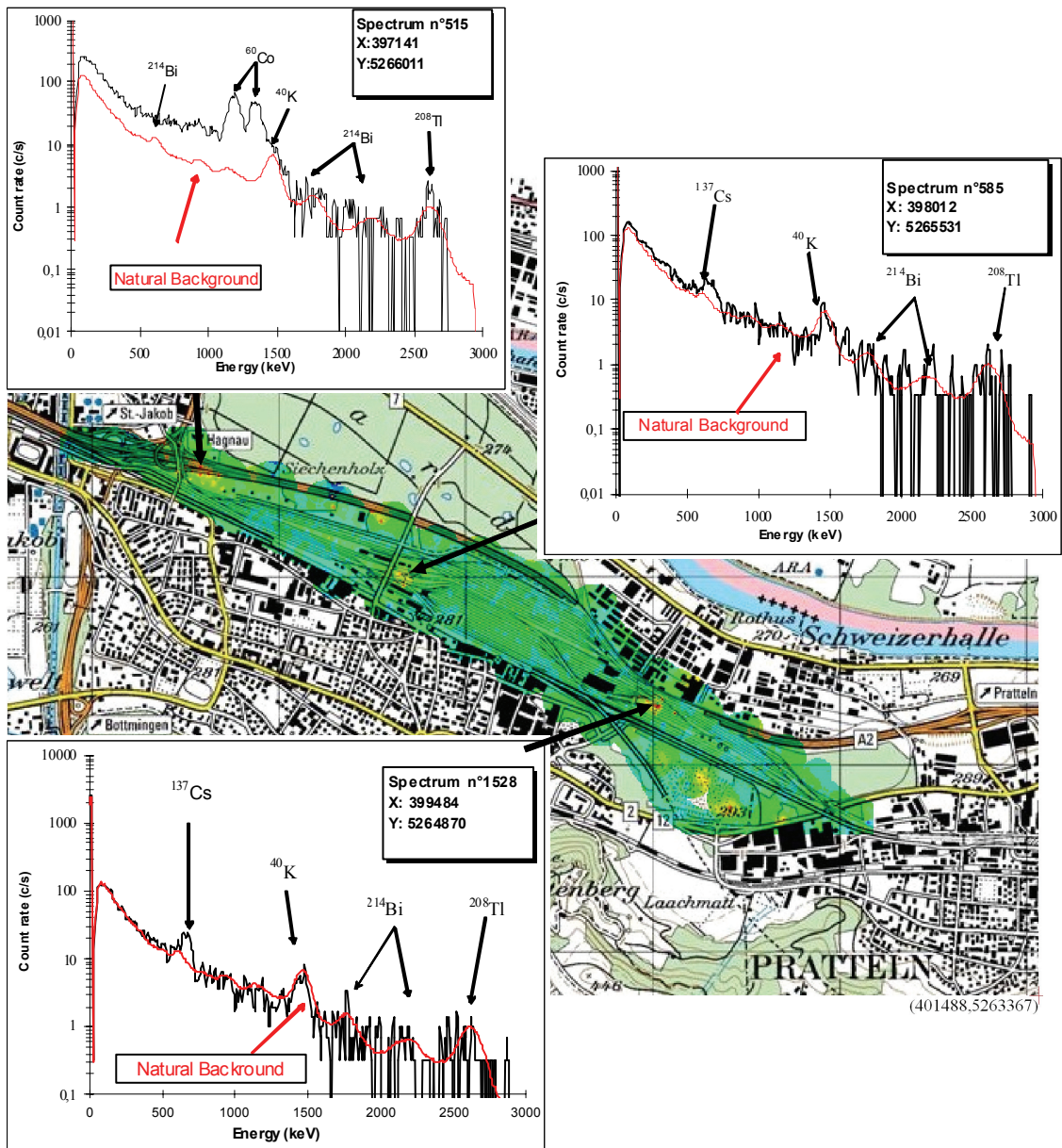
**Figure 52: Location of radioactive sources in the exercise area as reported by the French team. PK50©2005 swisstopo.**
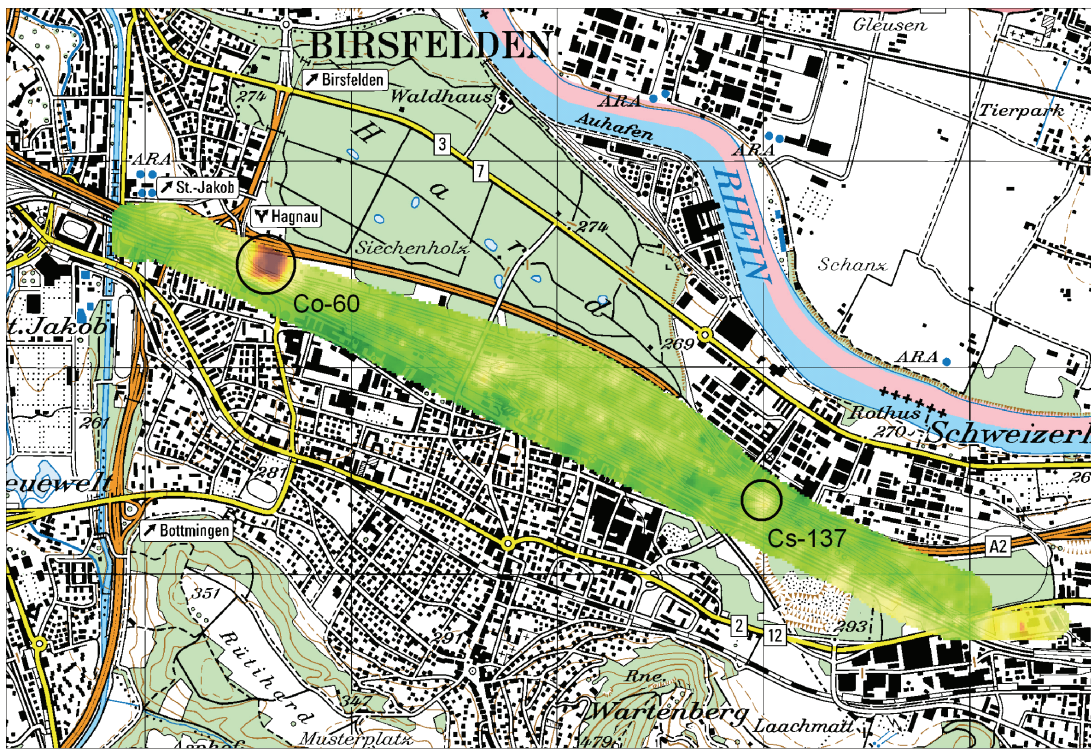
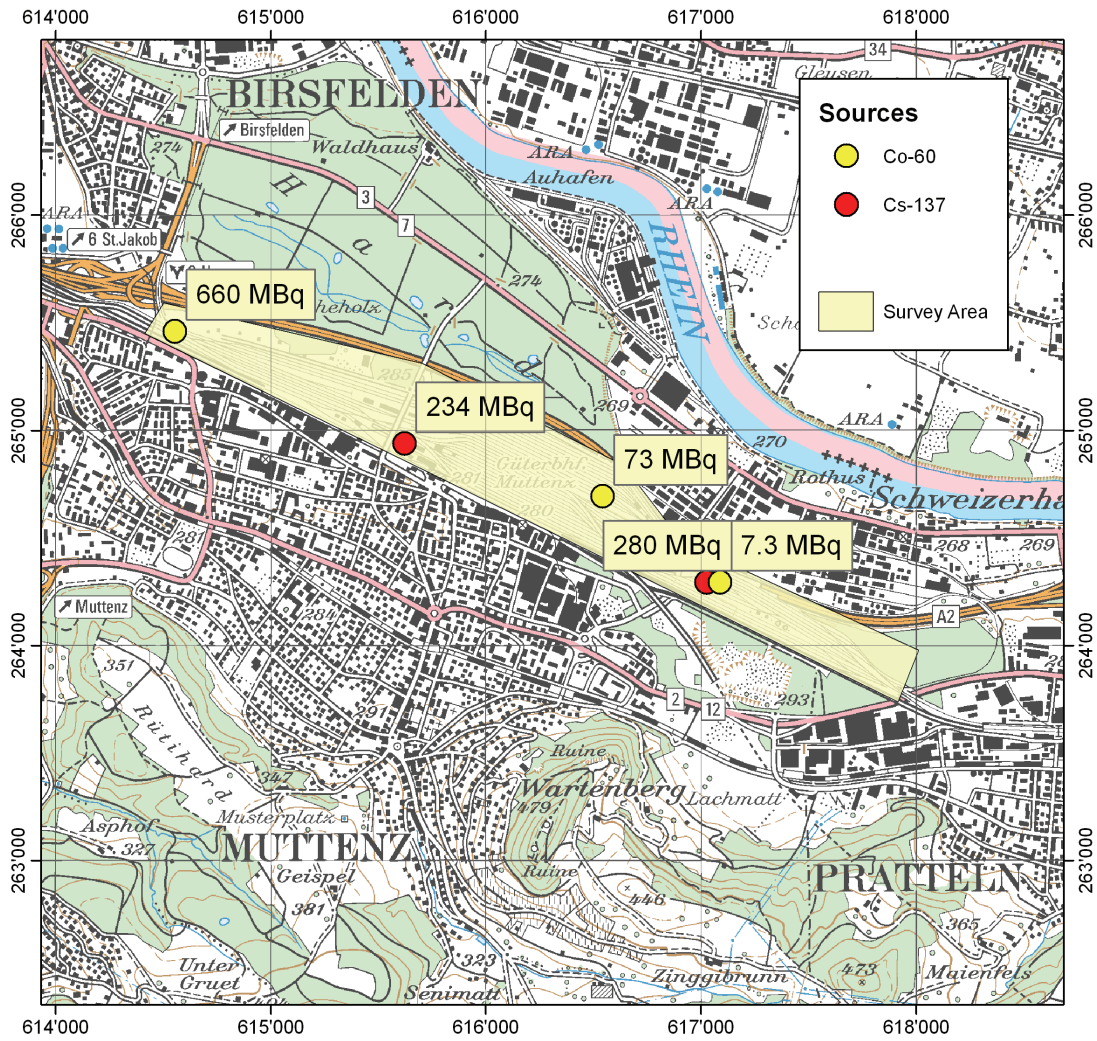**Figure 53: Location of radioactive sources in the exercise area as reported by the German team. PK50©2005 swisstopo.**
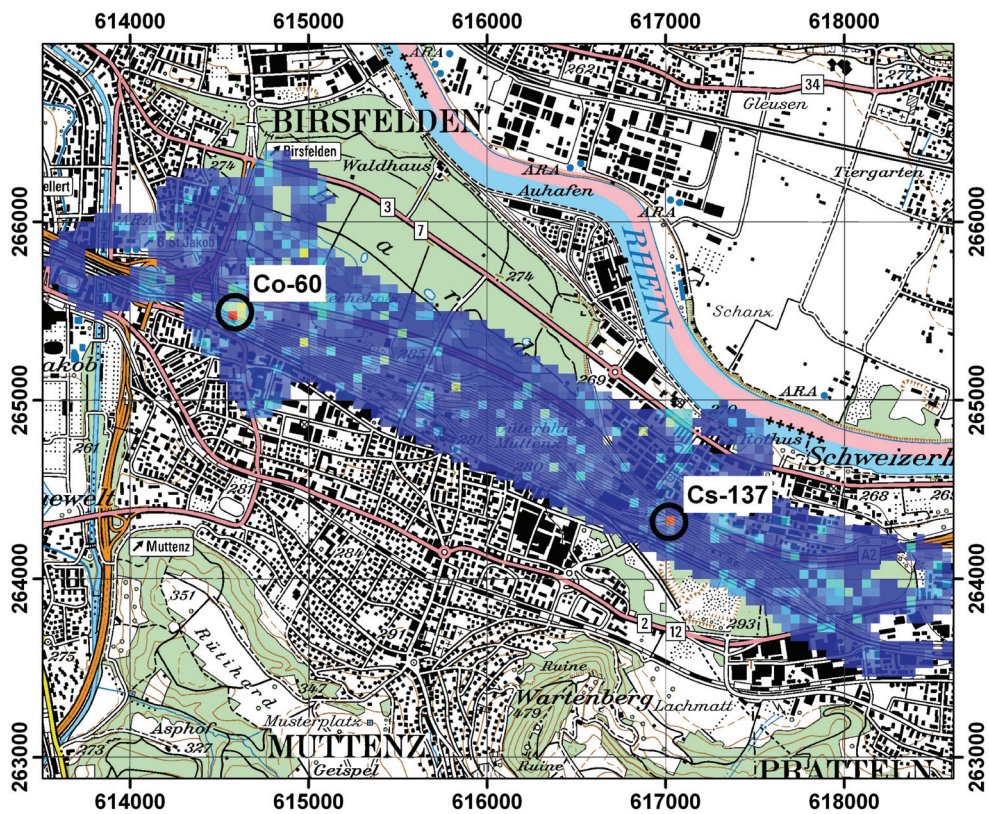


**Figure 54: Location of radioactive sources in the exercise area as reported by the Swiss team. PK50©2008 swisstopo.**

# 8 CONCLUSIONS

The joint exercise of areoradiometric teams from France, Germany and Switzerland showed clearly that the calibration of the measurement systems agree well for practical radiation protection purposes. The observed differences in reported activity concentrations are mainly of academic interest for further improvement of the measurement systems.
A major field of improvement is the standardisation of reporting methods. As the composite mapping exercise has shown, only compatible data and quantities enable a rapid exchange of results in emergencies which require the collaboration of international aeroradiometric teams. This requires the collaboration of international aeroradiometric teams and a strict adherence to the format description. The development of a standardised data format started with the NKS format introduced in the nordic countries. During the European ECCOMAGS (European Calibration and Coordination of Mobile and Airborne Gamma Spectrometry) projects, this data format was improved further to the PRD and finally ERS format. Nevertheless, the 2007 intercomparison exercise demonstrated a further need of harmonisation of reporting strategies and the application of the data format in routine measurements. The reported quantities should be based on the needs of the emergency response forces and a basic number of quantities should be reported by any team. The reported quantities should be associated with the corresponding uncertainties to render a direct access to data quality for the decision making processes. For mapping purposes no cut off is allowed. The use of a standard reference system as WGS84 for the coordinates and the exchange of transformation routines for local or national reference systems would be very useful.

For the first time foreign aeroradiometric teams had the opportunity to measure in the surroundings of Swiss nuclear power plants. The joint exercises over the environs of the Swiss nuclear power plants KKG and KKM confirmed the results found by the Swiss team in previous years. The radioactivity readings outside of the premises of KKG and KKM are completely attributable to natural radionuclides and fall-out from bomb testing and the Chernobyl accident.

The search exercise for abandoned radioactive sources showed clearly the advantages of low flight altitude and close-meshed distribution of flight lines for successful detection. For a source search in a limited area, the flight altitude should be as low as reasonable achievable because the detection limit is strongly depending on the distance between source and detector. The flight pattern should be very dense to achieve a low detection limit. This requests a very precise navigation by the pilots. The detection limit of the measuring system together with different search strategies should be considered prior to deployment of the airborne gamma-spectrometry system in a source search.

## 9 LITERATURE

Beck, H.L., DeCampo, J., Gogolak, C.: In-situ Ge(Li) and NaI(Tl) Gamma-Ray Spectrometry, U.S. Atomic Energy Commisssion Health and Safety Laboratory, Report HASL-258, New York, 1972.

Bourgeois, C., Bresson, J., Chiffot, T., Guillot, L.: RESUME 95, Exercice d'inter-comparaison des moyens mobiles de contrôle radiologique. Rapport n° 01/96, Commissariat à l'Énergie Atomique (CEA), Bruyères-le-Châtel, 1996.

Bucher, B., Rybach, L., Schwarz, G., Bärlocher, C.: Aeroradiometrische Messungen im Rahmen der Übung ARM97. Bericht für das Jahr 1997 zuhanden der Fachgruppe Aeroradiometrie (FAR). Interner Bericht, Institut für Geophysik, ETH Zürich, 1998.

Bucher, B., Rybach, L., Schwarz, G., Bärlocher, C.: Aeroradiometrische Messungen im Rahmen der Übung ARM98. Bericht für das Jahr 1998 zuhanden der Fachgruppe Aeroradiometrie (FAR). Interner Bericht, Institut für Geophysik, ETH Zürich, 1999.

Bucher, B., Rybach, L., Schwarz, G., Bärlocher, C.: Aeroradiometrische Messungen im Rahmen der Übung ARM99. Bericht für das Jahr 1999 zuhanden der Fachgruppe Aeroradiometrie (FAR). Interner Bericht, Institut für Geophysik, ETH Zürich, 2000.

Bucher, B., Rybach, L., Schwarz, G., Bärlocher, C.: Aeroradiometrische Messungen im Rahmen der Übung ARM00. Bericht für das Jahr 2000 zuhanden der Fachgruppe Aeroradiometrie (FAR). Interner Bericht, Institut für Geophysik, ETH Zürich, 2001.

Bucher, B.: Methodische Weiterentwicklungen in der Aeroradiometrie. Dissertation Nr. 13973, ETH Zürich, 2001.

Bucher, B., Rybach, L., Schwarz, G., Bärlocher, C.: Aeroradiometrische Messungen im Rahmen der Übung ARM01. Bericht für das Jahr 2001 zuhanden der Fachgruppe Aeroradiometrie (FAR). Interner Bericht, Paul Scherrer Institut, Villigen, Schweiz, 2002.

Bucher, B., Rybach, L., Schwarz, G., Bärlocher, C.: Aeroradiometrische Messungen im Rahmen der Übung ARM02. Bericht für das Jahr 2002 zuhanden der Fachgruppe Aeroradiometrie (FAR). Interner Bericht, Paul Scherrer Institut, Villigen, Schweiz, 2003.

Bucher, B., Rybach, L., Schwarz, G.: Aeroradiometrische Messungen im Rahmen der Übung ARM03. PSI-Bericht 04-14, ISSN 1019-0643, Paul Scherrer Institut, Villigen, Schweiz, 2004.

Bucher, B., Butterweck, G., Rybach, L., Schwarz, G.: Aeroradiometrische Messungen im Rahmen der Übung ARM04. PSI-Bericht 05-10, ISSN 1019-0643, Paul Scherrer Institut, Villigen, Schweiz, 2005.

Bucher, B., Butterweck, G., Rybach, L., Schwarz, G.: Aeroradiometrische Messungen im Rahmen der Übung ARM05. PSI-Bericht 06-06, ISSN 1019-0643, Paul Scherrer Institut, Villigen, Schweiz, 2006.

Deutsches Institut für Normung (DIN): In-situ-gamma ray spectrometry for nuclide specific environmental measurements. DIN 24462, Berlin, 2000.

Estier, S., Beuret, P., Byrde, F., Röllin, S., Schibli, M., Bucher, B., Buchillier, T., Froidevaux, P.: Mesures d'intercomparison en spectrométrie gamma in situ dans la region de La Chaux-de-Fonds 2006, Interner Bericht SUeR BAG, 2006.

Grasty, R.L.: Atmospheric absorption of 2,62 MeV gamma-ray photons emitted from the ground. Geophysics 40 (6), 1058-1065, 1975.

Guillot, L. : Spectrométrie gamma aéroportée : Etude de nouvelles méthodes de traitement spectral et de calibration permettant une interprétation qualitative et quantitative des mesures , PhD thesis, University of Burgundy, France, 1996.

Guillot, L.: Extraction of full absorption peaks in airborne gamma-spectrometry by filtering techniques coupled with a study of the derivatives. Comparison with the windows method. J. Environ. Radioact. 53, 381-398, 2001.

Gutierrez, S. : Mesures par spectrométrie gamma de l'abondance des radioéléments naturels et artificiels en surface et dans les sols par moyens mobiles (détecteurs au germanium embarqués à bord d'un hélicoptère ou d'un véhicule). Thèse de Doctorat de l'Université Paris XI, Paris, 2002.

Gutierrez, S.: Contribution of a germanium detector in mobile gamma-ray spectrometry. Spectral analysis and performances. Nucl. Instr. Meth. 482, 425-433, 2002.

International Atomic Energy Agency (IAEA): Gamma-ray surveys in uranium exploration, IAEA technical reports series 186, Vienna Austria, 1979.

International Atomic Energy Agency (IAEA): Airborne gamma-ray spectrometer surveying, IAEA technical reports series 323, Vienna Austria, 1991.

International Commission on Radiation Units and Measurements (ICRU): ICRU-Report 53, Gamma-Ray Spectrometry in the Environment. ISBN 0-913394-52-1, 1994.

International Organization for Standardization (ISO): Guide to the Expression of Uncertainty in Measurement. ISBN 92-67-10188-9, ISO, Geneva 1995

International Organization for Standardization (ISO):  X and gamma reference radiation for calibrating dosemeters and doserate meters and for determining their response as a function of photon energy - Part 3: Calibration of area and personal dosemeters and the measurement of their response as a function of energy and angle of incidence, ISO 4037-3:1999(E), 1999.

Ivanovich, M., Harmon, S. (eds.): Uranium series disequilibrium, Oxford Scientific Publications, Claredon Press, Oxford, 1992.

Karlsson, S., Mellander, H., Lindgren, J., Finck, R., Lauritzen, B.: RESUME 99 Rapid Environmental Surveying Using Mobile Equipment, Nordic nuclear safety research report NKS-15, ISBN 87-7893-065-0, 2000

Lauritzen, B., Sanderson, D.W., Cresswell, A., Scott, M., Finck, R.R., Karlsson, S.: ECCOMAGS: Initial results from the RESUME 2002 exercise, Nordic nuclear safety research report NKS-86, ISBN 87-7893-144-4, 2003

Rybach, L., Schwarz, G., Bucher, B.:  Aero-Gammaspektrometrie – Methodik und neue Anwendungen. Sonderband "DGG-Kolloquium AeroGeophysik", Deutsche Geophysikalische Gesellschaft e.V., I/2004, p. 61-73, ISSN-Nr. 0934-6554, 2004.

Sanderson, D.C.W., Cresswell, A.J., Lang, J.J.: An International Comparison of Airborne and Ground Based Gamma Ray Spectrometry,  SUERC, University of Glasgow, Glasgow, ISBN 0-85261-783-6, 2003.

Schwarz, G. F.: Methodische Entwicklungen zur Aerogammaspektrometrie. Beiträge zur Geologie der Schweiz, Geophysik Nr.23, Schweizerische Geophysikalische Kommission, 1991.

Schwarz, G. F., Klingelé, E. E., Rybach, L.: Aeroradiometrische Messungen in der Umgebung der schweizerischen Kernanlagen. Bericht für das Jahr 1991 zuhanden der Hauptabteilung für die Sicherheit der Kernanlagen (HSK). Interner Bericht, Institut für Geophysik, ETH Zürich, 1991.

Schwarz, G. F., Klingelé, E. E., Rybach, L.: Airborne Radiometric Mapping in Switzerland. Geophysique Nr. 25, Schweizerische Geophysikalische Kommission, 1992.

Schwarz, G. F., Rybach, L.: Aeroradiometrische Messungen im Rahmen der Übung ARM94. Bericht für das Jahr 1994 zuhanden der Fachgruppe Aeroradiometrie (FAR). Interner Bericht, Institut für Geophysik, ETH Zürich, 1995.

Schwarz, G. F., Rybach, L.: Aeroradiometrische Messungen im Rahmen der Übung ARM95. Bericht für das Jahr 1995 zuhanden der Fachgruppe Aeroradiometrie (FAR). Interner Bericht, Institut für Geophysik, ETH Zürich, 1996.

Schwarz, G. F., Rybach, L., Bärlocher, C.: Aeroradiometrische Messungen im Rahmen der Übung ARM96. Bericht für das Jahr 1996 zuhanden der Fachgruppe Aeroradiome-trie (FAR). Interner Bericht, Institut für Geophysik, ETH Zürich, 1997.

**Figure 55: Flightlines of the German team in the environs of KKM nuclear power plant. PK100©2008 swisstopo.**

**Figure 56: Flightlines of the Swiss team in the environs of KKM nuclear power plant. PK100©2008 swisstopo.**

**Figure 57: Total dose rate measured by the German team in the environs of KKM nuclear power plant. PK100©2008 swisstopo.**

**Figure 58: Total dose rate measured by the Swiss team in the environs of KKM nuclear power plant. PK100©2008 swisstopo.**

**Figure 59: $^{137}$Cs activity concentration measured by the German team in the environs of KKM nuclear power plant. PK100©2008 swisstopo.**

**Figure 60: $^{137}$Cs activity concentration measured by the Swiss team in the environs of KKM nuclear power plant. PK100©2008 swisstopo.**

**Figure 61: $^{40}$K activity concentration measured by the German team in the environs of KKM nuclear power plant. PK100©2008 swisstopo.**

Figure 62: $^{40}$K activity concentration measured by the Swiss team in the environs of KKM nuclear power plant. PK100©2008 swisstopo.

**Figure 63: $^{238}$U activity concentration measured by the German team in the environs of KKM nuclear power plant. PK100©2008 swisstopo.**

**Figure 64: $^{238}$U activity concentration measured by the Swiss team in the environs of KKM nuclear power plant. PK100©2008 swisstopo.**
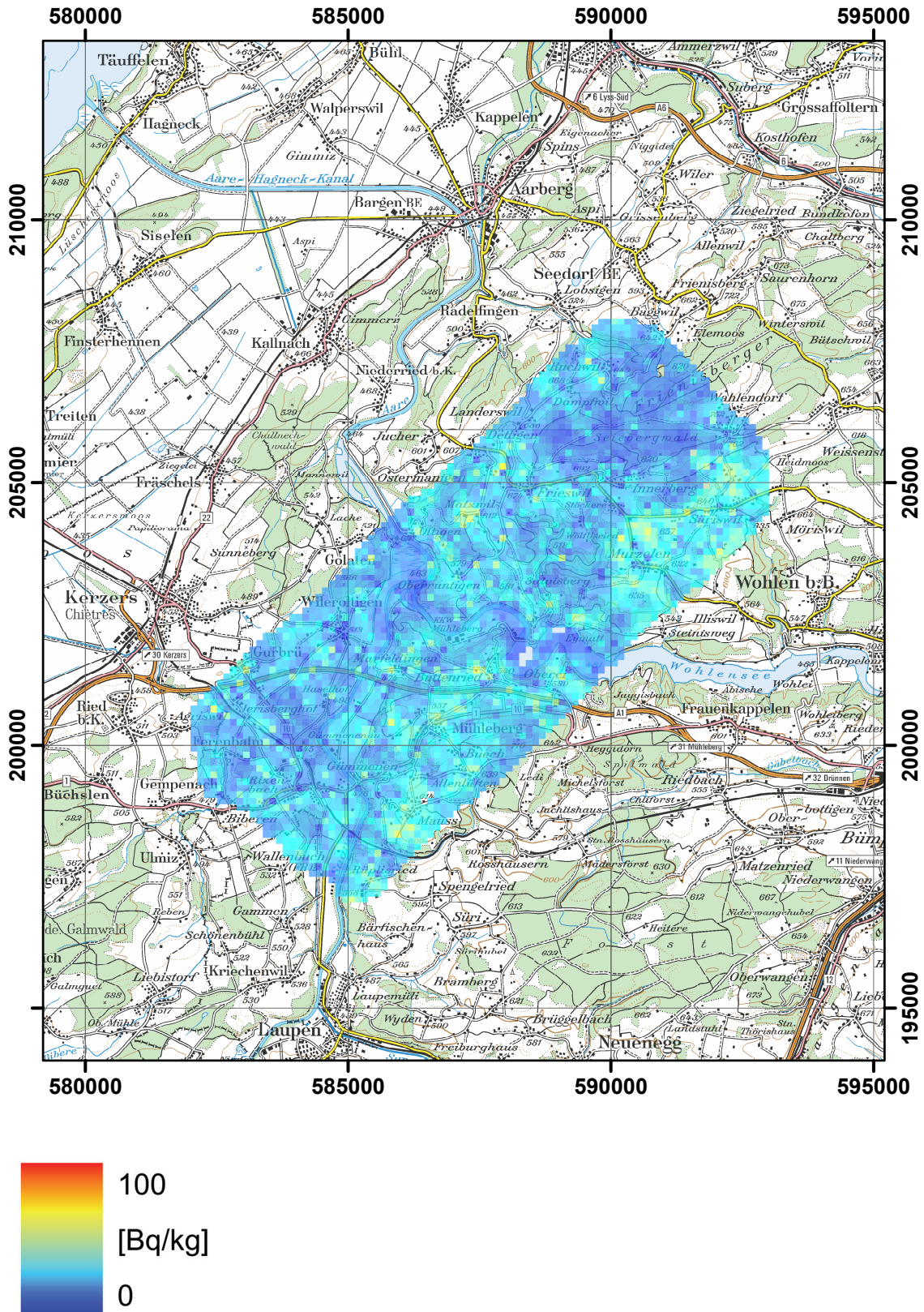
**Figure 65: $^{232}$Th activity concentration measured by the German team in the environs of KKM nuclear power plant. PK100©2008 swisstopo.**
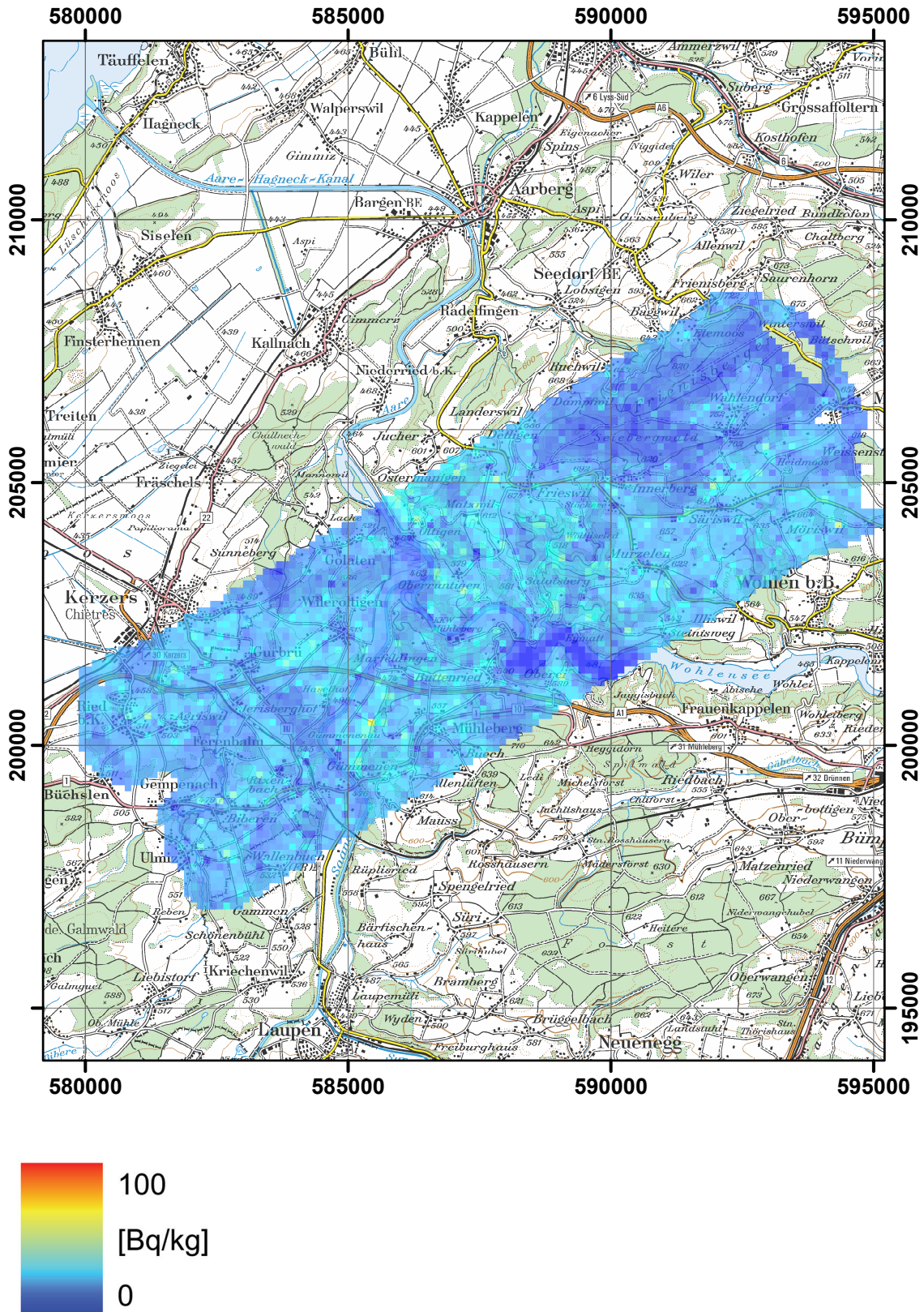
**Figure 66: <sup>232</sup>Th activity concentration measured by the Swiss team in the environs of KKM nuclear power plant. PK100©2008 swisstopo.**

82
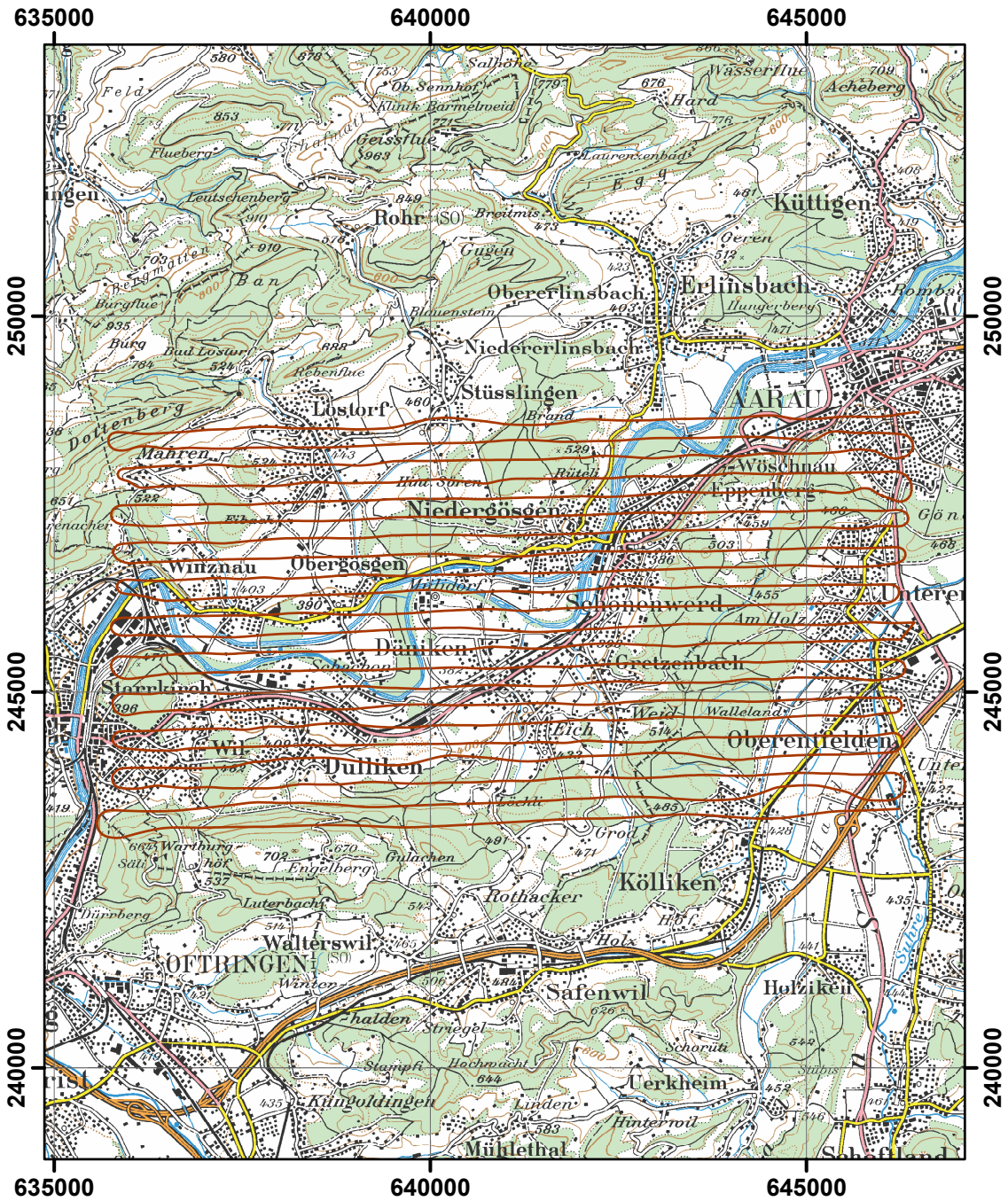


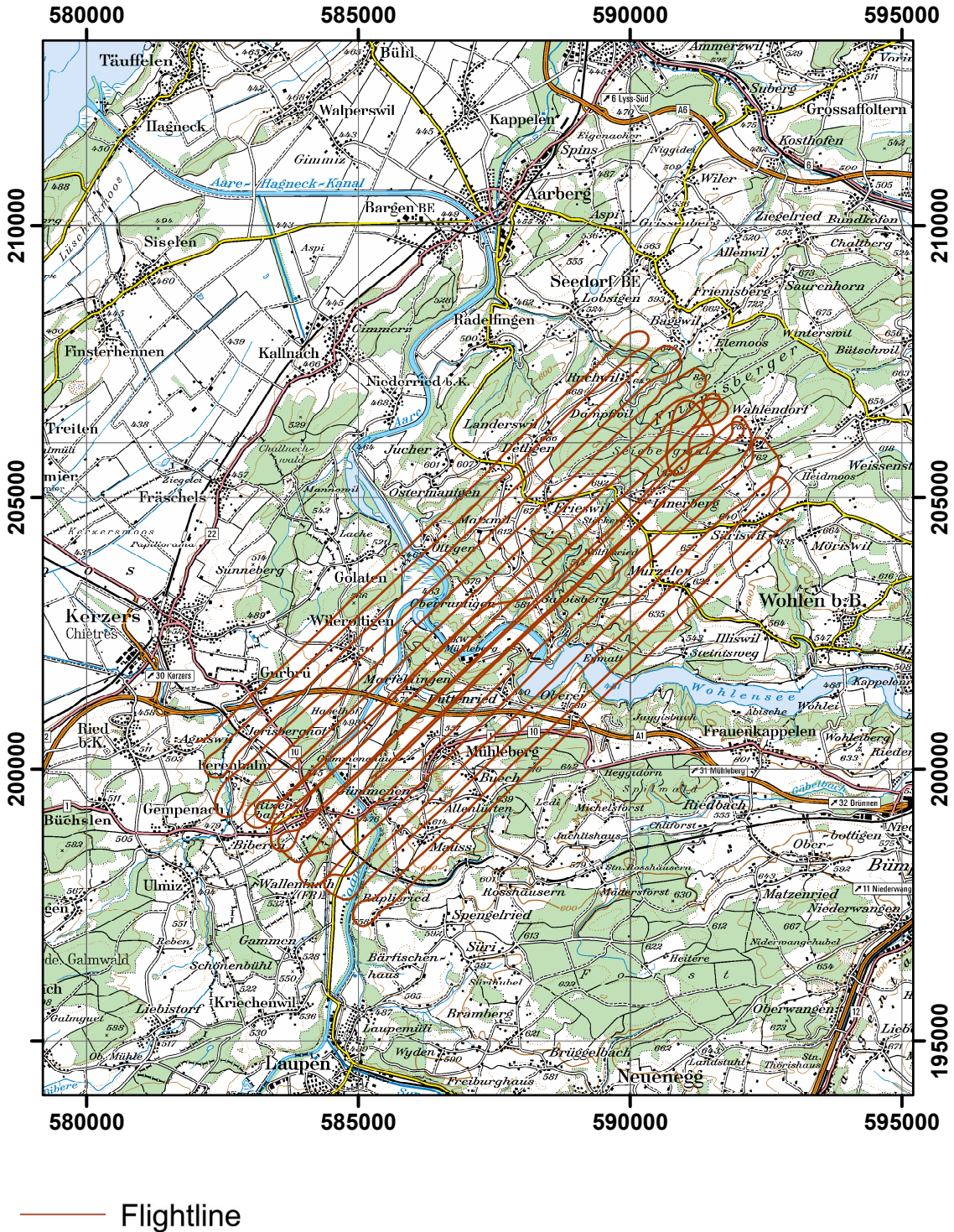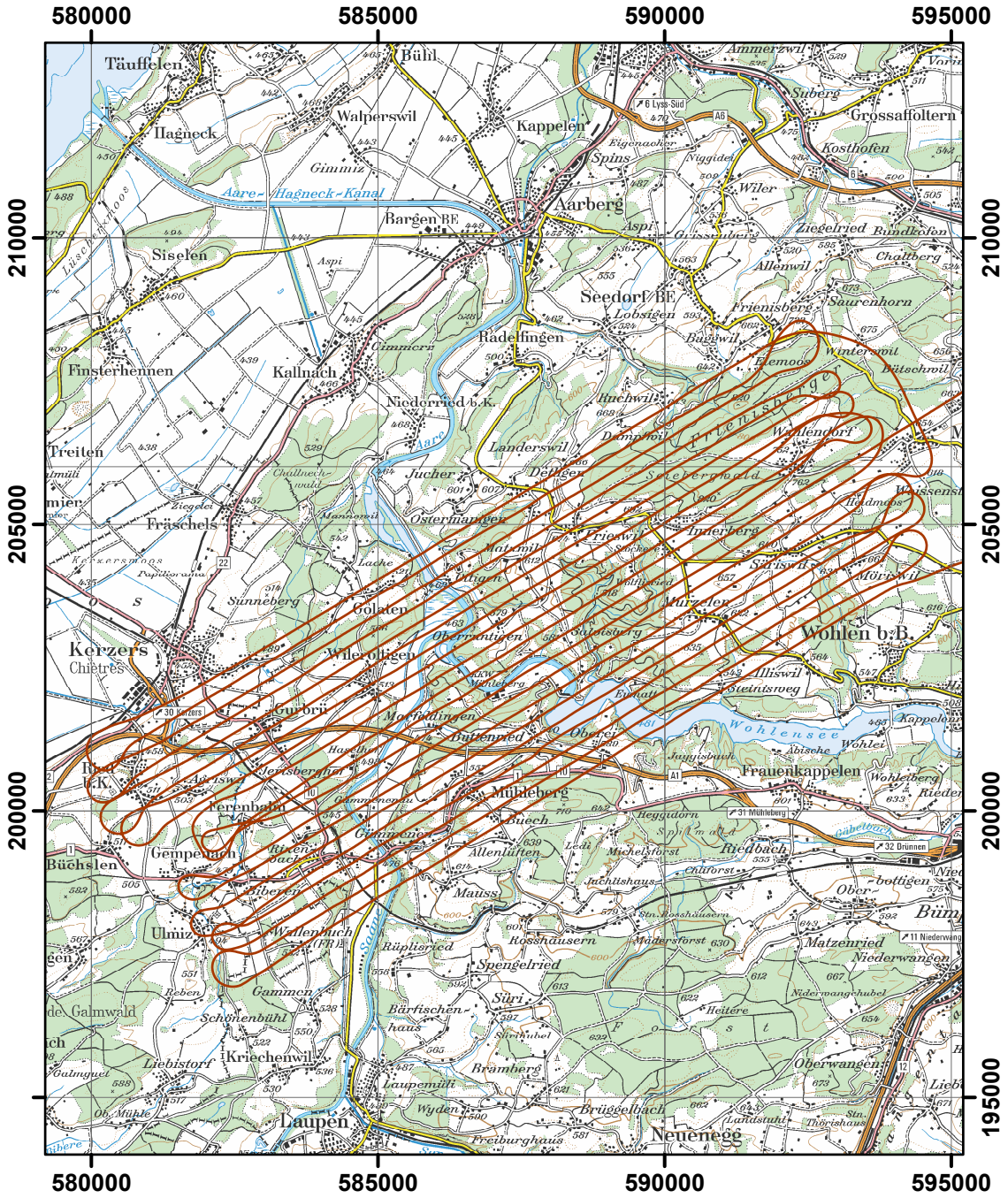**Figure 67: Flightlines of the French team in the environs of KKG nuclear power plant. PK100©2003 swisstopo.**
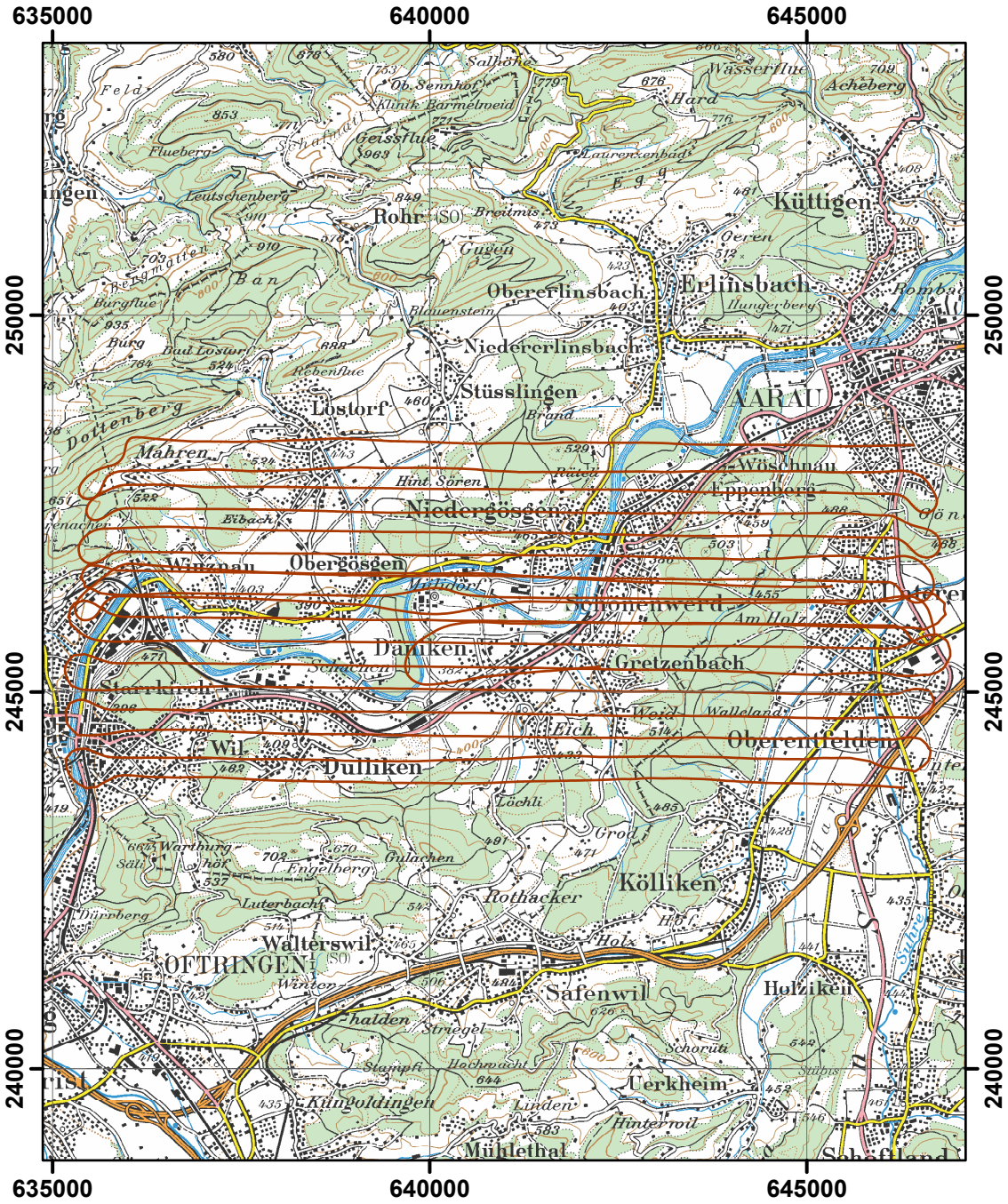
**Figure 68: Flightlines of the German team in the environs of KKG nuclear power plant. PK100©2003 swisstopo.**
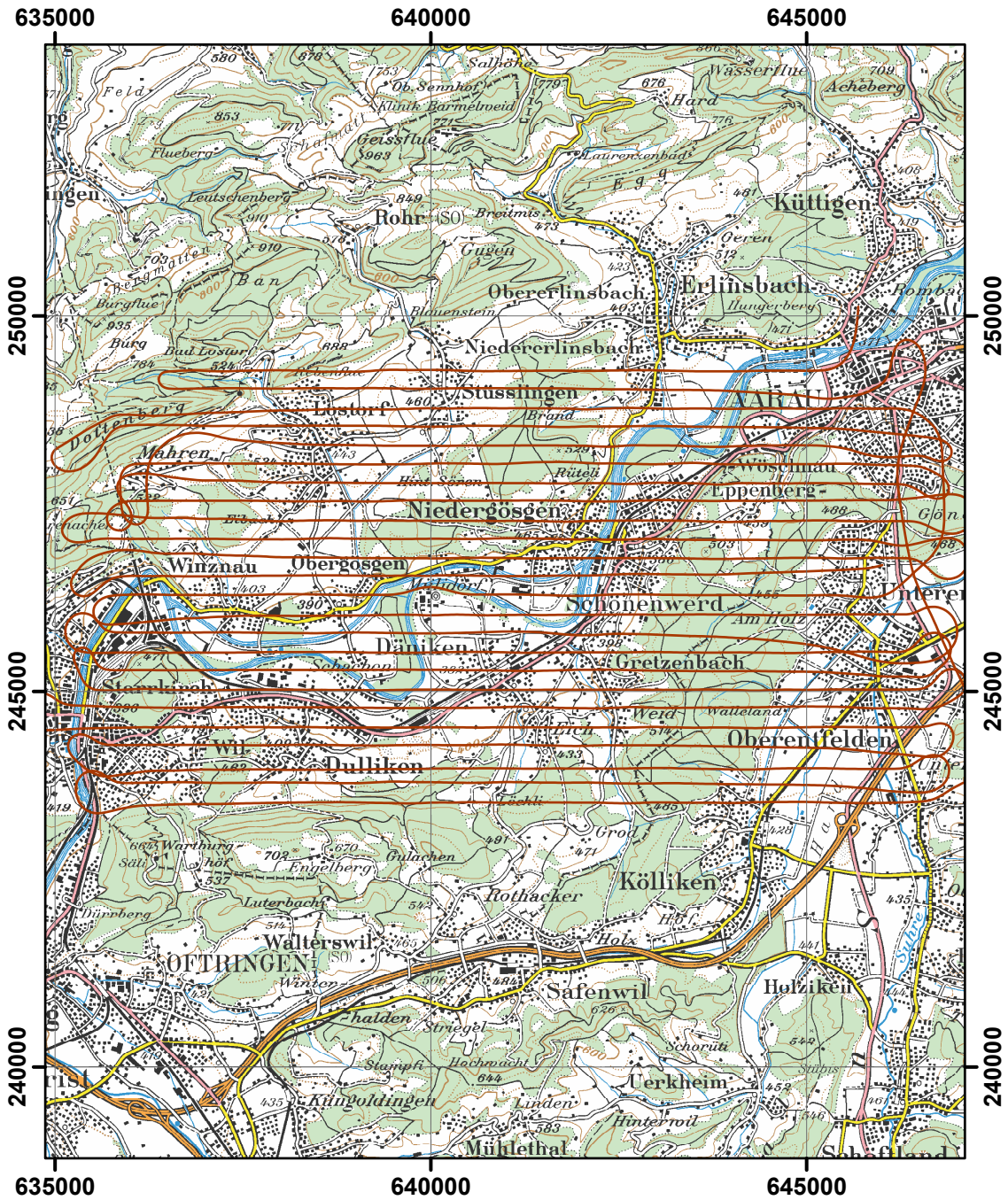
**Figure 69: Flightlines of the Swiss team in the environs of KKG nuclear power plant. PK100©2003 swisstopo.**
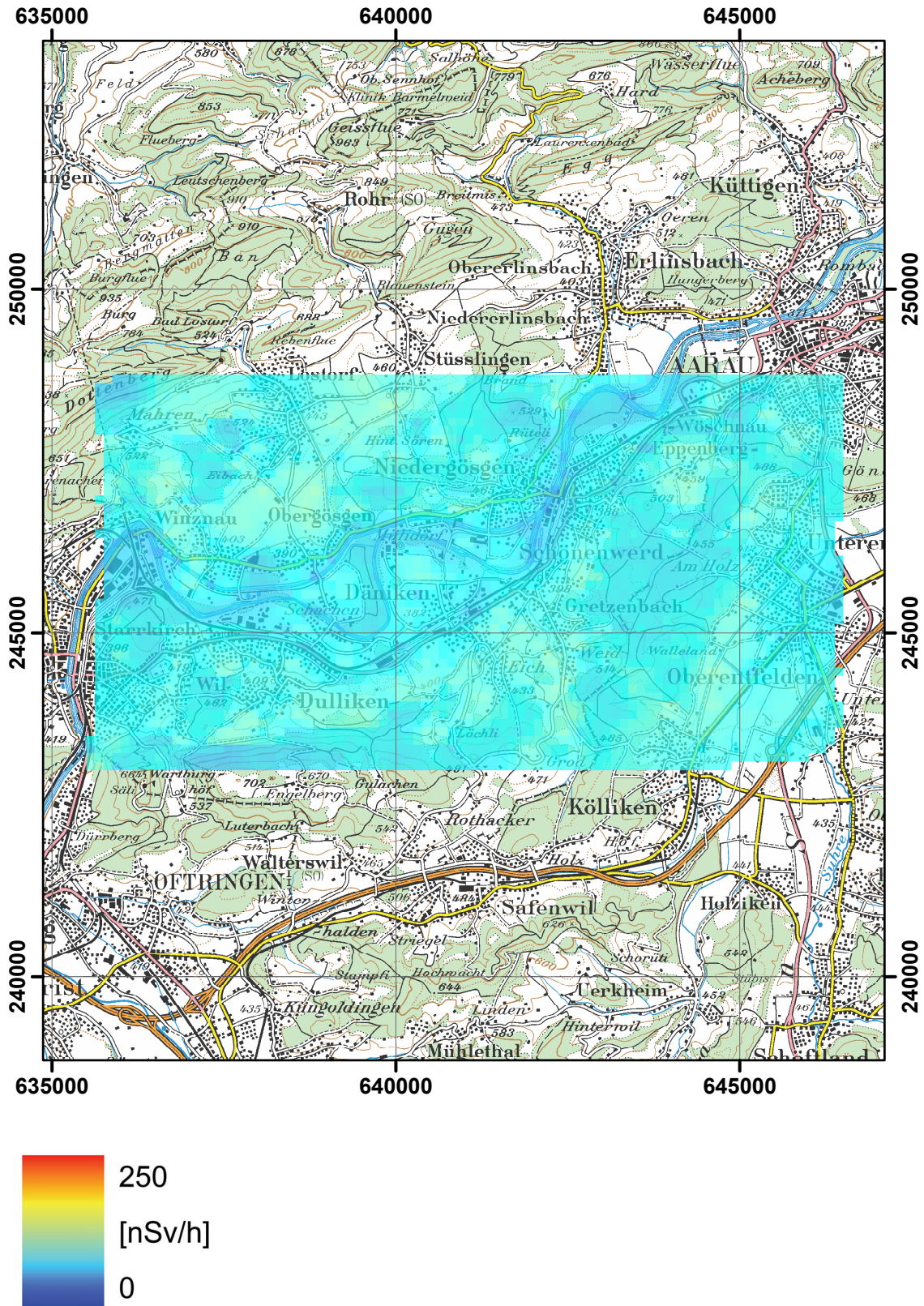
Figure 70: Total dose rate measured by the French team in the environs of KKG nuclear power plant. PK100©2003 swisstopo.
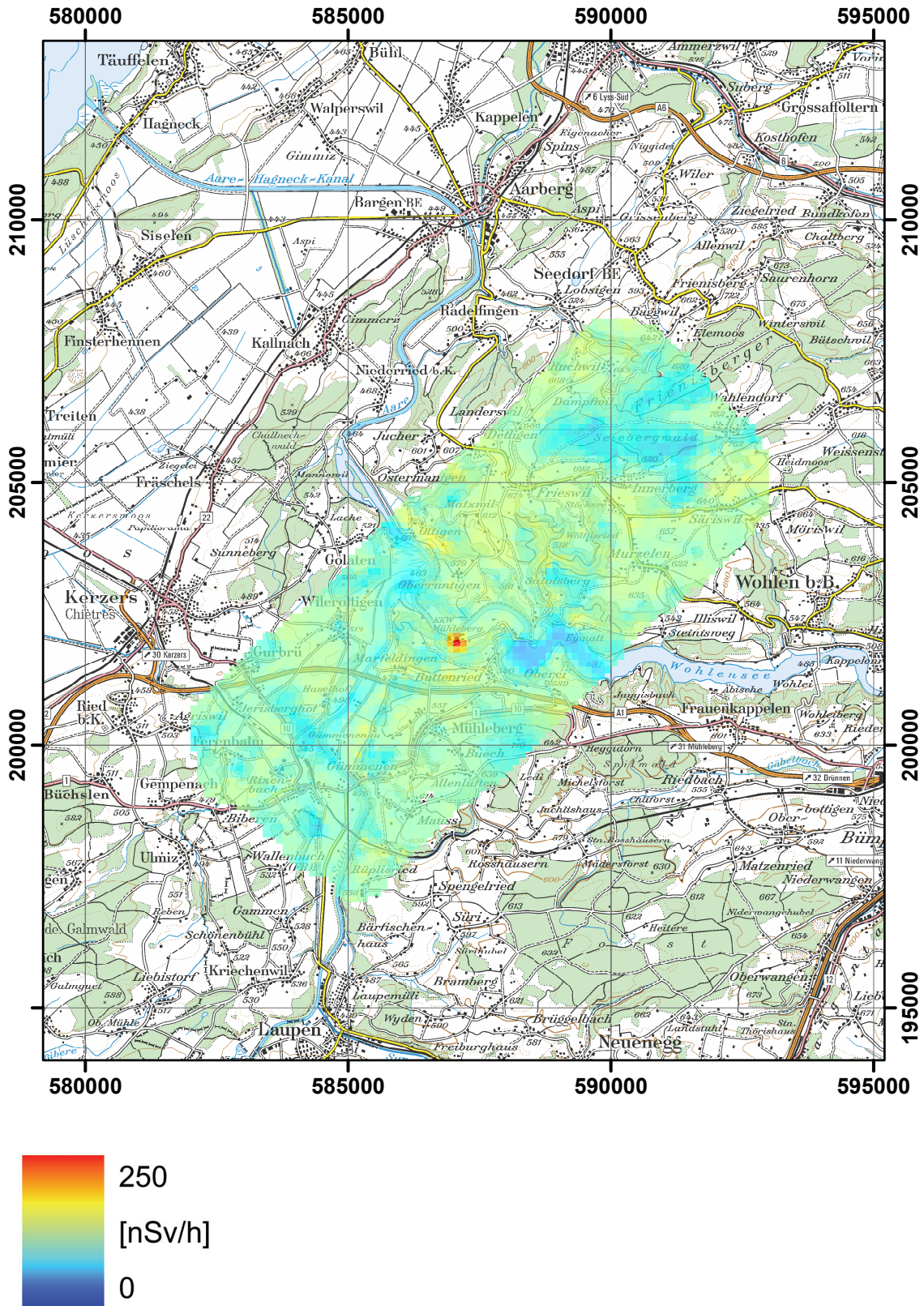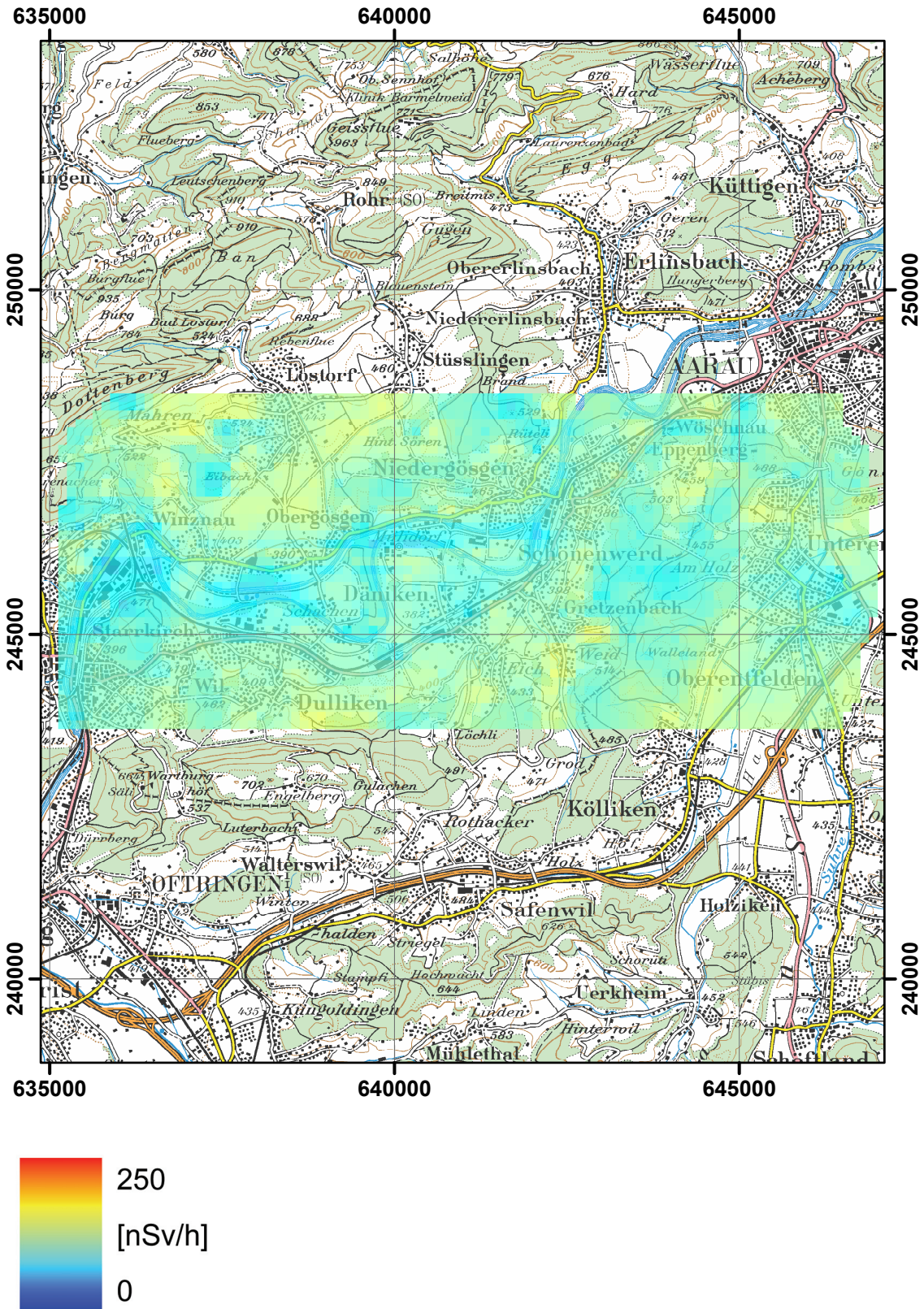
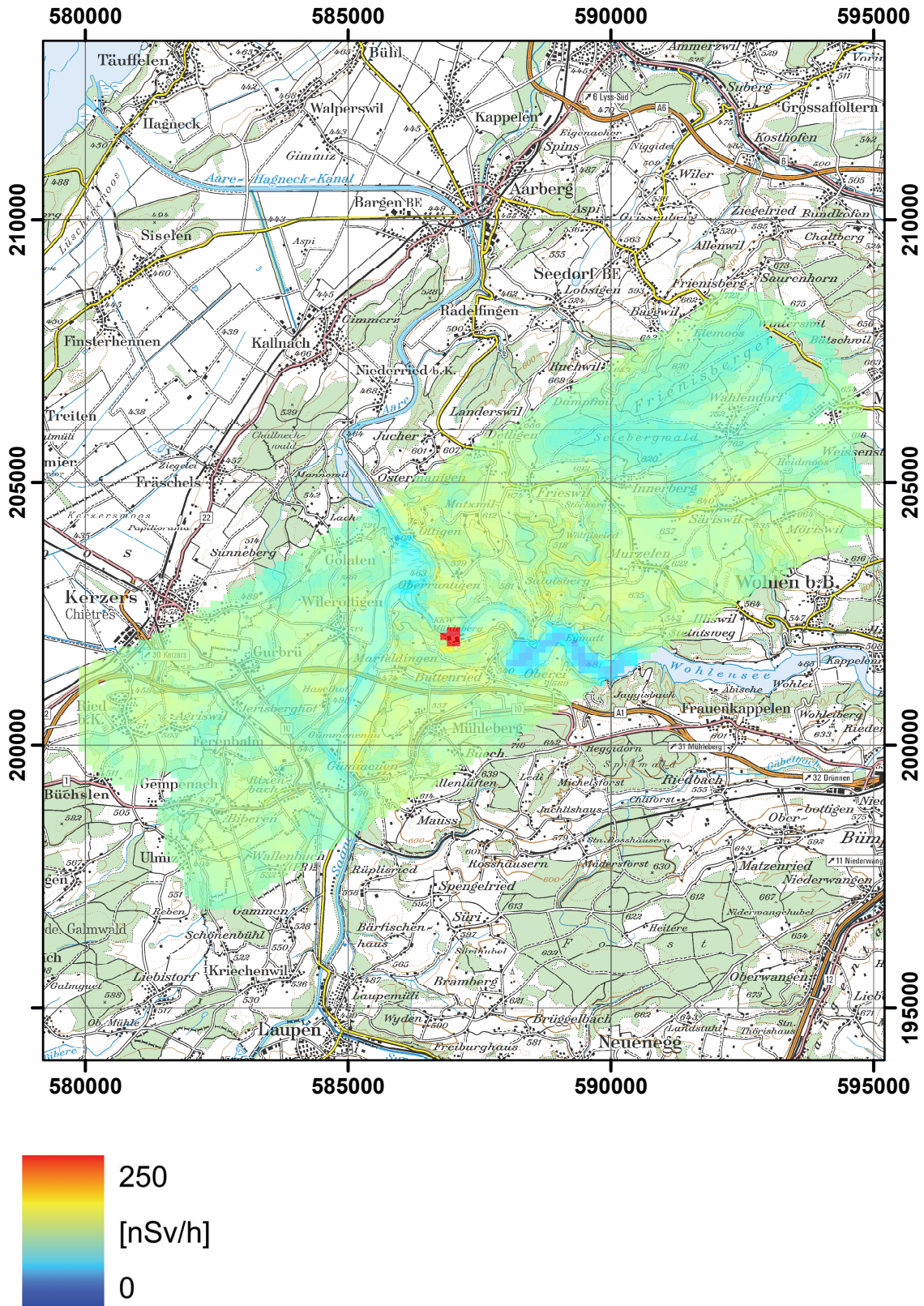**Figure 71: Total dose rate measured by the German team in the environs of KKG nuclear power plant. PK100©2003 swisstopo.**
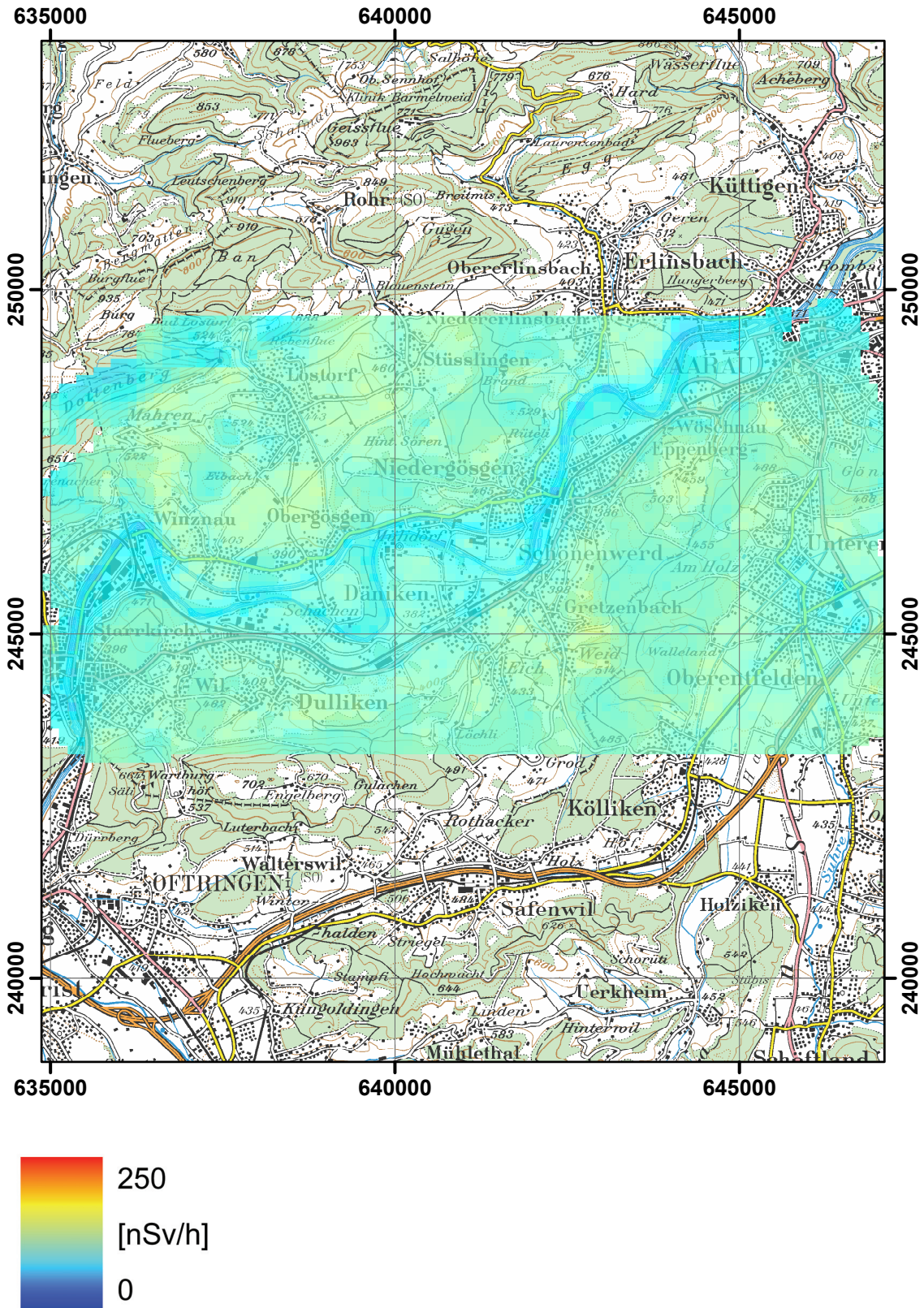
**Figure 72: Total dose rate measured by the Swiss team in the environs of KKG nuclear power plant. PK100©2003 swisstopo.**
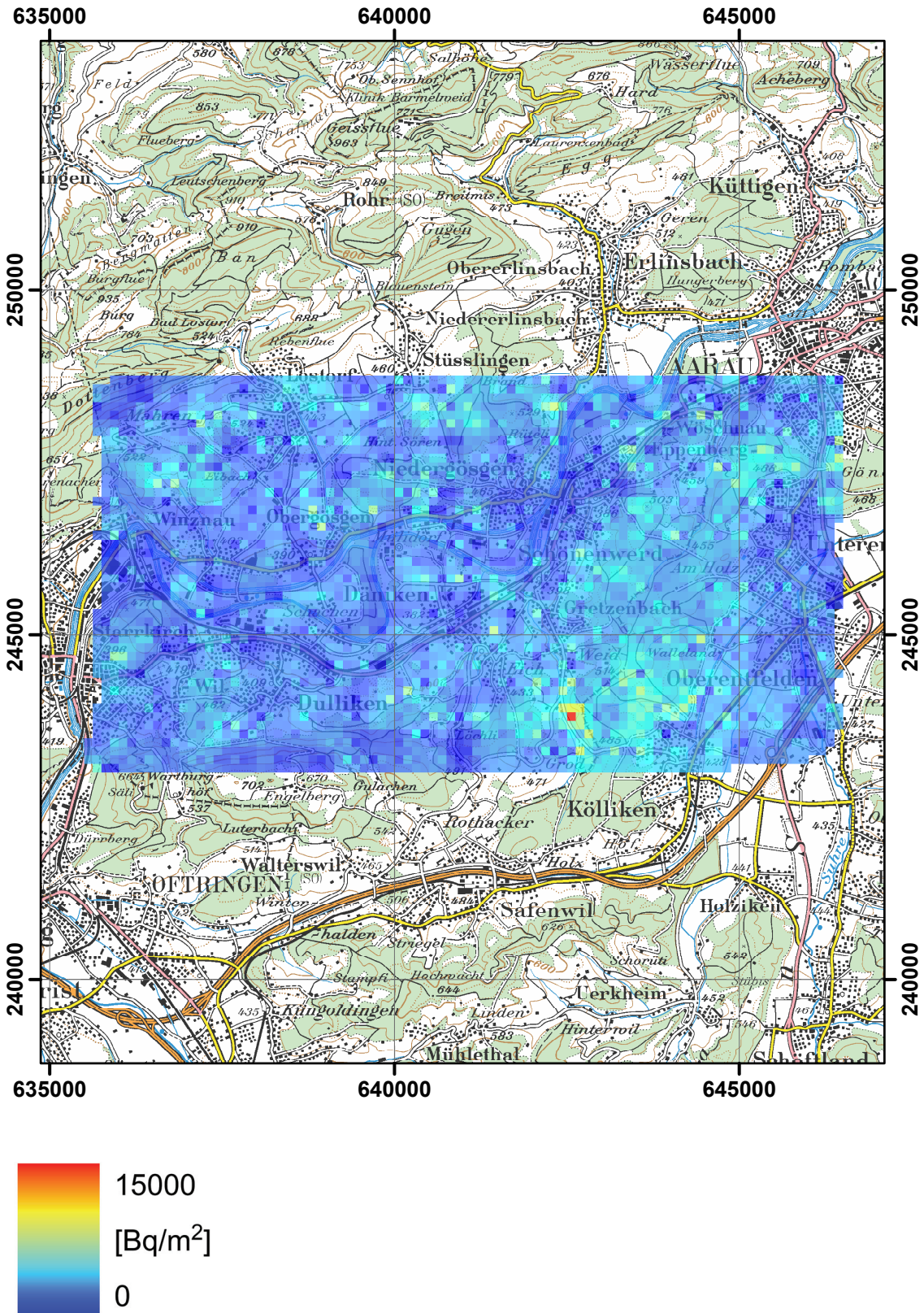
**Figure 73: $^{137}$Cs activity concentration measured by the French team in the environs of KKG nuclear power plant. PK100©2003 swisstopo.**
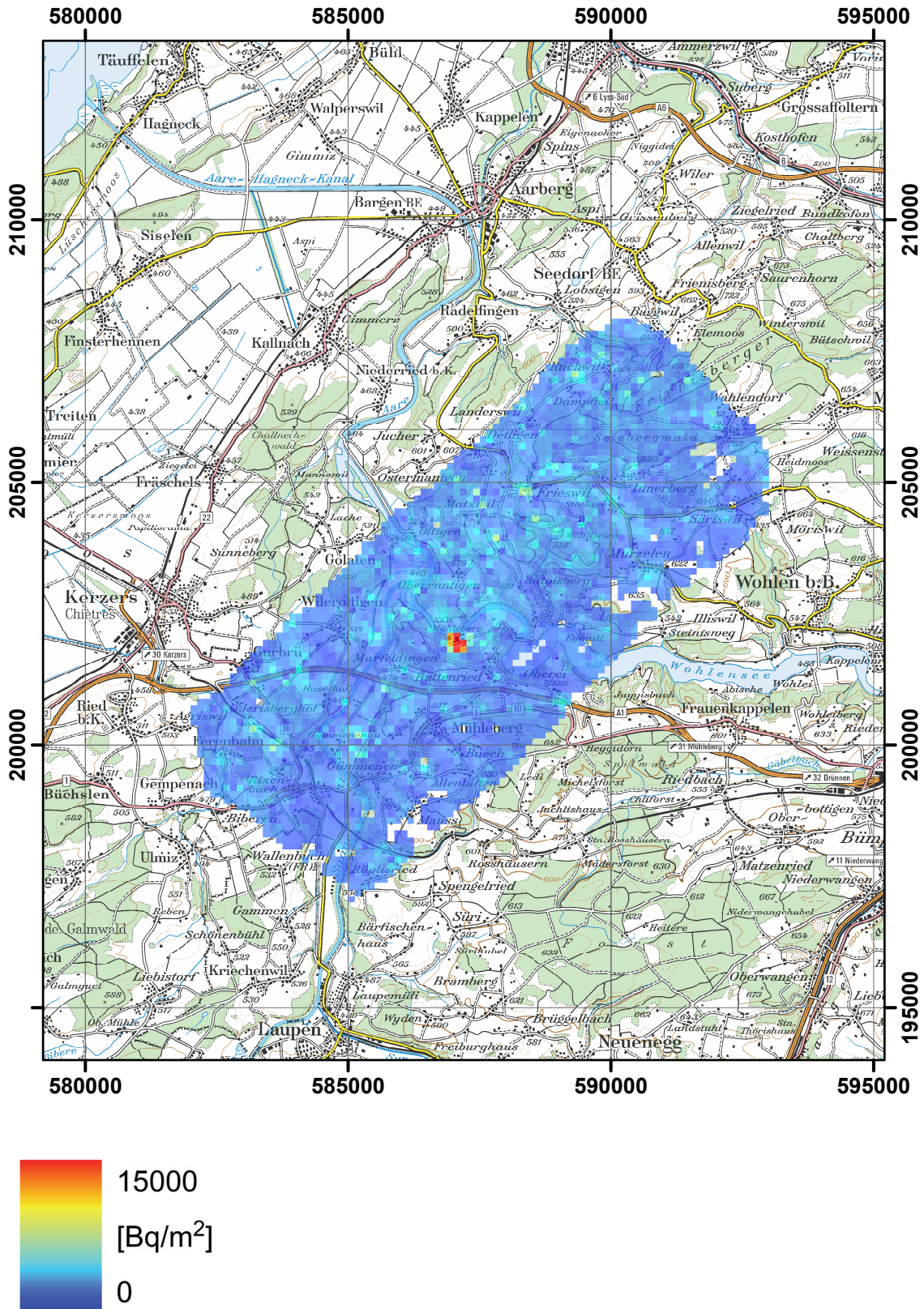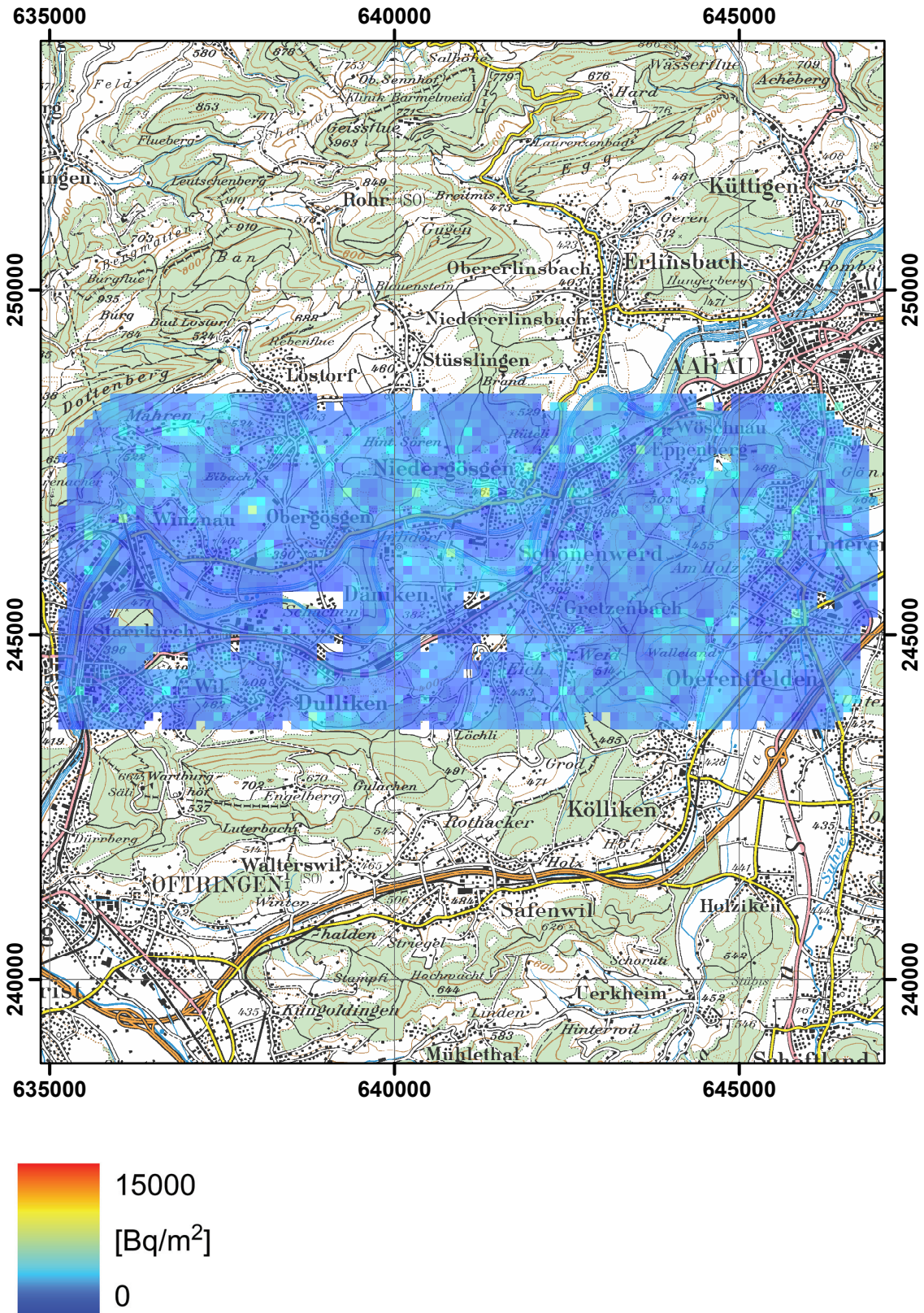
**Figure 74: $^{137}$Cs activity concentration measured by the German team in the environs of KKG nuclear power plant. PK100©2003 swisstopo.**
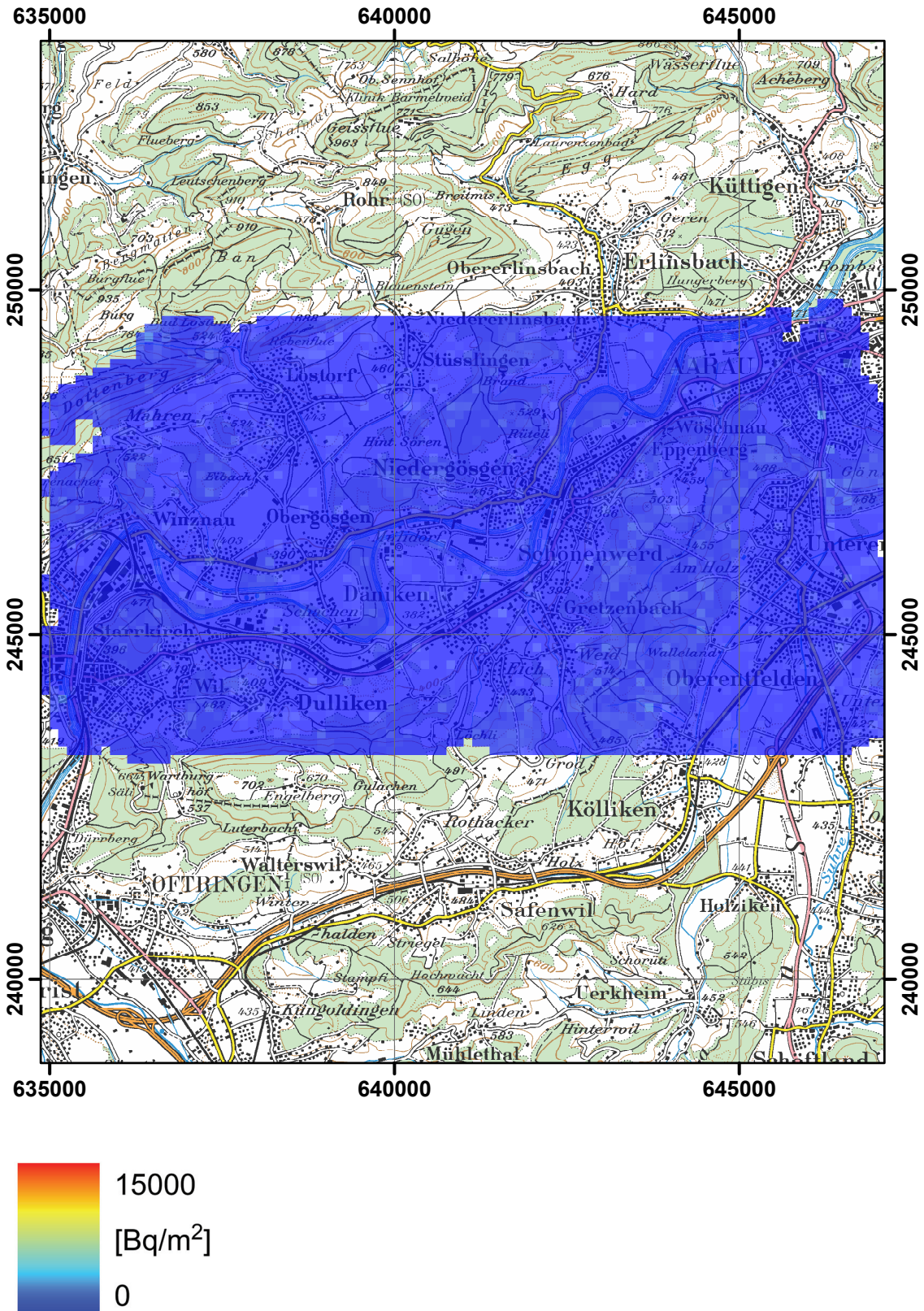
**Figure 75: $^{137}$Cs activity concentration measured by the Swiss team in the environs of KKG nuclear power plant. PK100©2003 swisstopo.**
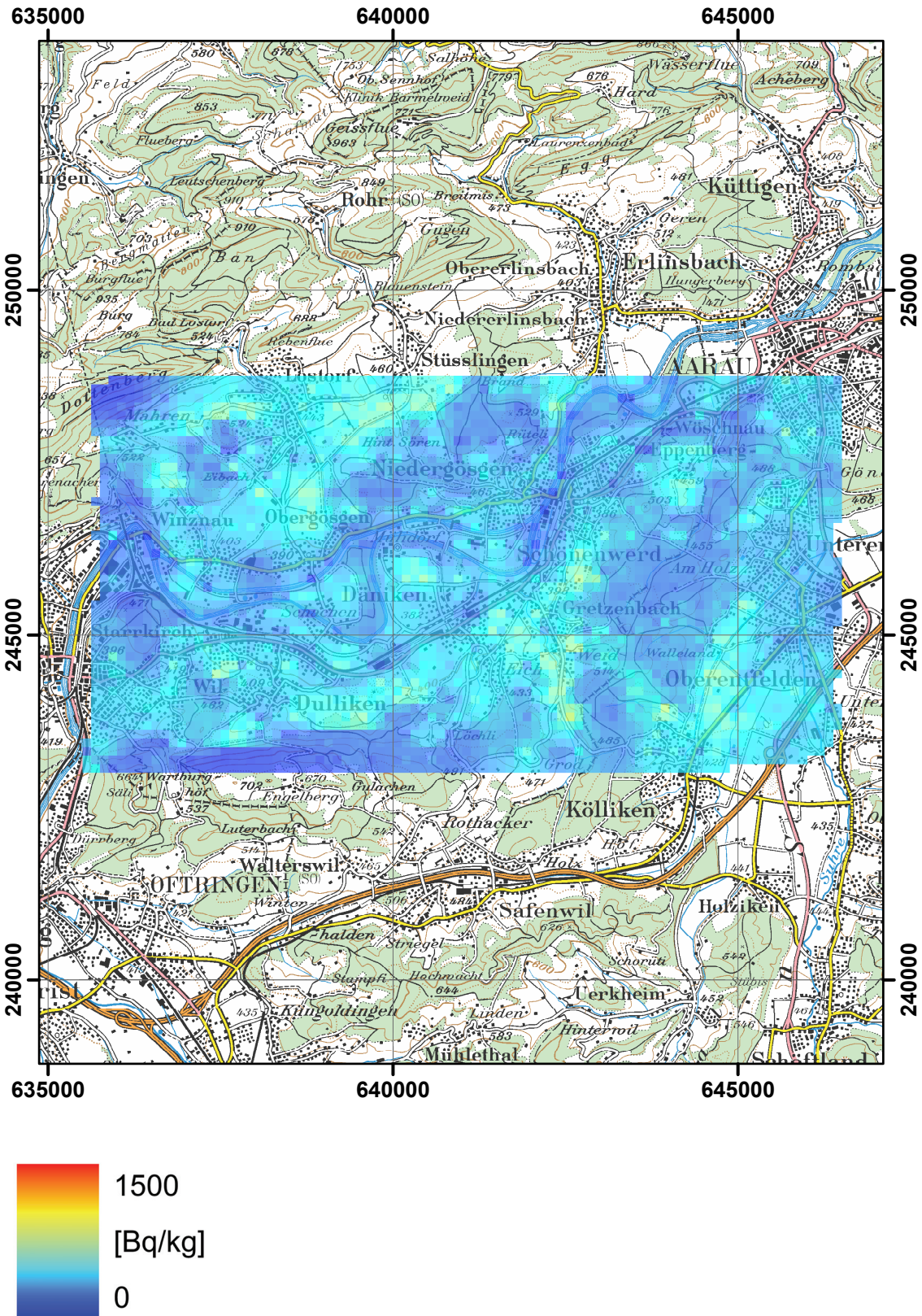
**Figure 76: $^{40}$K activity concentration measured by the French team in the environs of KKG nuclear power plant. PK100©2003 swisstopo.**
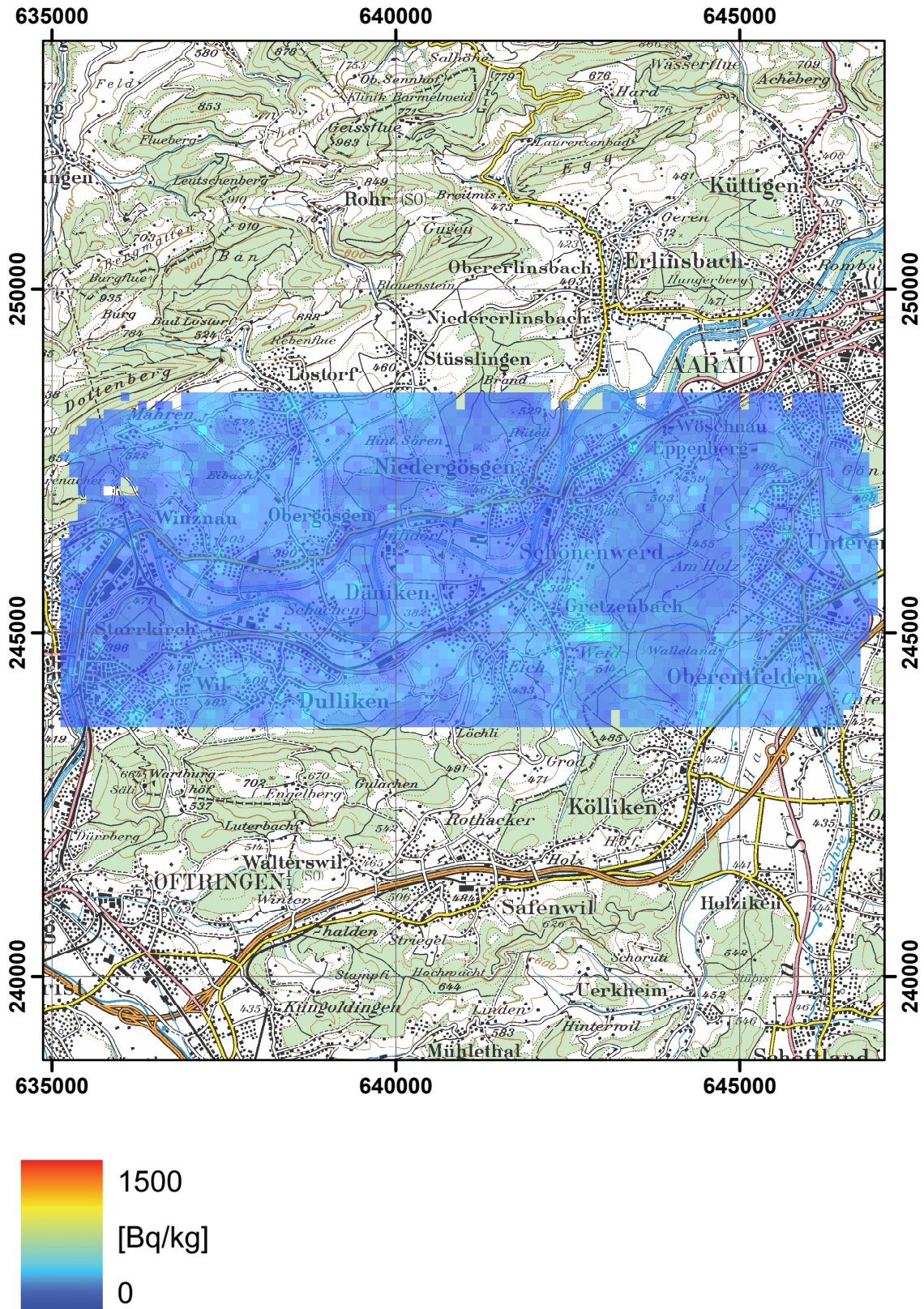
**Figure 77: $^{40}$K activity concentration measured by the German team in the environs of KKG nuclear power plant. PK100©2003 swisstopo.**
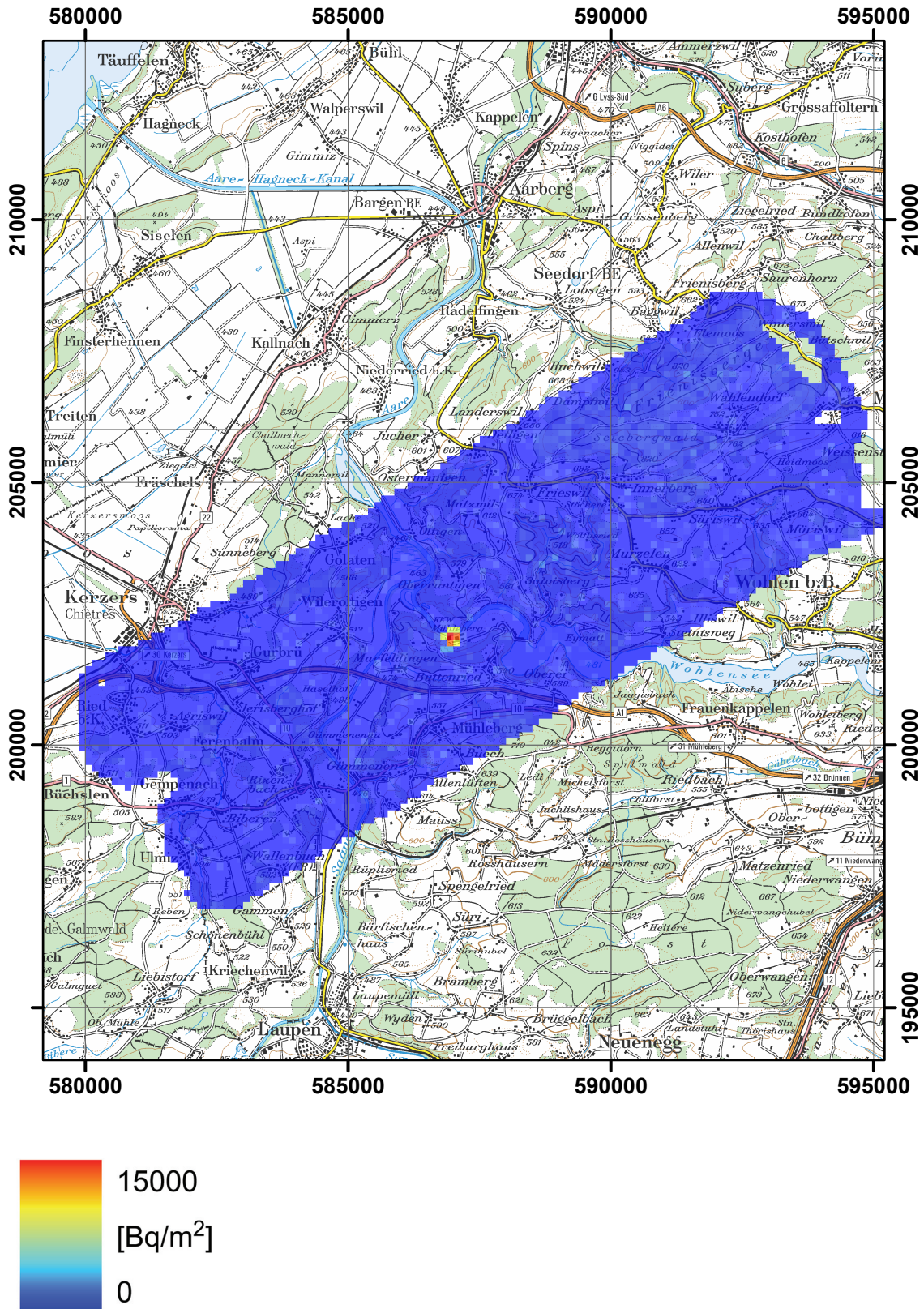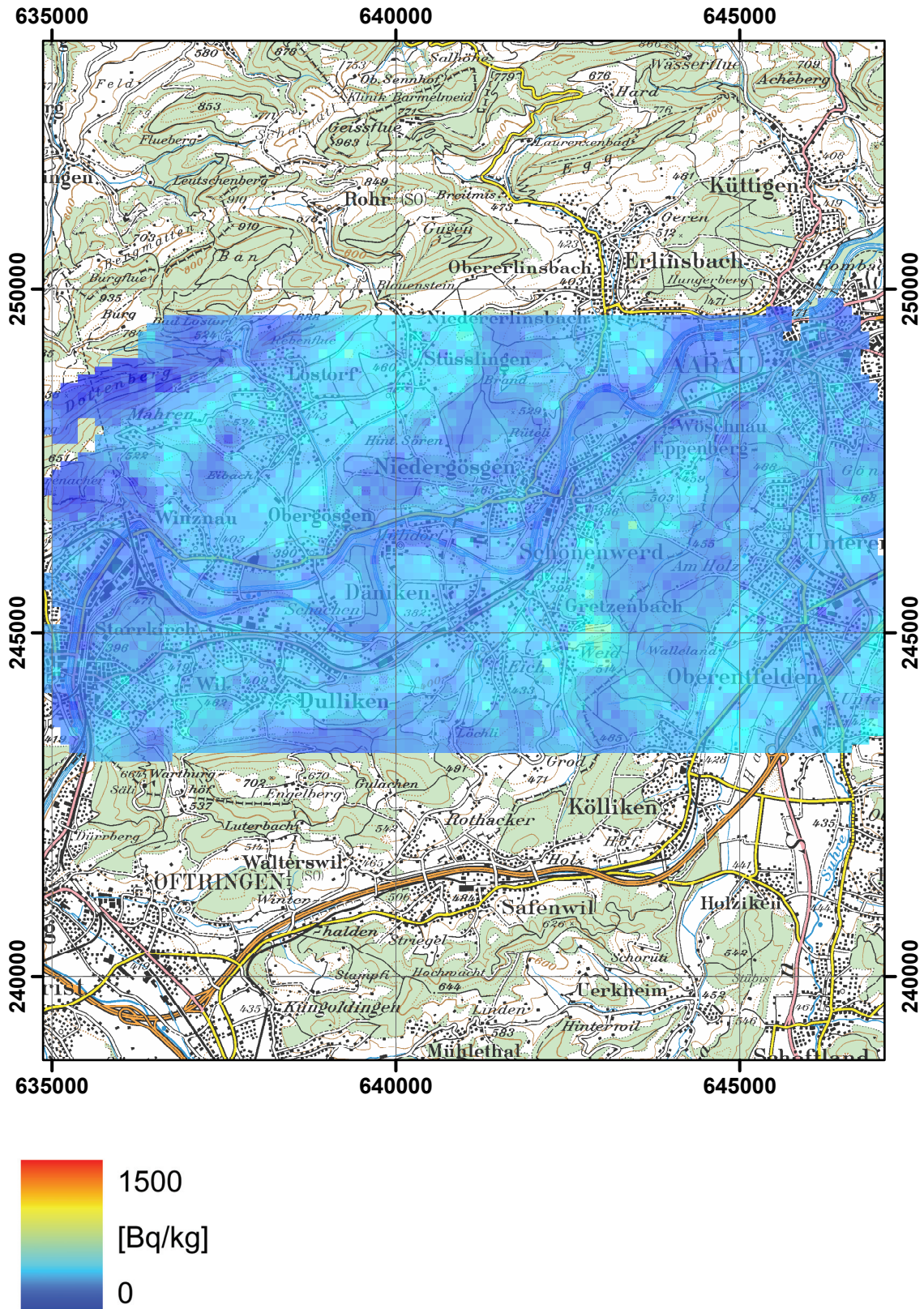
Figure 78: <sup>40</sup>K activity concentration measured by the Swiss team in the environs of KKG nuclear power plant. PK100©2003 swisstopo.
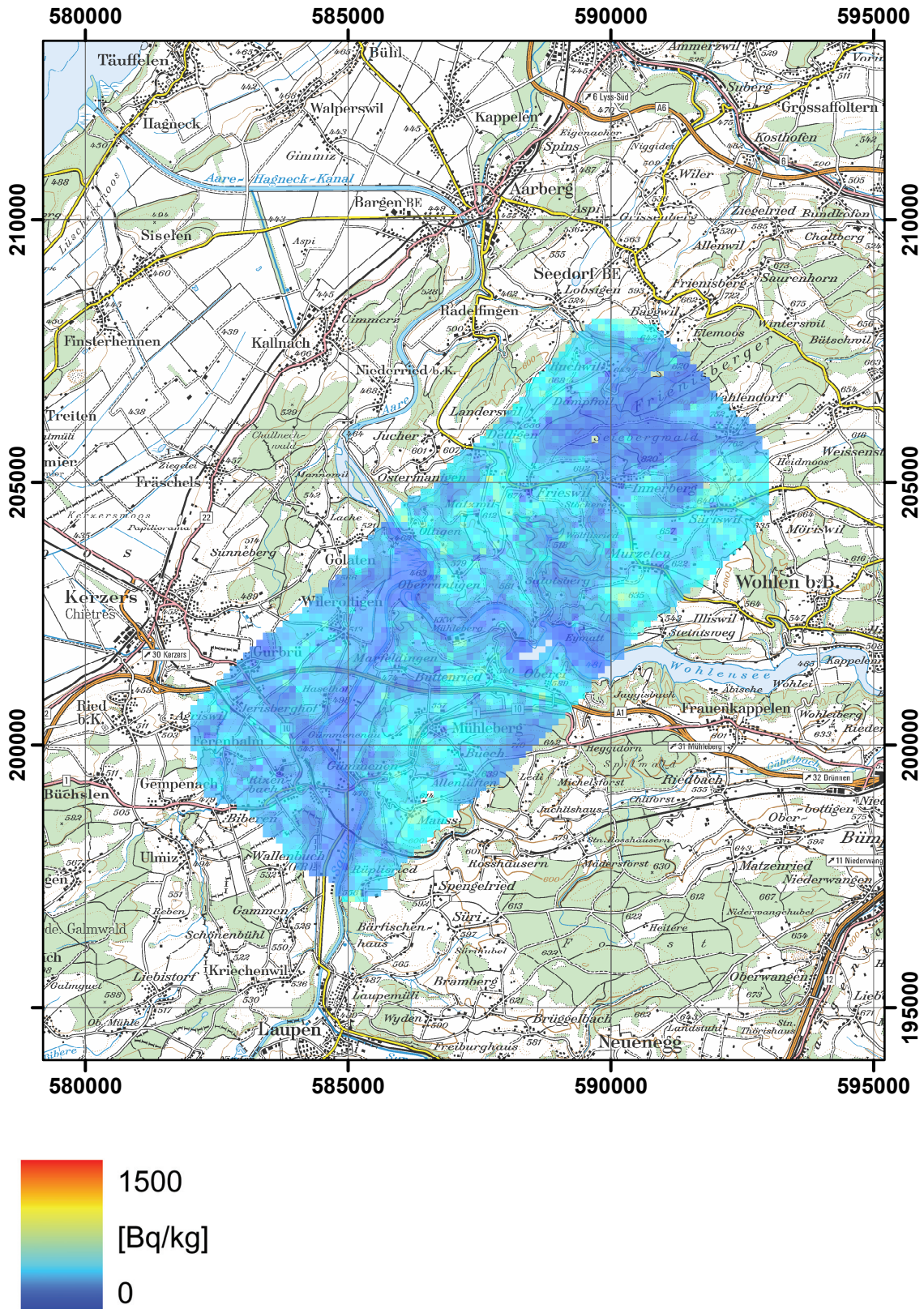
94
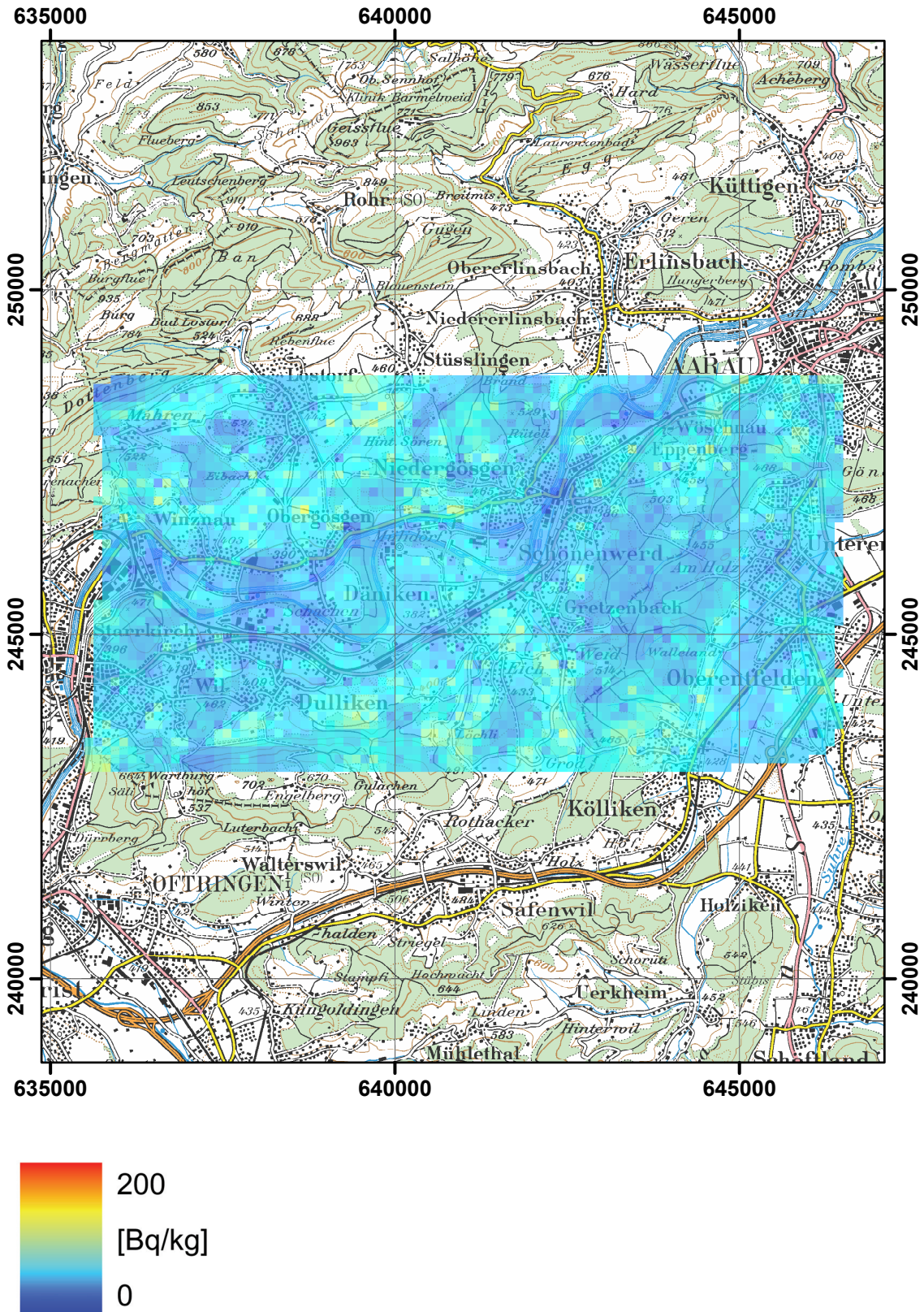


**Figure 79: $^{238}$U activity concentration measured by the French team in the environs of KKG nuclear power plant. PK100©2003 swisstopo.**
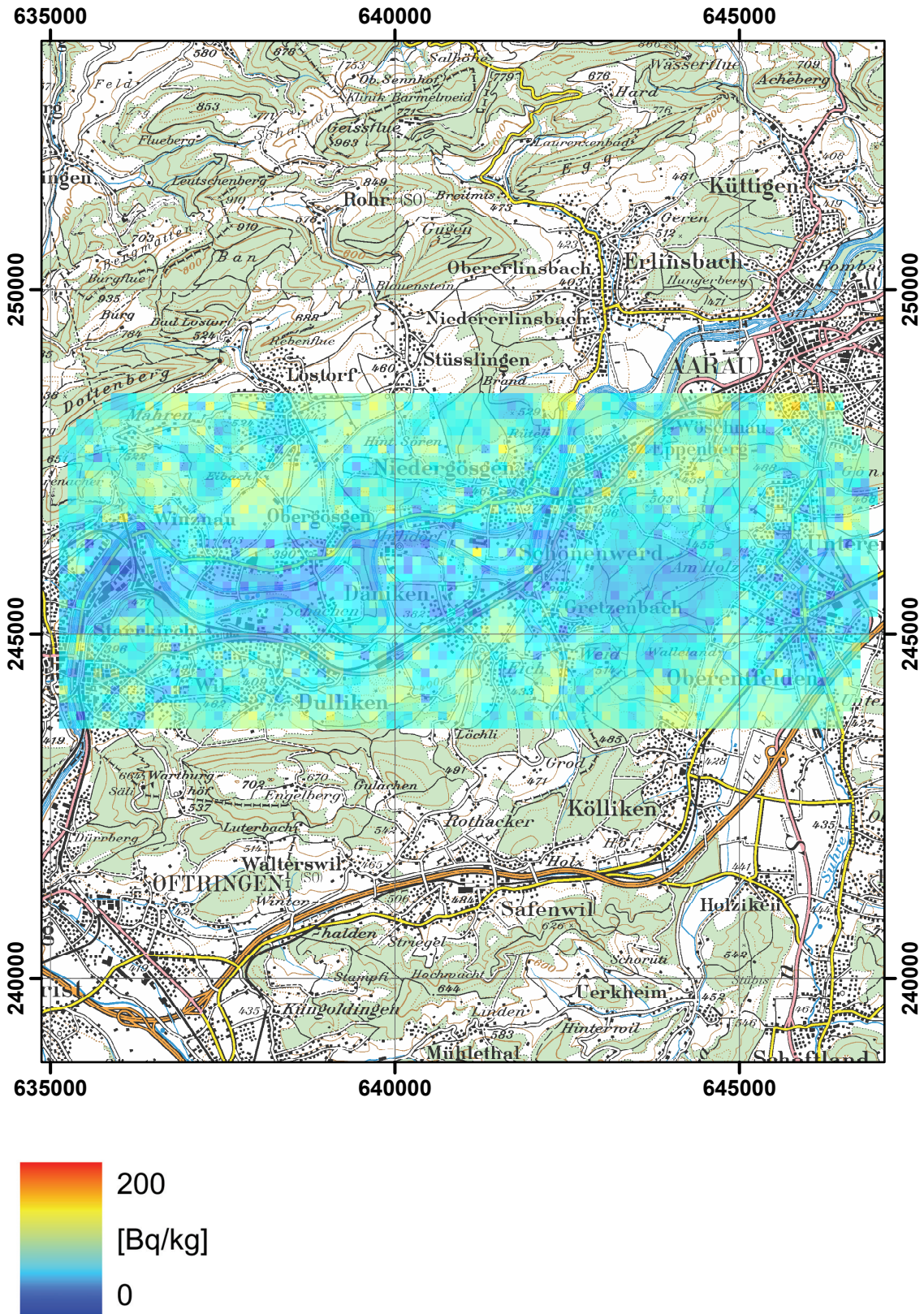
Figure 80: $^{238}$U activity concentration measured by the German team in the environs of KKG nuclear power plant. PK100©2003 swisstopo.
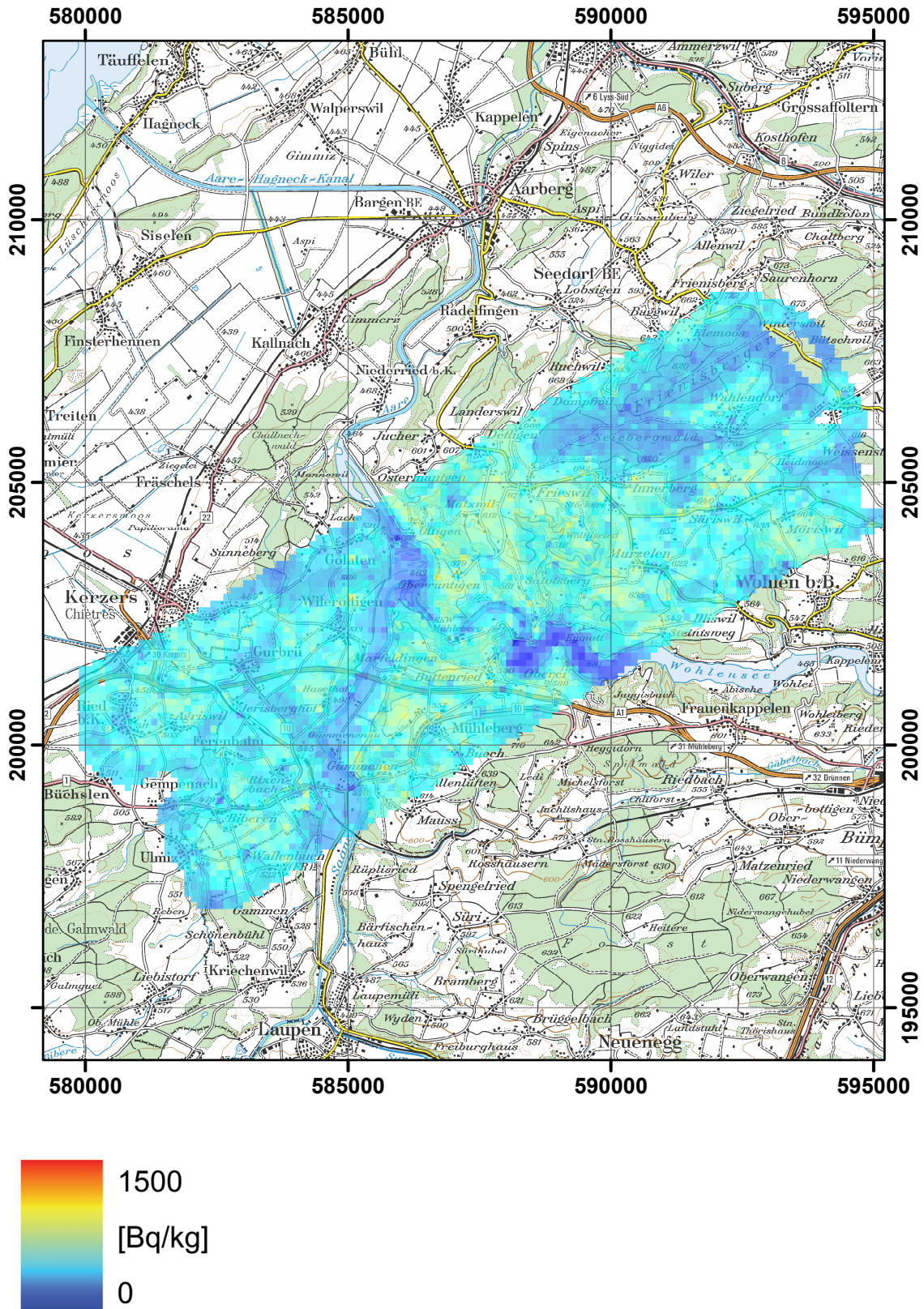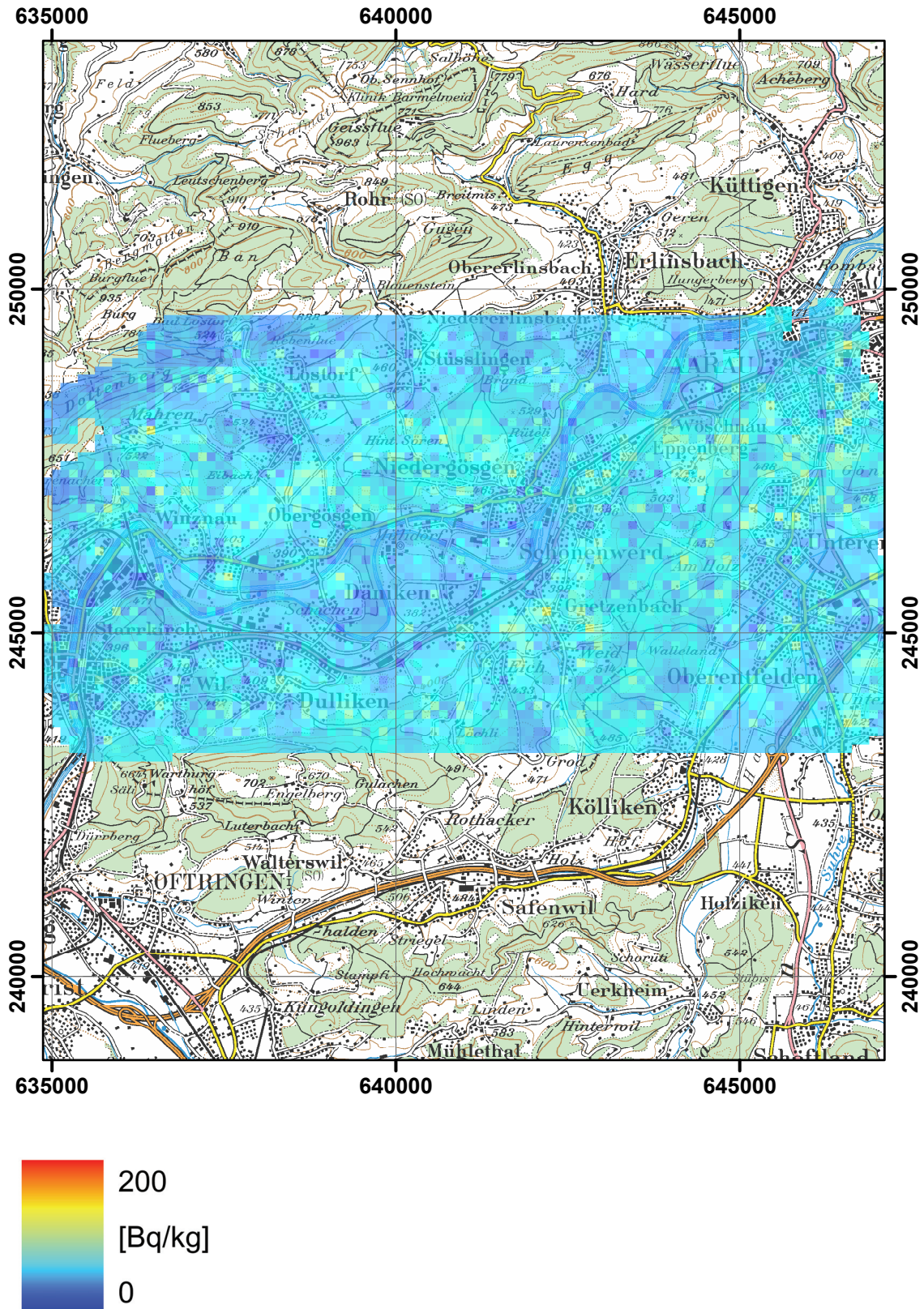
**Figure 81: $^{238}$U activity concentration measured by the Swiss team in the environs of KKG nuclear power plant. PK100©2003 swisstopo.**
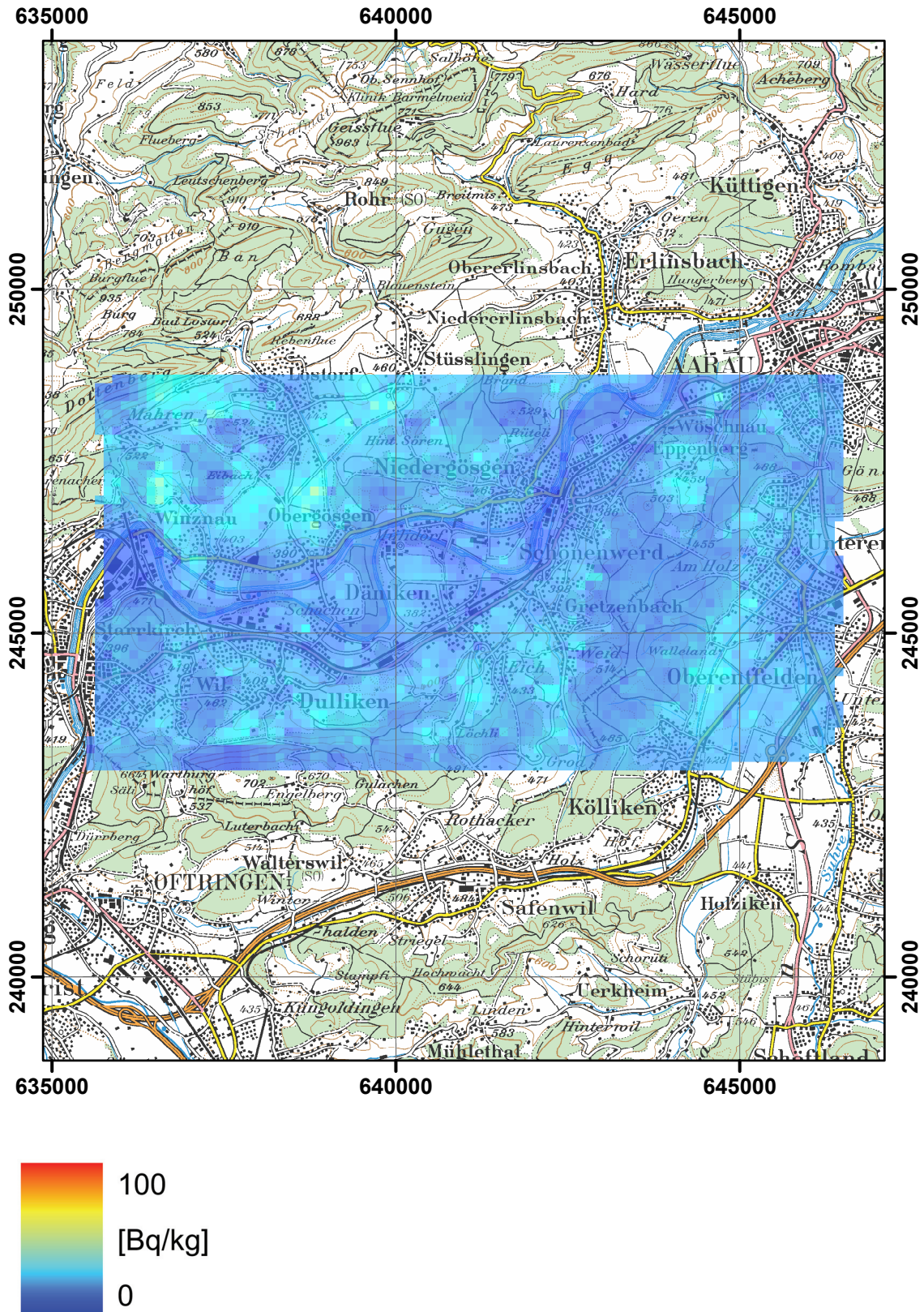
Figure 82: $^{232}$Th activity concentration measured by the French team in the environs of KKG nuclear power plant. PK100©2003 swisstopo.
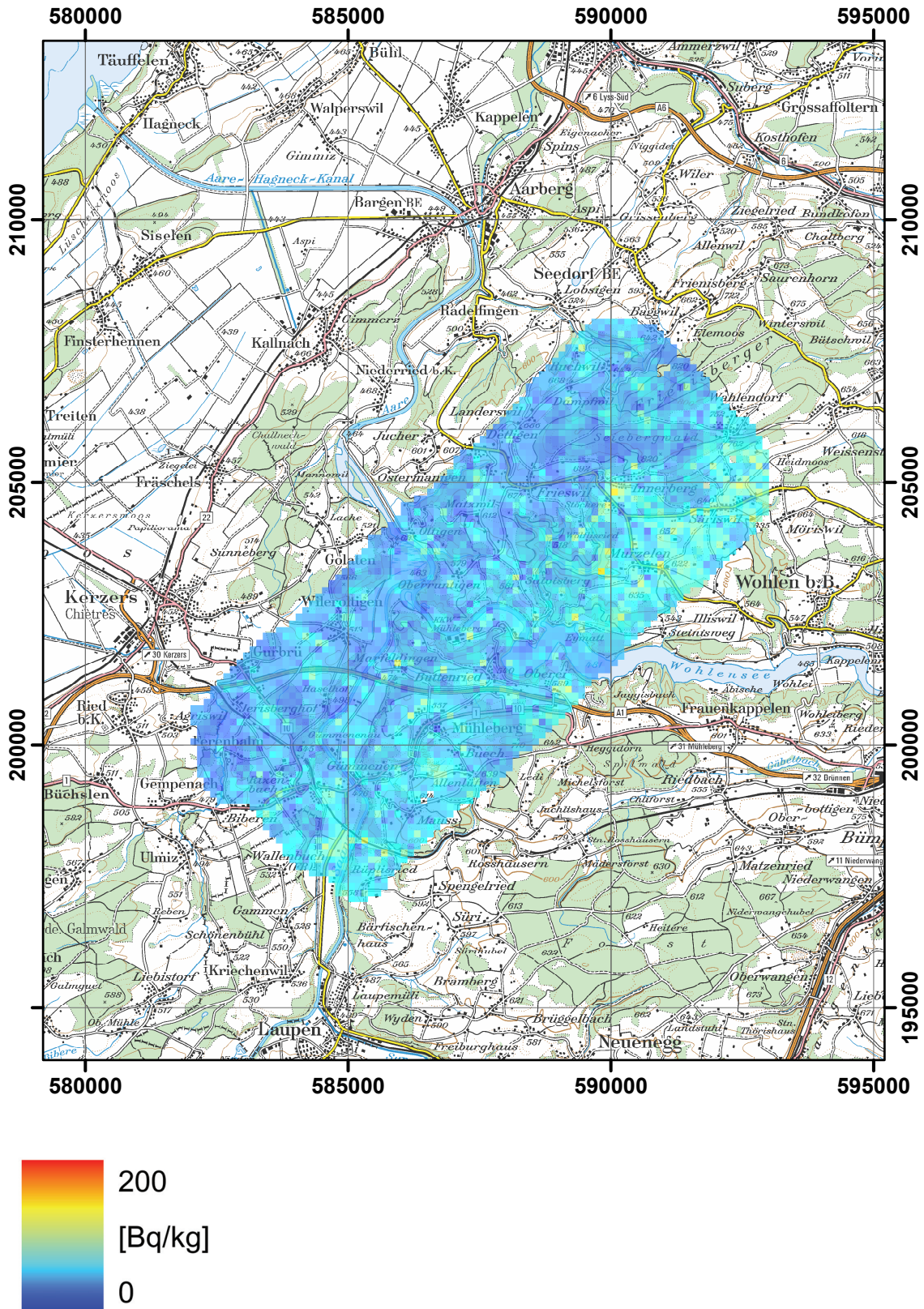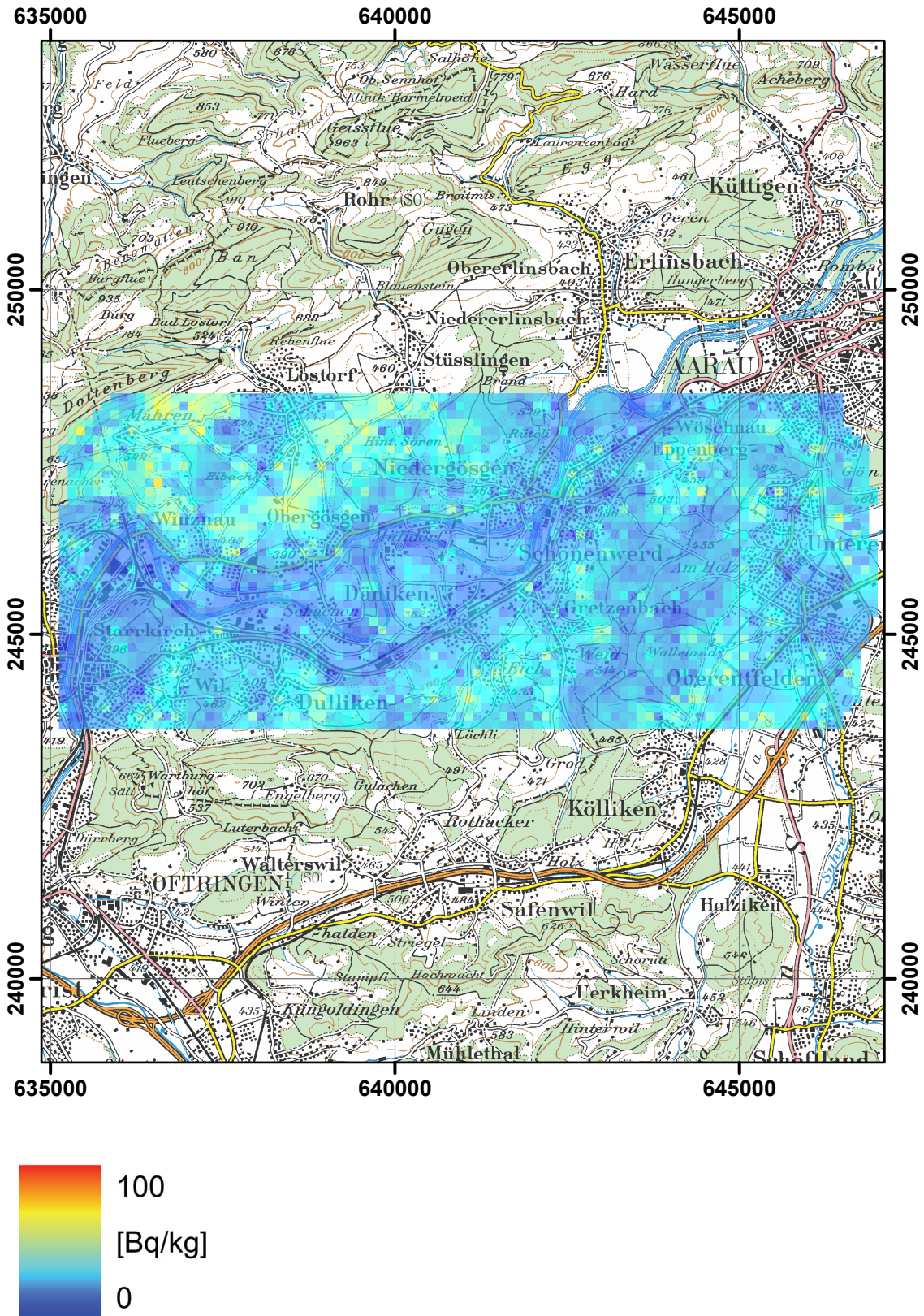
Figure 83: $^{232}$Th activity concentration measured by the German team in the environs of KKG nuclear power plant. PK100©2003 swisstopo.
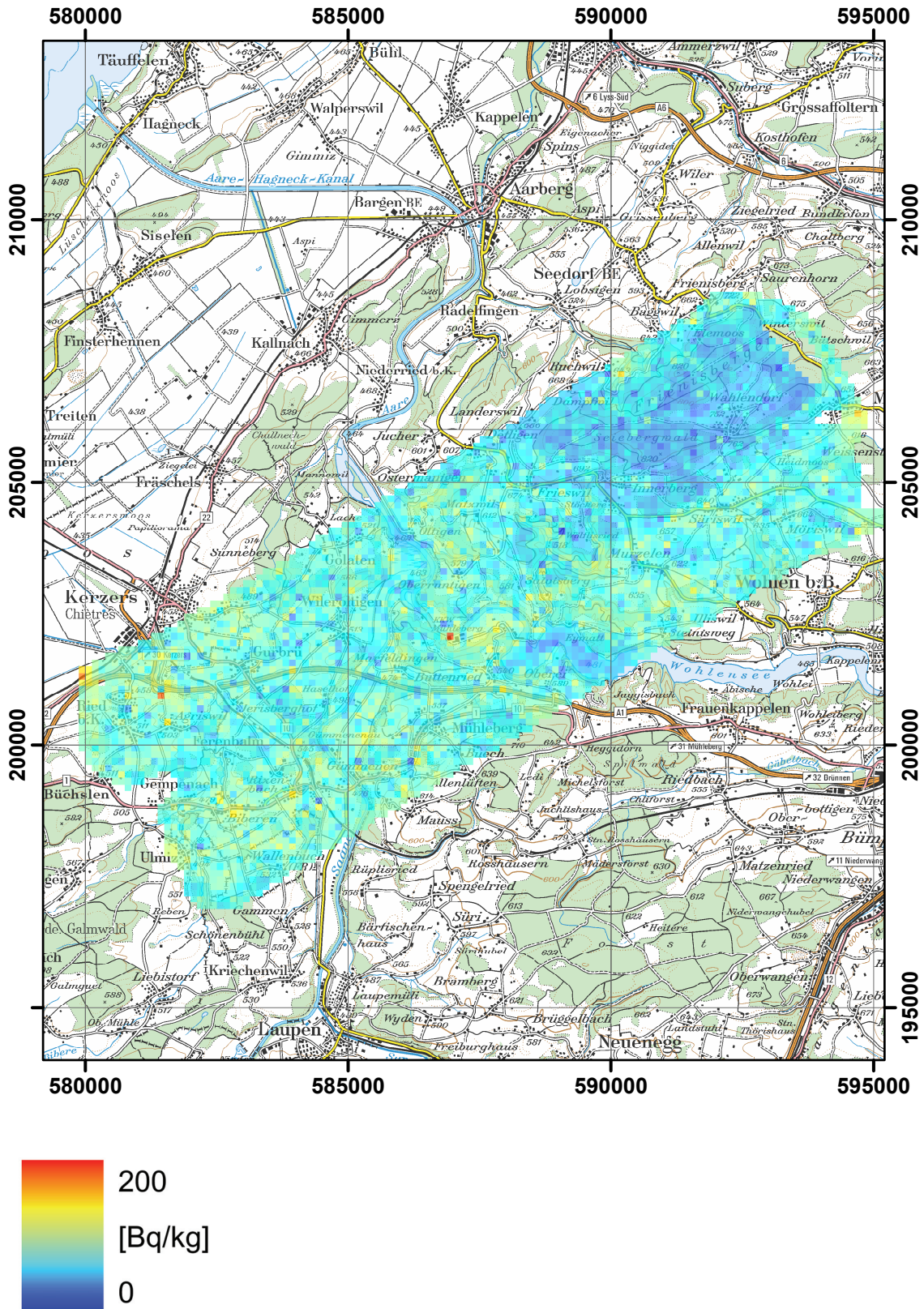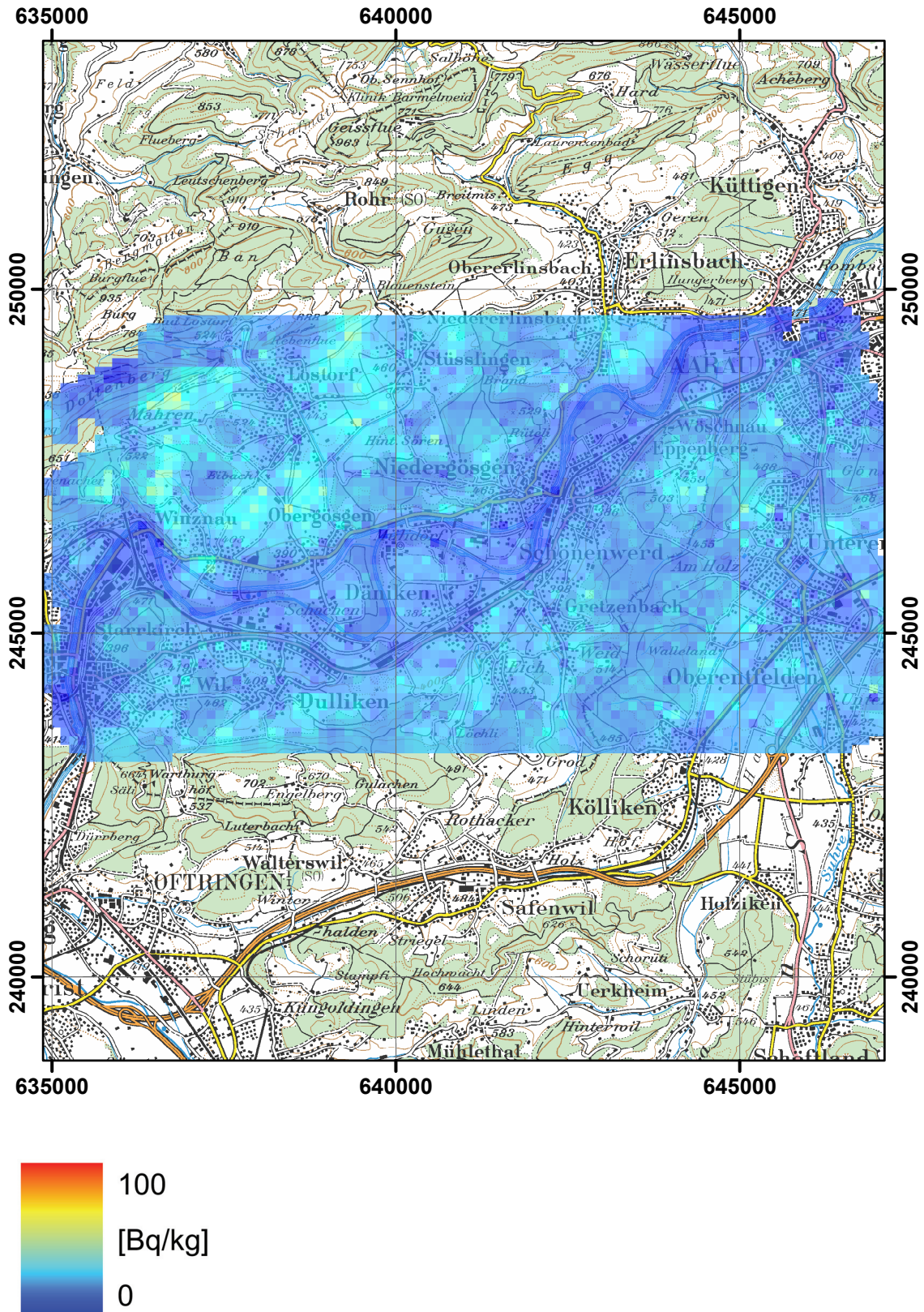
**Figure 84: $^{232}$Th activity concentration measured by the Swiss team in the environs of KKG nuclear power plant. PK100©2003 swisstopo.**
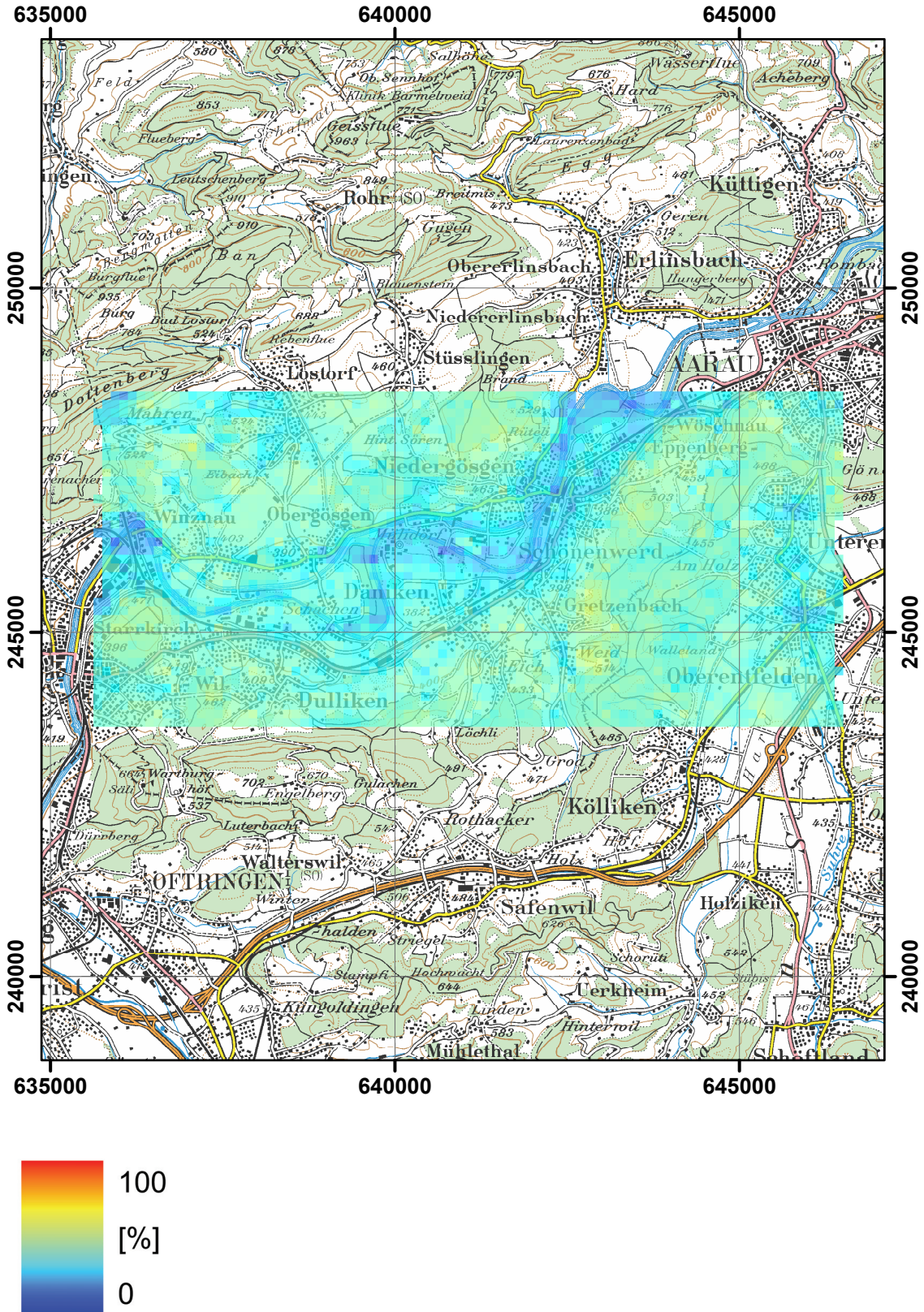
**Figure 85: Relative standard deviation of the terrestric dose rate in the environs of KKG nuclear power plant. PK100©2003 swisstopo.**
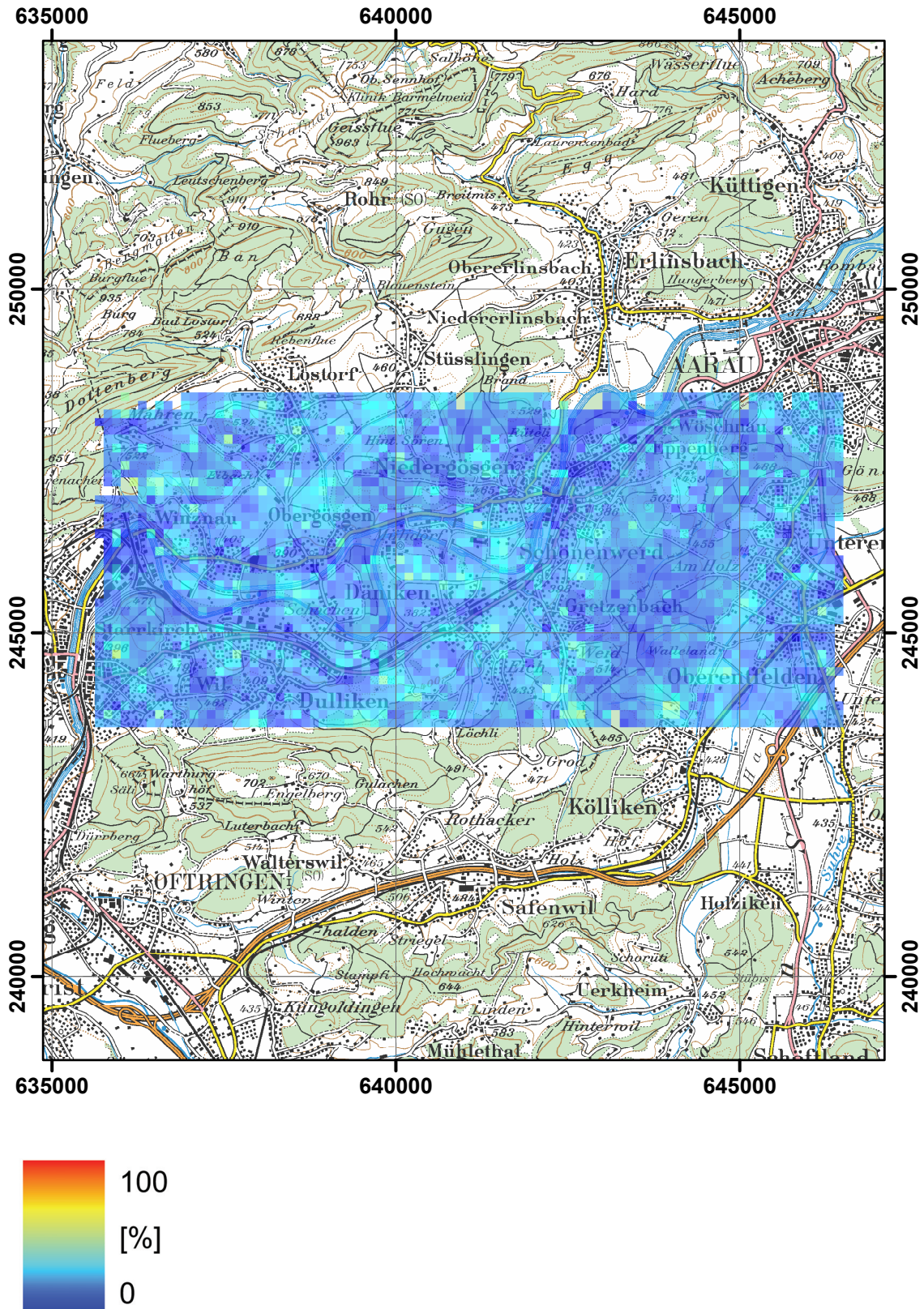
**Figure 86: Relative standard deviation of the $^{40}$K activity concentration in the environs of KKG nuclear power plant. PK100©2003 swisstopo.**
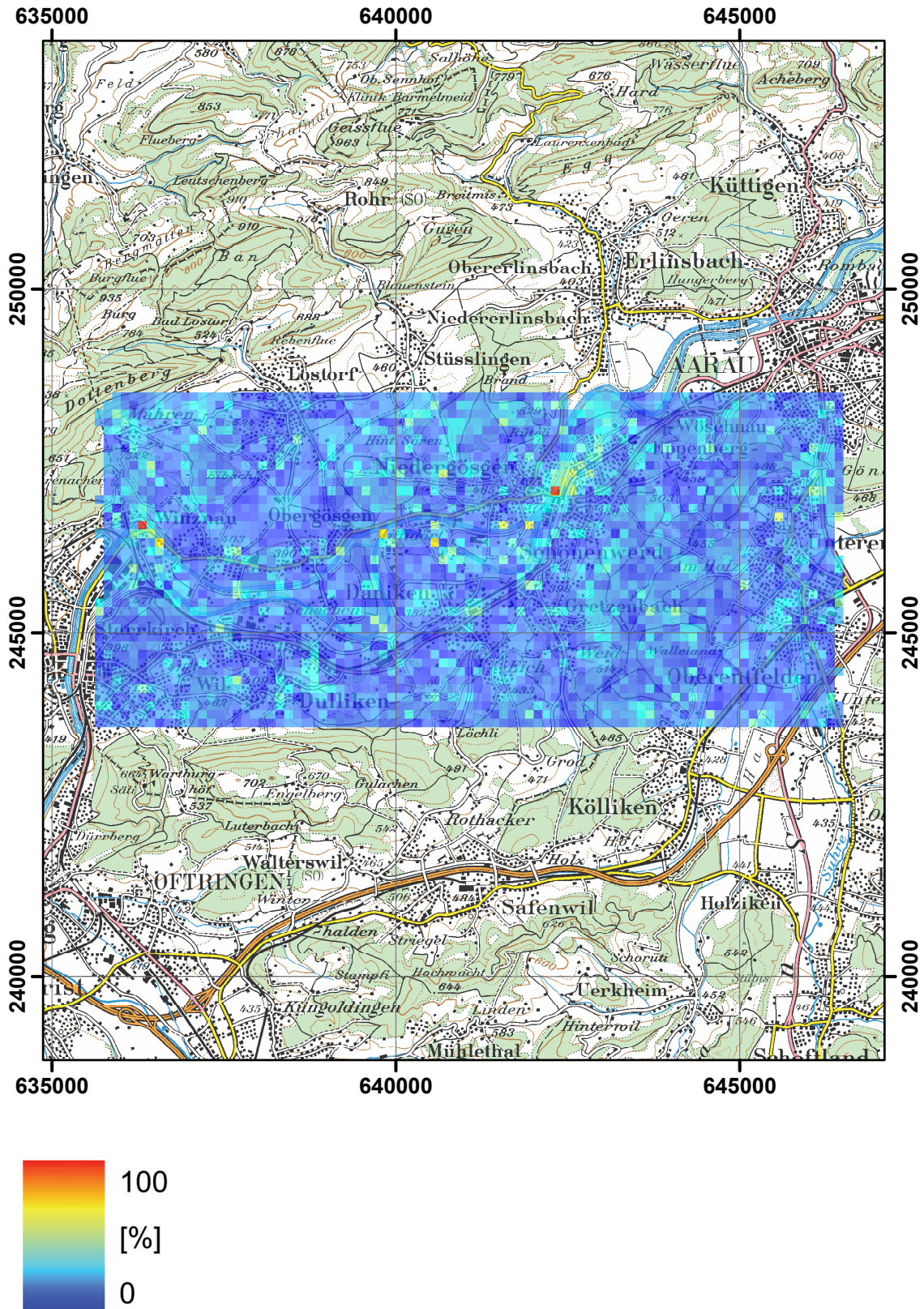
Figure 87: Relative standard deviation of the $^{232}$Th activity concentration in the environs of KKG nuclear power plant. PK100©2003 swisstopo.
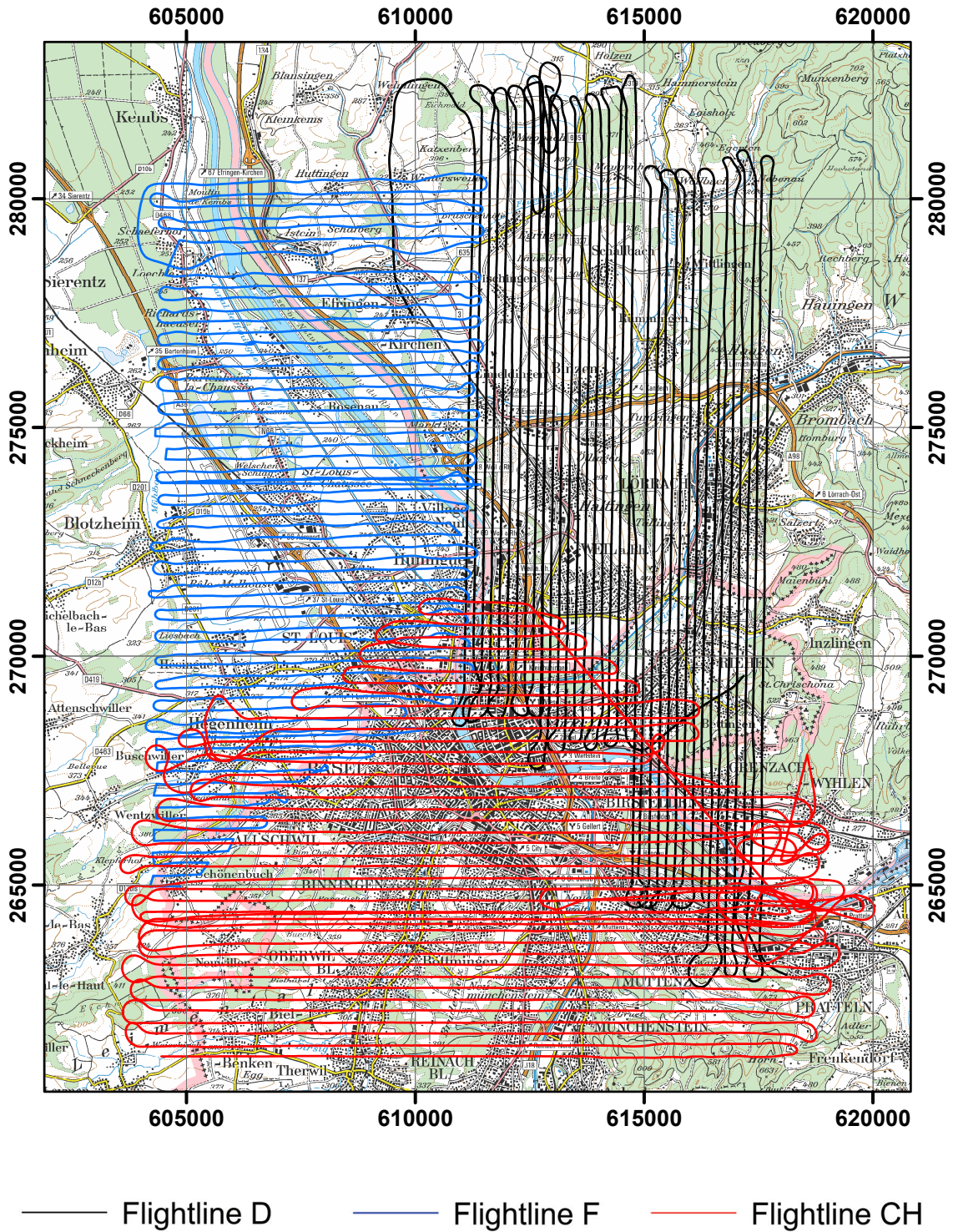
**Figure 88: Flightlines in the environs of Basel. PK100©2008 swisstopo.**
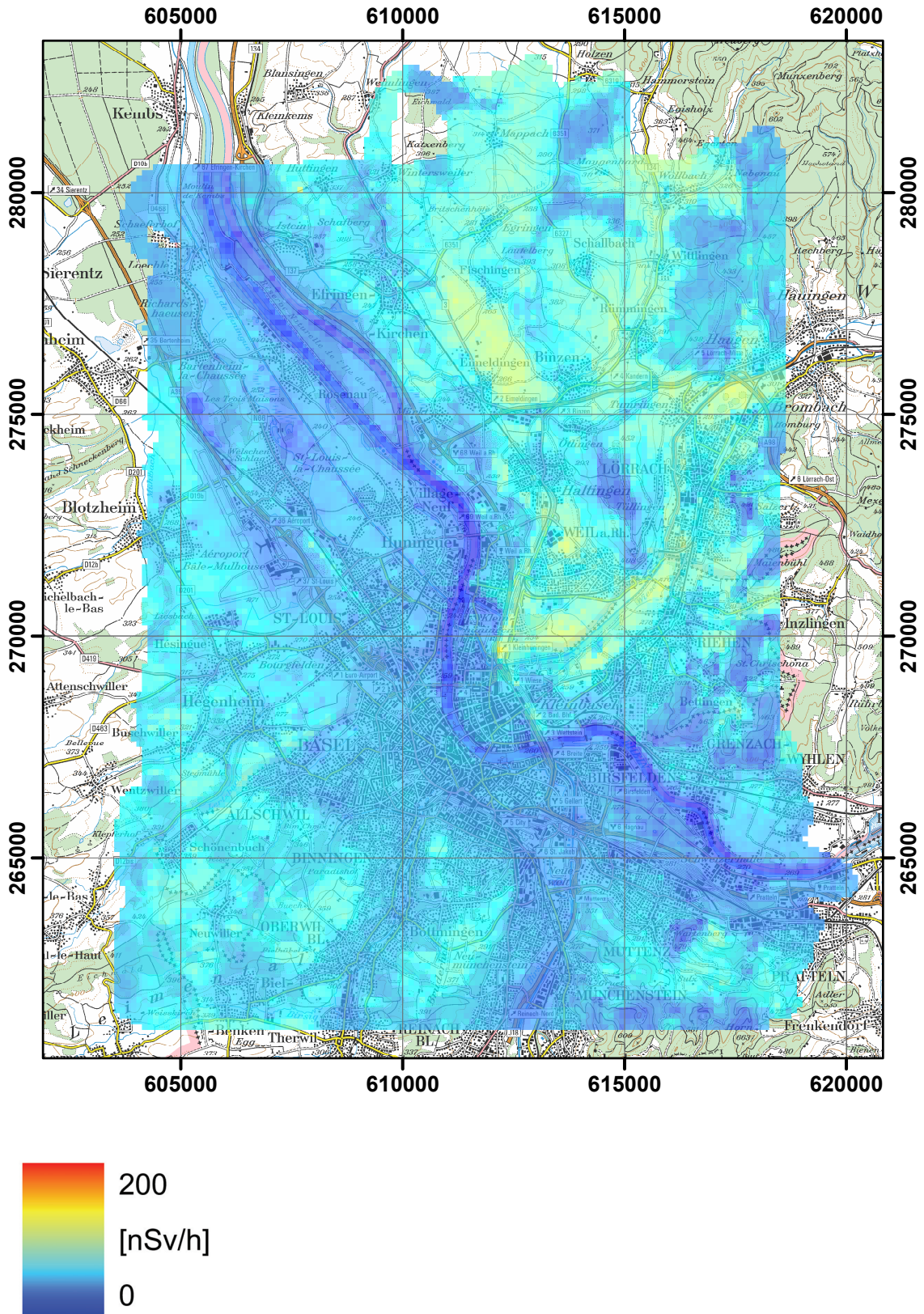
**Figure 89: Composite map of the terrestric dose rate in the environs of Basel. PK100©2008 swisstopo.**
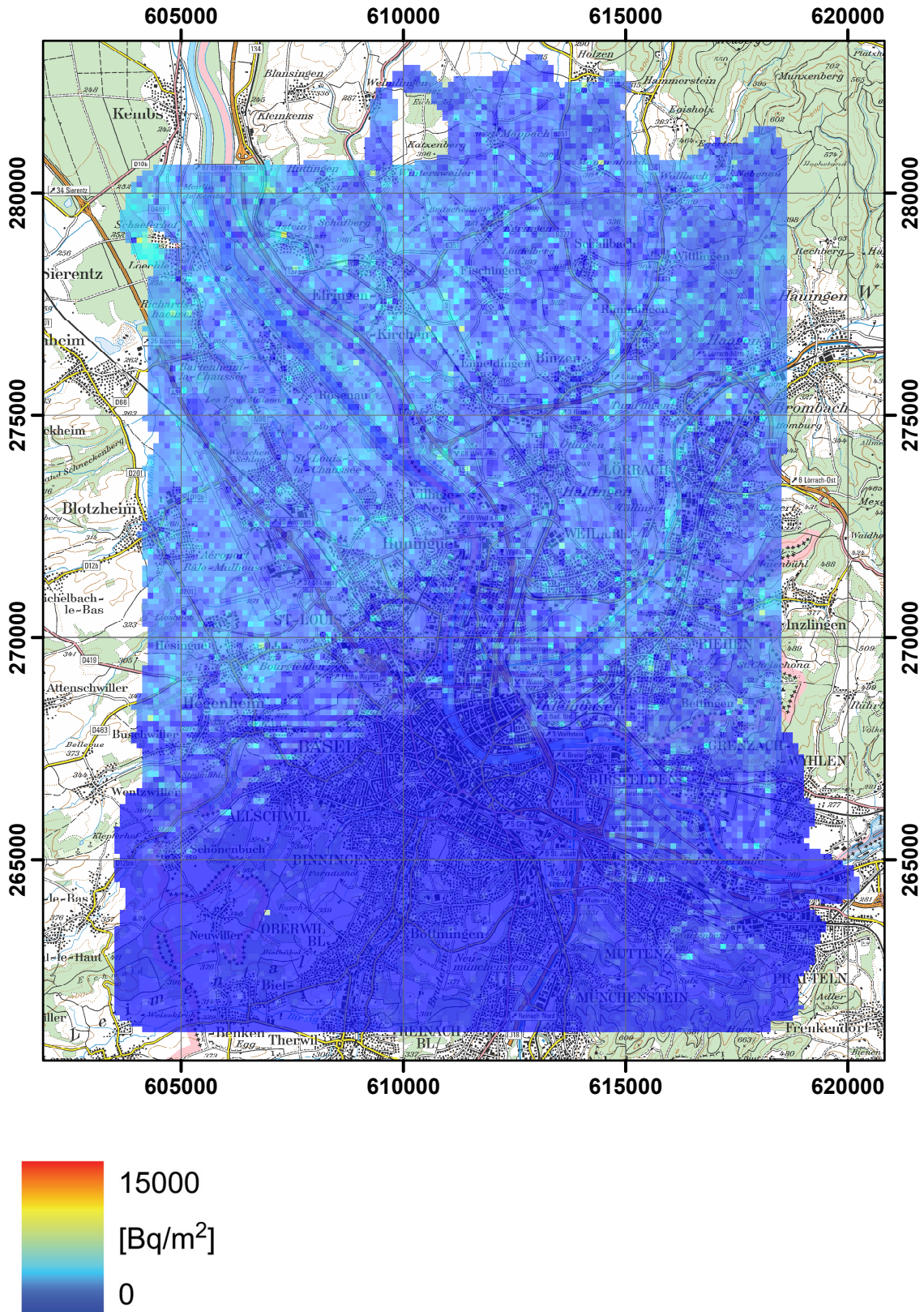
Figure 90: Composite map of the $^{137}$Cs activity concentration in the environs of Basel. PK100©2008 swisstopo.
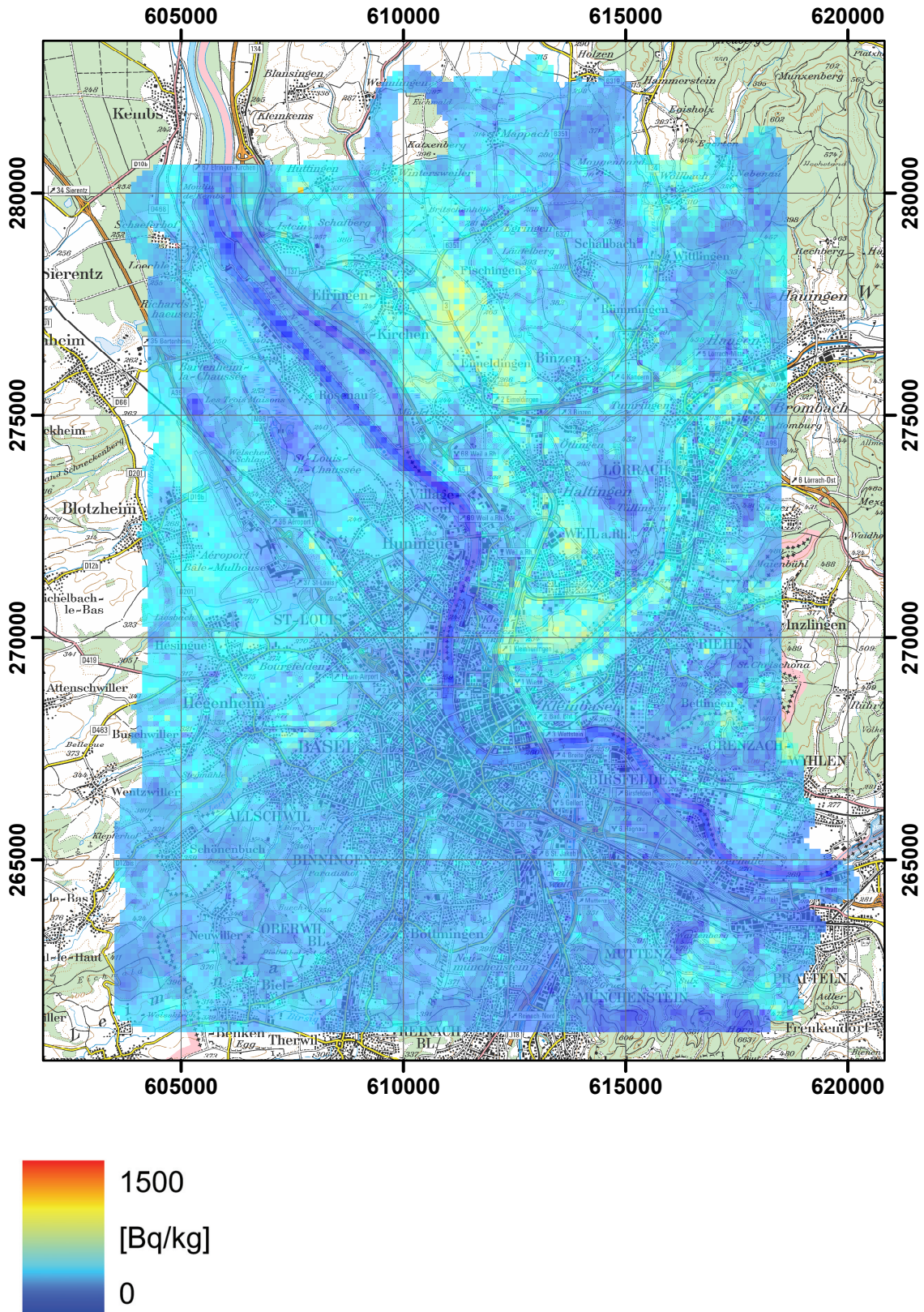
Figure 91: Composite map of the $^{40}$K activity concentration in the environs of Basel. PK100©2008 swisstopo.
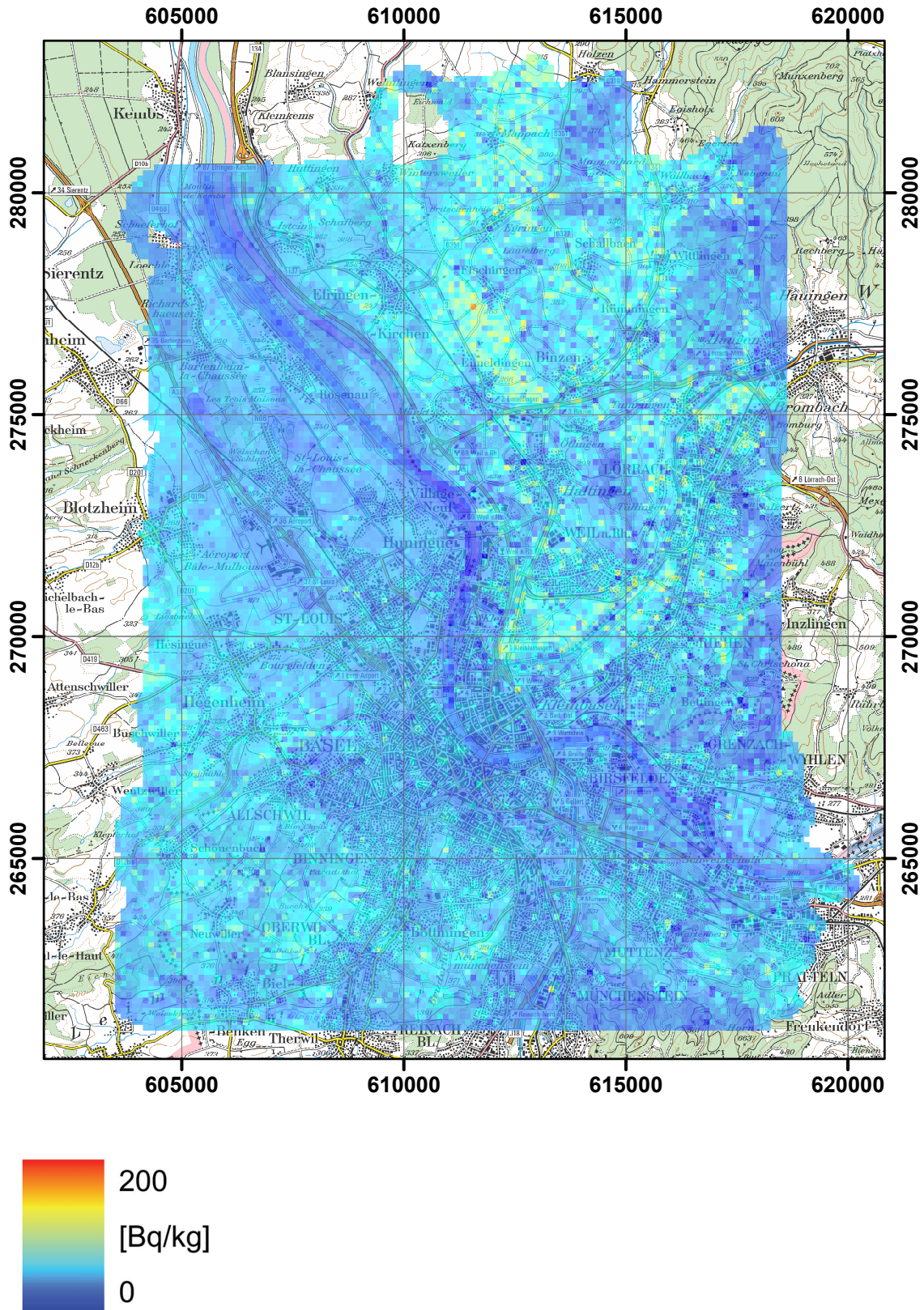
**Figure 92: Composite map of the $^{238}$U activity concentration in the environs of Basel. PK100©2008 swisstopo.**
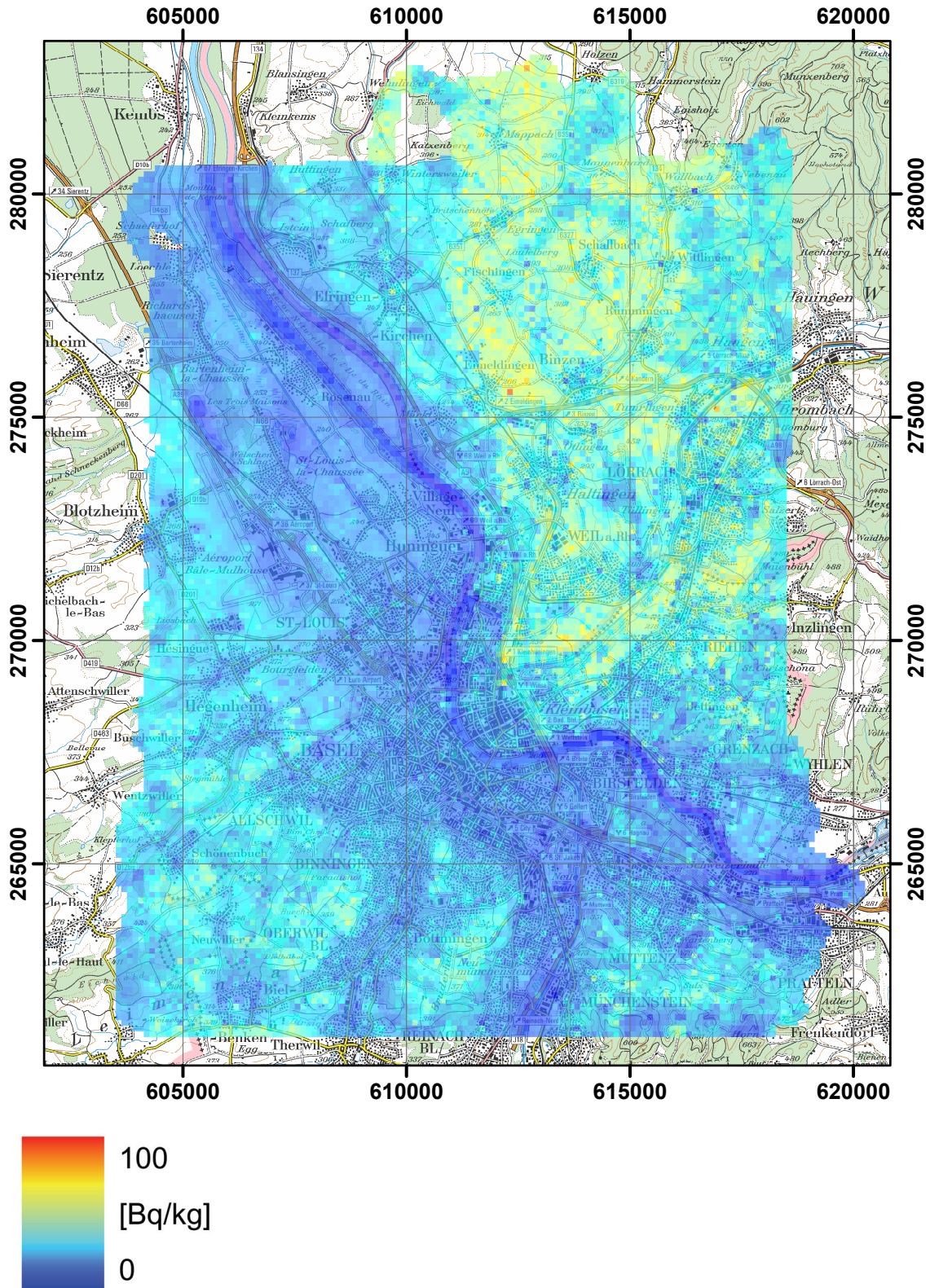
**Figure 93: Composite map of the $^{232}$Th activity concentration in the environs of Basel. PK100©2008 swisstopo.**

## A1 DESCRIPTION OF THE ERS FORMAT

A major goal of the European ECCOMAGS-project was the creation of a common data format for uncomplicated transfer between the participating measurement teams. The following chapter consists of an excerpt of the definition of the data format specification published at „http://www.gla.ac.uk/ECCOMAGS/ERSFormat.pdf".

### A1.1 General principles

The ERS-format (European Radiometric and Spectrometry format) is primarily designed for mobile measurements but can also be applied to In-situ measurements, to measurements on soil samples, to laboratory gamma spectrometry, to fixed measurement stations and so on. The objective is to have a general format, enough flexible to fit with the needs of various measurement techniques. In agreement with the format syntax, each community of users would recommend some rules to standardize the use of this format.

The ERS-format uses ASCII characters to provide easy access and easy use. There is no need to have reading and writing routines just to see the data. An ASCII format is also more flexible. It would make it easier to compose files with various contents. Some files would content spectral data, processed data or both. The syntax should be simple and easily readable. A format based on entities consisting of identifiers-value pairs describing the quantities and measured values was introduced in the PRD (Paired Radiation Data)-format defined by R.Finck (SSI) in 2002. The ERS-format uses the same syntax. It allows flexibility in the file content while providing good readability. A list of identifiers is defined and would be upgraded when needed. To maintain backward compatibility of the upgraded versions with the lower versions, all identifiers defined in the lower versions should be kept unchanged.

### A1.2 Major news in the ERS exchange format

This format is built on the PRD-format for exchanging processed data of the ECCOMAGS exercise. This format is fully described in the exercise protocol "Description of Data Management and Exchange". The major change between PRD and ERS format concerns the storage of the spectral data and information required to process the spectra.

In the Header section, a group of identifiers describing the spectral calibration factors required to process the spectral data is added (S group). The definition is primarily focused on parameters usable with the window method: background and cosmic factors, stripping factors, air attenuation coefficients and calibration factors. In the future, calibration parameters of a new method would be added following the same logic of structure.

An identifier, HSURVEY, has been added to allow the description of a survey, including the nominal ground clearance and line spacing aimed for, the area sur-

veyed, the dates of the survey and other information. If the file reports data from an area within a larger survey, the HSITE identifier may be used to describe this area.

In the Measurement data section, an identifier #S is added to store the spectral data. It would be used to store spectra of apparatus defined in the header section IA. In order to optimise the storage volume, a single identifier is used for the whole spectrum. The spectrum is put within double quotes (" "). It is recommended to start the spectra on a new line and to store 128 channels per line. A Checksum identifier #SC containing the total counts of the spectral data is defined.

The maximum characters per line shouldn't exceed 1024 bytes.

If a value (mostly strings like for the spectra) doesn't fit to one line it can be continued on a new line with the same identifier in combination with identifier tail _+. The line begins with this identifier (ex: S_+ "ch1 ch2 ch3…").

The comment identifier /* has been modified to conform to the identifier-value structure, with the value being a text string enclosed in quotes. The */ end of quote identifier is no longer used.

The IP header section has been modified to conform to the grammar of the identifier-value structure. Thus IPWGS84 "Garmin 12XL" to identify the map datum and GPS instrument has been replaced with IPR "Garmin 12XL" and IPC "WGS84". Optional (sysid) and (coordid) values are added to recognise that more than one instrument may be used, and generally more than one coordinate system is reported (eg: WGS84 and national grid). Also, earth centred coordinate systems can be used, in which case PE, PN and PZ are used to report X,Y and Z respectively.

## A2 RECOMMENDATIONS FOR IMPLEMENTATION OF ERS-FORMAT FOR REPORTING AGS SPECTRAL DATA

The ERS-format has been designed for storing and exchanging radiation measurement data in a general form. To simplify the use of this format for the AGS purposes some recommendations are defined, in agreement with the syntax of the ERS-format. Files generated by the teams following these recommendations are going to have an identical structure, and simple reading and writing procedures could then be used.

The file structure will consist of a header section describing the survey during which the data was collected, the instrumentation used and calibration parameters. A data section consisting of repeated records follows this. It contains positional information, activities and dose rate resulting of data processing and the spectra. It should be noticed that the data section can contain processed data or raw data or both. In the third case, it is recommended to put the results before the raw data. In case of value not available, replace it by –999. It is recommended to store the same number of pairs per line.

## A3 IDENTIFIERS OF THE ERS FORMAT

### A3.1 Header identifiers

Should be placed in records at the beginning of the file

**Table A1: ERS - Header identifiers V**

| V | File format version | Value format |
|---|---|---|
| V | Format version. The value for this version is 1.0 | Text |

**Table A2: ERS - Header identifiers H**

| H | General heading information | Value format |
|---|---|---|
| HCTRY | Country | Text |
| HORG | Organisation | Text |
| HMODE | Operational mode. Values are REAL, EXERCISE or TRAINING | Text |
| HTEAM | Team | Text |
| HSITE | Site (can be used to describe part of a survey) | Text |
| HFILE | File name or other code | Text |
| HSURVEY | Survey information: should include information about survey name, aimed ground clearance, aimed line spacing, speed, etc.) | Text |

**Table A3: ERS - Header identifier IA**

| IA(sysid) | Instrumentation, apparatus<br>sysid - system identification is optional. The third character in the code for instrumentation is the same as the EURDEP code for apparatus type. Common types are given here. Value should describe the apparatus. | Value format |
|---|---|---|
| IAB | Alpha - ZnS scintillator | Text |
| IAD | Alpha - solid state detector | Text |
| IAY | Alpha - alpha spectrometry | Text |
| IAE | Alpha - other | Text |
| IAG | Beta - Geiger-Muller counter | Text |
| IAJ | Beta - solid state detector | Text |
| IAK | Beta - other | Text |
| IAM | Beta and gamma - other | Text |
| IA1 | Gamma - Geiger-Muller tube | Text |
| IAN | Gamma - TLD | Text |
| IAO | Gamma - ionisation chamber | Text |
| IAP | Gamma - sodium iodide detector | Text |
| IAU | Gamma - gamma spectrometry scintillator | Text |
| IAQ | Gamma - solid state detector, Ge(Li) or HPGe | Text |
| IAR | Gamma - other | Text |
| IAZ | Other | Text |

**Table A4: ERS - Header identifier IC**

| IC(sysid) | **Instrumentation, carrier or platform** sysid - system identification is optional. Value should describe the carrier. | **Value format** |
|---|---|---|
| ICA | Airborne (Type and registration number of the air-craft) | Text |
| ICF | Fixed (Type and registration number of the aircraft) | Text |
| ICG | Ground vehicle (Type and registration number of the vehicle) | Text |
| ICI | In situ | Text |
| ICL | Laboratory | Text |
| ICP | Portable | Text |
| ICZ | Other | Text |

**Table A5: ERS - Header identifier IM**

| IM(sysid) | **Instrumentation, method** sysid - system identification is optional. Value should describe the method. | **Value format** |
|---|---|---|
| IM4 | $4\pi$-geometry | Text |
| IMC | With collimator | Text |
| IMS | With shield | Text |
| IMT | Cosmic reduction | Text |
| IMZ | Other | Text |

**Table A6: ERS - Header identifier IP**

| IP(sysid) | Instrumentation, Localization<br>sysid - system identification is optional; Value should describe the instrument for positioning. | Value format |
|---|---|---|
| IPR(sysid) | Description of GPS receiver | Text |
| IPC(coor-did)(sysid) | Type of coordinates system (e.g. "WGS84", or "RT90"). Coordid is the identification number of the coordinates system. | Text |
| IPU(coor-did)(sysid) | Describes the unit of the coordinates system. | Text |
| IPG | Ground clearance determination system | Text |
| IPP | Unit of position precision (meters or PDOP etc.) | Text |

Several coordinates systems can be define to store several sets of coordinates. For example, coordinates provided by the GPS (latitude and longitude in WGS84) should be stored because it can considered as the raw coordinates. For mapping a projection in a local coordinates system such like RT90 is needed.

**Table A7: ERS - Header identifier IS**

| IS(sysid) | Spectral processing parameters<br>sysid - system identification is optional.<br>Value should describe the method. | Value format |
|---|---|---|
| ISW | Window method | Text |
| ISWE1_Xx-000m | Lower energy of window centred on Xx-000m | KeV |
| ISWE2_Xx-000m | Upper energy of window centred on Xx-000m | KeV |
| ISWE1_TOT | Lower energy of total count window | KeV |
| ISWE2_TOT | Upper energy of total count window | KeV |
| ISWC_Xx-000m | Cosmic ratio between Xx-000m window and the cosmic window | Numeric |
| ISWC_TOT | Cosmic ratio between the total count window and the cosmic window | Numeric |
| ISWB_Xx-000m | Background in the Xx-000m window | C/s |

**Table A7: ERS - Header identifier IS (Continued)**

| IS(sysid) | Spectral processing parameters<br>sysid - system identification is optional.<br>Value should describe the method. | Value format |
|---|---|---|
| ISWB_TOT | Background in the total count window | C/s |
| ISWRA1 | Radon correction sky shine A1 | C/s |
| ISWRA2 | Radon correction sky shine A2 | C/s |
| ISWRA_Xx-000m | Radon correction sky shine AXx | Numeric |
| ISWRA_TOT | Radon correction sky shine ATC | Numeric |
| ISWRB_Xx-000m | Radon correction factor BXx | Numeric |
| ISWRB_TOT | Radon correction factor BTC | Numeric |
| ISWS_Xx-000m_Yy-000m | Stripping factor Xx-000m/Yy-000m | Numeric |
| ISWT | Attenuation model  (ex: exp(-mu*H)) | Text |
| ISWT_Xx000m | Attenuation parameter mu for Xx-000m window | $m^{-1}$ |
| ISWT_TOT | Attenuation parameter mu for total count window | $m^{-1}$ |
| ISWA_Xx000m | Calibration factor for Xx-000m activity. Several calibration factors can be defined depending on activity distribution: PWAP, PWAL, PWAAc | c/s per unit of Activity distribution |
| ISWA0_Xx000m | Calibration factor intercept for Xx-000m activity. Several calibration factors can be defined depending on activity distribution: PWAP0, PWAL0, PWAA0c | C/s |
| ISDT | Calibration factor for dose rate calculated from the total count rate | C/s per nGy $h^{-1}$ |
| ISC | Number of channels per spectra | Numeric |
| Ismethodid | methodid . Identification of a method different than the window method. | Text |

If a calibration factor doesn't match to 0 at intercept, A 0 can be added to an identifier to create an additional identifier to declare the value at intercept.

**Table A8: ERS - Header identifier &**

| & | **Additionally defined identifiers**<br>Value should describe the identifier and the unit. | **Value format** |
|---|---|---|
| DEFINE&idf | Define additional identifier. The identifier is &idf. This definition must occur before the identifier can be used. Example: DEFINE&DRCOSM "Cosmic dose rate, nSv/h" defines a new identifier &DRCOSM | Text |
| &idf | An additional identifier &idf that can be used any-where in the file. | Unit as defined by DEFINE |

Identifier-value pairs of the header type should be placed in the beginning of the file. The comment marker should be handled as identifier and the comment as text string, for example:
/* „Start of heading section"
Identifier-value pairs
/* „End of heading section"

**A3.2 Quoted values and comment marks**

Can be placed anywhere in the file.

**Table A9: ERS - Quotes and comments**

| | **Quotes and comments** | **Format** |
|---|---|---|
| „ | Values that include spaces must be enclosed within the double quote character. Example „this is a valide value" | Text |
| /* | Start of comment mark. There will not be any deco-ding of values between start of comment and end of comment markers. Comments cannot automati-cally continue to new lines. A comment on a new line must be preceded by the start of comment mark. | Text |

117

## A3.3 Weather and environment identifiers

Can be placed anywhere in the file, but preferably in the header.

**Table A10: ERS - Identifier W**

| W | Weather | Value unit |
|---|---------|------------|
| WP | Precipitation yes or no. Values are Y or N | Text |
| WPR | Precipitation rate | mm/h |
| WPS | Snow cover depth | m |
| WAT | Air temperature | °C |
| WAH | Air humidity | % |
| WAD | Air density | $kg/m^3$ |
| WGD | Ground density | $kg/m^3$ |
| WGH | Ground moisture content, wet weight /dry weight | Numeric |

## A3.4 Measurement data identifiers

Can be placed anywhere in the file after the heading

**Table A11: ERS - Identifier C**

| C | Calendar date and time | Value format |
|---|------------------------|--------------|
| CD | Measurement date (YYYY-MM-DD) Example: 2002-04-28 | ISO8601 |
| CT | Measurement time of day (hh:mm:ss) Example: 13:35:12 13:35:12Z 14:35:12+01 | ISO8601 |
| CDR | Reference date | ISO8601 |
| CTR | Reference time | ISO8601 |
| CDS | Measurement date start | ISO8601 |
| CTS | Measurement time start | ISO8601 |
| CDP | Measurement date stop | ISO8601 |
| CTP | Measurement time stop | ISO8601 |

**Table A11: ERS - Identifier C (Continued)**

| C | Calendar date and time | Value format |
|---|---|---|
| CDM | Measurement date middle | ISO8601 |
| CTM | Measurement time middle | ISO8601 |
| CDSS | Sampling date start | ISO8601 |
| CTSS | Sampling time start | ISO8601 |
| CDSP | Sampling date stop | ISO8601 |
| CTSP | Sampling time stop | ISO8601 |
| CDSM | Sampling date middle | ISO8601 |
| CTSM | Sampling time middle | ISO8601 |

The letter Z following the date and time indicates Universal Time, UTC. Adding the string +hh or . hh to the time of day, where hh is the time difference relative to UTC, indicates local time. Example: 12:00 UTC is written 12:00Z. Central European Time, CET, is 1 hour ahead of UTC. At 12:00Z, the CET during winter will be 13:00+01 and during summer - when daylight saving time - 14:00+02.

**Table A12: ERS - Identifier A**

| A(sysid) | Activity<br>sysid - system identification is optional. | Value unit |
|---|---|---|
| AP | Activity of a point source | Bq |
| AL | Activity per unit length of a source distributed along a line | Bq/m |
| AA | Activity per unit area of source distributed over an area | $Bq/m^2$ |
| AV | Activity per unit volume of a source distributed in a volume | $Bq/m^3$ |
| AD | Activity per unit dry weight of a source distributed in a volume | Bq/kg |
| AW | Activity per unit wet weight of a source distributed in a volume | Bq/kg |
| AE | Activity per unit area as equivalent surface deposition (1 m above ground) | $Bq/m^2$ |
| AF | Activity per unit area as equivalent surface activity (at the measurement height) | $Bq/m^2$ |

119

**Table A13: ERS - Identifier D**

| D(sysid) | Dose and dose rate<br>sysid - system identification is optional. | Value<br>unit |
|---|---|---|
| DA | Dose to air in free air | µGy |
| DAR | Dose rate to air in free air | µGy/h |
| DK | Air kerma in free air | µGy |
| DKR | Air kerma rate in free air | µGy/s |
| DX | Exposure | µR |
| DXR | Exposure rate | µR/s |
| DHS | Ambient dose equivalent H*(10) | µSv |
| DHSR | Ambient dose equivalent rate H*(10) | µSv/s |
| DHI | Directional dose equivalent H' | µSv |
| DHIR | Directional dose equivalent rate H' | µSv/s |
| DHP | Personal dose equivalent Hp (ICRU 1993) | µSv |
| DHPR | Personal dose equivalent rate Hp | µSv/s |
| DE | Effective dose (not measurable quantities) | µSv |
| DER | Effective dose rate | µSv/s |
| DEAP | Effective dose AP geometry | µSv |
| DEAPR | Effective dose rate AP geometry | µSv/s |
| DEPA | Effective dose PA geometry | µSv |
| DEPAR | Effective dose rate PA geometry | µSv/s |
| DELA | Effective dose LAT geometry | µSv |
| DELAR | Effective dose rate LAT geometry | µSv/s |
| DELL | Effective dose LLAT geometry | µSv |
| DELLR | Effective dose rate LLAT geometry | µSv/s |
| DERL | Effective dose RLAT geometry | µSv |
| DERLR | Effective dose rate RLAT geometry | µSv/s |
| DERO | Effective dose ROT geometry | µSv |
| DEROR | Effective dose rate ROT geometry | µSv/s |
| DEIS | Effective dose ISO geometry | µSv |
| DEISR | Effective dose rate ISO geometry | µSv/s |

**Table A14: ERS - Identifier F**

| F(sysid) | **Fluence**<br>sysid - system identification is optional. | **Value unit** |
|---|---|---|
| F | Fluence | /m$^2$ |
| FR | Fluence rate | /m$^2$s |

**Table A15: ERS - Identifier T**

| T(sysid) | **Acquisition time**<br>sysid - system identification is optional. | **Value unit** |
|---|---|---|
| TL | Acquisition live time | s |
| TR | Acquisition real time | s |

**Table A16: ERS - Identifier N**

| N | **Numbering** | **Value format** |
|---|---|---|
| N | Record number or measurement number | Number or text |

**Table A17: ERS - Identifier P**

| P | **Location, geographic coordinates**<br>The coordinate system (map datum) is defined by the IPC identifier that should be given before measured data. | **Value format or unit** |
|---|---|---|
| PA | Name or code for the measurement or sample point | Text |
| PB | Additional description of the measurement or sample point | Text |
| PN(coor-did) | Measurement or sample point coordinate N-S (latitude) Negative values allowed, when appropriate. If used for Earth centred coordinates (X, Y and Z), PN corresponds to Y) | Numeric |

**Table A17: ERS - Identifier P (Continued)**

| P | Location, geographic coordinates<br>The coordinate system (map datum) is defined by the IPC identifier that should be given before measured data. | Value format or unit |
|---|---|---|
| PE(coor-did) | Measurement or sample point coordinate E-W (longitude) Negative values allowed, when appropriate. If used for Earth centred coordinates (X, Y and Z), PE corresponds to X) | Numeric |
| PZ(coor-did) | Measurement or sample point, altitude above datum. If used for Earth centred coordinates (X, Y and Z), PZ corresponds to Z | m |
| PH | Measurement or sample point, ground clearance | m |
| PP | Position precision | Numeric |

**Table A18: ERS - Identifier PR**

| PR | Relative location related to the source | Unit |
|---|---|---|
| PRA | Relative position of measurement or sample point, horizontal distance to centre of source | m |
| PRH | Relative position of measurement or sample point, height above the centre of a source, negative values allowed | m |
| PRB | Direction (bearing) of the measurement or sample point relative to the North direction (0-360 degrees).<br>Example: A measurement point North of the source is 0 degrees. A measurement point East of the source is 90 degrees. | degrees |

**Table A19: ERS - Identifier #**

| # | Raw data | Value format or unit |
|---|---|---|
| #PHD(sysid) | Pulse height distribution data from spectrometer follows. sysid - system identification is optional. Value should give some description of what has been measured and selected . | Text |
| #Cnumber | Counts in channel number | Numeric |
| #CRnumber | Count rate in channel number | /s |
| #ROI(sysid) | Region of interest data from spectrometer follows. sysid - system identification is optional. Value should give some description of what has been measured and selected. | Text |
| #RCnumber | Counts in region of interest number | Numeric |
| #RCRnumber | Count rate in region of interest number | /s |
| #ECenergy | Counts for energy in keV. Example #EC662 | Numeric |
| #ECRenergy | Count rate for energy keV. Example #ER352 | /s |
| #ECenergy1-energy2 | Count between energy1 and energy2. Energy in keV Example #EC640-680 | Numeric |
| #ECRenergy1-energy2 | Count rate between energy1 and energy2. Energy in keV Example #EC640-680 | /s |
| #S | Full Raw spectrum. The spectrum is put within double quotes and values separated by spaces ("ch0 ch1 ch2 …"). The number of channels is given by ISC. | Numeric |
| #SWstartingchannel | Spectral data within a region of interest starting with startingchannel. | Numeric |
| #SC | Checksum of the spectral data = total counts in the spectrum. | Numeric |

## A3.5 Source description identifiers

Should be placed before processed data.

**Table A20: ERS - Identifier SG**

| SG | Source geometry in ground, general description<br>Description of the source geometry in ground without specification of source coordinates. Can be combined with the Q-identifier to specify geographical coordinates. The identifier can take on a radionuclide tail. | Value unit |
|---|---|---|
| SGP | Point source in ground at depth | m |
| SGL | Line source in ground at depth | m |
| SGA | Plane source in ground at depth | m |
| SGSS | Slab source in ground, start at depth | m |
| SGSP | Slab source in ground, stop at depth | m |
| SGV | Uniform source in ground start at depth | m |
| SGE0 | Exponential source in ground, coefficient at air ground interface or zero ground clearance height | m |
| SGEM | Exponential source, exponent coefficient (mass depth) | $m^2/kg$ |
| SGEL | Exponential source, exponent coefficient (linear depth) | /m |
| SGM | Description of a measured depth distribution containing information about site, name, position and distribution. | Text |

**Table A21: ERS - Identifier SA**

| SA | Source geometry in air, general description<br>Description of the source geometry in air without specification of source coordinates. Applicable for airborne, mobile, carried and in situ measurements. Can be combined with the Q-identifier to specify geographical coordinates. The identifier can take on a radionuclide tail. | Value unit |
|---|---|---|
| SAP | Point source in air at ground clearance height. | m |
| SAL | Line source in air at ground clearance height. | m |
| SASS | Uniform slab source in air, start at ground clearance. | m |
| SASP | Uniform slab source in air, stop at ground clearance. | m |
| SAV | Uniform source in air start at ground clearance, infinite height. | m |
| SACHH | Cylindrical source in air, horizontal axis, centre at ground clearance height. | m |
| SACHR | Cylindrical source in air, horizontal axis, radius. | m |
| SACV | Cylindrical source in air, vertical axis, start at ground clearance height, infinite height. | m |
| SACVS | Cylindrical source in air, vertical axis, start at ground clearance height. | m |
| SACVP | Cylindrical source in air, vertical axis, stop at ground clearance height. | m |
| SACVR | Cylindrical source in air, vertical axis, radius. | m |
| SAE0 | Exponential source in air at zero ground clearance. | m |
| SAEM | Exponential coefficient (mass height) | $m^2/kg$ |
| SAEL | Exponential coefficient (linear height) | /m |

**Table A22: ERS - Identifier SS**

| SS | Source sample description<br>Specific description of sampled sources.<br>Coordinates for source samples should be given with the P identifier. | Value format or unit |
|---|---|---|
| SSI | Sample identification code | Text |
| SSH | Sample description | Text |
| SSTYPE | Sample type code where the value is the 1 - 4 letter EURDEP sample type code.<br>For example:<br>A1 air sample      A11 outdoor air<br>A2 water sample    A21 surface water<br>A3 soil sample      A212 lake water<br>A4 deposition       A23 waste water<br>A5 external radiation   A32 soil + grass<br>A6 sediment        A33 in situ<br>A44 aerial gamma   A411 total deposition<br>A422 snow melt water   A421 rain water<br>AZ environmental sample   A43 grass | Text code |
| SSTREA | Sample treatment code where the value is the one letter EURDEP sample treatment code. For example:<br>A unspecific        K deep frozen<br>B no treatment      M liquid reduced to its residue<br>E measured immediately   V Sample washed<br>I radiochemical separation   W evaporation + ashing<br>L oven dried        X dried + homogenised<br>Q homogenization   Y mixed<br>U air dried          Z others | Text code |
| SSVALU | Sample value type code where the value is the one let-ter EURDEP value code. For example:<br>A discrete single meas.   G highest value<br>B bulked sample average   O lowest value<br>C time average       H time average month<br>D geograph average   L time average year<br>F time and geograph aver.   Z not specified<br>J discrete sample from bulked source | Text code |
| SSV | Sample volume | $m^3$ |
| SSY | Sample density | $kg/m^3$ |

**Table A22: ERS - Identifier SS (Continued)**

| SS | Source sample description<br>Specific description of sampled sources.<br>Coordinates for source samples should be given<br>with the P identifier. | Value<br>format<br>or unit |
|---|---|---|
| SSW | Sample wet weight | kg |
| SSD | Sample dry weight | kg |
| SSA | Sample area | $m^2$ |
| SSS | Sample depth start | m |
| SSP | Sample depth stop | m |
| SSL | Sample linear depth thickness | m |
| SSM | Sample mass depth thickness | $m^2$/kg |

**A3.6 Source coordinate identifiers**

Should be placed together with measurement data.

**Table A23: ERS - Identifier Q**

| Q | Location of a source in the environment.<br>The coordinate system (map datum) is defined by<br>the IP identifier that should be given before<br>measurement data. The identifier can take on a<br>radionuclide tail. | Value<br>format<br>or unit |
|---|---|---|
| QA | Name or code for the source | Text |
| QB | Additional description of the source | Text |
| QCPN | Point source coordinate N-S (latitude) | Numeric |
| QCPE | Point source coordinate E-W (longitude) | Numeric |
| QCPZ | Point source, altitude above sea level | m |
| QCPH | Point source, ground clearance | m |
| QCLN1 | Line source first coordinate N-S | Numeric |
| QCLE1 | Line source first coordinate E-W | Numeric |
| QCLN2 | Line source first coordinate N-S | Numeric |

**Table A23: ERS - Identifier Q (Continued)**

| Q | Location of a source in the environment.<br>The coordinate system (map datum) is defined by the IP identifier that should be given before measurement data. The identifier can take on a radionuclide tail. | Value format or unit |
|---|---|---|
| QCLE2 | Line source first coordinate E-W | Numeric |
| QCLZ | Line source, average altitude above sea level | m |
| QCLH | Line source, average ground clearance | m |
| QCCN | Circular source centre coordinate N-S | Numeric |
| QCCE | Circular source centre coordinate E-W | Numeric |
| QCCR | Circular source radius | m |
| QCCZ | Circular source, average altitude above sea level | m |
| QCCH | Circular source, average ground clearance | m |
| QCAN1 | Area source coordinate N1 | Numeric |
| QCAE1 | Area source coordinate E1 | Numeric |
| QCAN2 | Area source coordinate N2 | Numeric |
| QCAE2 | Area source coordinate E2 | Numeric |
| QCAN3 | Area source coordinate N3 | Numeric |
| QCAE3 | Area source coordinate E3 | Numeric |
| QCAN4 | Area source coordinate N4 | Numeric |
| QCAE4 | Area source coordinate E4 | Numeric |
| QCAZ | Area source, average altitude above sea level | m |
| QCAH | Area source, average ground clearance | m |
| QCVN1 | Volume source coordinate N1 | Numeric |
| QCVE1 | Volume source coordinate E1 | Numeric |
| QCVN2 | Volume source coordinate N2 | Numeric |
| QCVE2 | Volume source coordinate E2 | Numeric |
| QCVN3 | Volume source coordinate N3 | Numeric |
| QCVE3 | Volume source coordinate E3 | Numeric |
| QCVN4 | Volume source coordinate N4 | Numeric |

**Table A23: ERS - Identifier Q (Continued)**

| Q | Location of a source in the environment. The coordinate system (map datum) is defined by the IP identifier that should be given before measurement data. The identifier can take on a radionuclide tail. | Value format or unit |
|---|---|---|
| QCVE4 | Volume source coordinate E4 | Numeric |
| QCVZ1 | Volume source, start at average altitude above sea level | m |
| QCVZ2 | Volume source, stop at average altitude above sea level | m |
| QCVH1 | Volume source, start at average ground clearance | m |
| QCVH2 | Volume source, stop at average ground clearance | m |

**A3.7 Identifier tails**

Should be connected to the body of certain identifiers.

**Table A24: ERS - Identifier tail Type 1**

| | Identifier tail Type 1: Detection limit, uncertainty, apparent and estimated values. Can be used for activity, dose, dose rate, fluence and fluence rate. Should be written before identifier tail Type 2. | Value unit |
|---|---|---|
| _LC | Decision limit<br>Example: Decision limit for activity per unit area: AA_LC | * |
| _LD | Detection limit | * |
| _LQ | Determination limit | * |
| _UR | Random uncertainty | * |
| _US | Systematic uncertainty | * |
| _UT | Combined total uncertainty | * |
| _URP | Random uncertainty percent | % |
| _USP | Systematic uncertainty percent | % |

**Table A24: ERS - Identifier tail Type 1 (Continued)**

| | **Identifier tail Type 1:** Detection limit, uncertainty, apparent and estimated values. Can be used for activity, dose, dose rate, fluence and fluence rate. Should be written before identifier tail Type 2. | **Value unit** |
|---|---|---|
| _UTP | Combined total uncertainty percent | % |
| _UEx | Error type where x is the EURDEP-code for denoting error type using the letters A . Z. Example: _UEA standard deviation _UED standard error of the mean | ** |
| _A | Apparent value assuming a specific source geometry that probably is not the correct geometry. Applicable for reporting activity when the source geometry is unknown. | * |
| _G | Estimated or guessed value, not a measured value. Ap-plicable for a source in the environment that has not yet been thoroughly quantified. | * |
| _+ | Continuation character (e.g. #S_+) | |

**Table A25: ERS - Identifier tail Type 2**

| | **Identifier tail Type 2:** Radionuclide, energy Can be used for activity, dose, dose rate, fluence, fluence rate, source descriptions and source coordinates. | **Value Unit** |
|---|---|---|
| _Xx-000m | Radionuclide. All radionuclides allowed. Examples: _Cs-137, _Tc-99m Decision limit for Cs-137 per unit area: AA_LC_Cs-137 | * |
| _TOT | Total for all radionuclides | * |
| _NAT | Natural radionuclides | * |
| _ANT | Antropogenic radionuclides | * |
| _COS | Cosmic | * |
| _Eenergy | Energy (given in keV). Example: _E662 | * |

* The unit should be the same as for the body of the identifier

\*\* The unit depends on the definition of the quantity related to the EURDEP error code

**A3.8 These identifiers are not yet fully defined**

**Table A26: ERS - Incomplete Identifiers**

| Identifier | Quantity, description | Unit |
|---|---|---|
| SA | Source geometry in air<br>Description of source geometry without geographical position | |
| SAP | Point source in air at ground clearance | m |
| SAL | Line source in air at ground clearance | m |
| SAA | Plane source in air at ground clearance | m |
| SASS | Slab source in air, start at ground clearance | m |
| SASP | Slab source in air, stop at ground clearance | m |
| SAV | Uniform source in air start at ground clearance | m |
| SAE0 | Exponential source in air at zero ground clearance | m |
| SAEM | Exponential coefficient (mass height) | $m^2/kg$ |
| SAEL | Exponential coefficient (linear depth) | /m |

PAUL SCHERRER INSTITUT

**PSI**